

Study of Atomic and Molecular Many-Body Processes in Astrophysics

*A Thesis
Submitted for the Degree of
Doctor of Philosophy*

*In
Faculty of Science
Bangalore University*

Sonjoy Majumder



**Indian Institute of Astrophysics
Bangalore 560 034, India**

March 2001

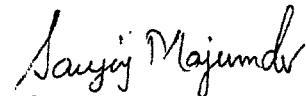
Declaration

I hereby declare that this thesis, submitted to Bangalore University, Bangalore, for the award of a Ph.D. degree, is a result of the investigations carried out by me at Indian Institute of Astrophysics, Bangalore, under the supervision of Bhanu Ptatap Das. The results presented herein have not been subject to scrutiny, by any university or institute, for the award of a degree, diploma, associateship or fellowship whatsoever.



Prof. Bhanu Pratap Das

(Thesis Supervisor)



Sonjoy Majumder

(Ph.D. Candidate)

Indian Institute of Astrophysics
Bangalore 560 034, India

2001 March

Certificate

This is to certify that the thesis entitled 'Study of Atomic and Molecular Many-Body Processes in Astrophysics' submitted to the Bangalore University by Sonjoy Majumder for the award of the degree of Doctor of Philosophy in the faculty of Science, is based on the results of the investigations carried out by him under my supervision and guidance, at the Indian Institute of Astrophysics. This thesis has not been submitted for the award of any degree, diploma, associateship, fellowship, etc. of any university or institute.


Prof. Bhanu Pratap Das
(Supervisor)

Bangalore 560034

2001 March

To my Jathya (Uncle)

Late Lalit Mohan Majumder

Acknowledgements

It has taken many a long nights and days to finish this little piece of work. A work built on the work of others and a study upon a miniscule fraction among mammoths. I consider myself lucky to get the opportunity of working in physics in general and the area of my work in particular, for which I am greatly indebted to Prof. Bhanu Pratap Das, who with his generosity and a lot of past experience considered me as a doctoral student when I was at loss after my earlier supervisor left the institute. All along, the help I got from you and the discussion I had with you were my motivations to do better each time. I thank you for the lessons learnt in the process. It is difficult to convey my indebtedness to Dr. Rajat K. Chaudhuri, without whose valuable help and advice it would have been impossible to proceed with this work. He has been my adviser in matters of research work as well as personal life since the first time we met. Any words will be too less to express my thanks to him for the ever helpful inspiration and guidance he provided during the whole course of this work. I have a very special indebtedness to Prof. Palash B. Pal. I am indeed fortunate to start my research career under your guidance. I am very grateful to you for teaching me the basics of physics as a whole and helping me to step into research activities, although it is unfortunate for me that we could not continue to work together. I am grateful to the Director of the Institute Prof. Ramanath Cowsik for all the help I got.

My association with all the NAPP group members, Dilip, Geetha, Prafulla, Holger, Nirmalya, Hasi-di, Latha and Sahoo was extremely beneficial, especially, the group discussions we had through out this work. In addition, I have had innumerable, illuminating discussions with several other members of the institute, whose names are too numerous to mention. I wish to express my thanks to all of you.

I thank Bangalore University for making the official processing smooth and remain indebted to Prof. Ananthram, Chairman Physics Dept., Bangalore University for his help in official matters. The officials at PhD section, Bangalore University, Central College are always being helpful to me on all issues of official matters, thank you all and especially Mr. Krishnamurthy.

I wish to express my thanks to all the staff of our Institute. The Library and canteen staff, the computer personnel have also been very helpful. I am indebted to Mr.

Prabhakara, Mr. Venkatesh, Mr. Yarappa and Mr. Kanakaraj in the library. Mr. Narashima Raju and Mr. Mohan Kumar in the administration, Mr. Iyenger. Mr. Prabhakara and Mr. Selvakumar in the store, Mr. Aragyaswami, Mr. Dhanaanjay. Mr. Alagiri, Mr. Venu, Mr. Murthy, Mr. Mariappa, Mr. Nagaraj (beloved Naga) of the canteen, Mr. Murali Das of air-conditioning plant, Mr. Shankar and Mrs. Jain of the telephone Exchange for their constant help.

It was my pleasure to have warm association with all my seniors, Dr. Dipankar Banerjee, Dr. Eshwar Reddy, Dr. R.D. Prabhu, Dr. Gajendra Pandey, Dr. Arun Thampan, Dr. Sivarani, Dr. Swara Ravindranath during first part of this work. you have given me precious lessons on many things in academic and personal life. Dr. Sujan Sengupta, our Sujan-da, your attitude towards science left me spell bound and admiring, and our precious company with Dr. Kaustav Das, our Kaustav-da, for many many days are memorable, especially on the eve of new millennium days on Kovalam Beach and all the Saturday nights we spent together with lots of fun. The many discussions I had with Partha-da, Dr. Partha Joarder, though mostly on non-academic matters sustained my views and his precious, humorous, enjoyable company kept me lively this work, thank you Partha-da. I should acknowledge you, Manas and Hasi-di for your enjoyable and constructively critical company all through the overlap we had.

Srik I always remain a fan of your many activities academic and non-academic, especially your way of discussions on quantum computer. I am grateful to you for going through manuscript of my thesis carefully and your valuable suggestions. Thank you Rajguru for exposing me to the climate-Sun relationship and all the fun we used to have during the dinners.

All my friends at IIA have made working here an enjoyable experience. I would especially like to thank my 'batchmates', Pavan, Jana, Sankar, Rajesh, Mangala. The friendship of Bhargavi, Dharam, Sridharan, Suresh, Raji, Ramachandra, Sudip, Subhabrata, Manoj, Ravindra, Ravindar, Kathi, Maheshwaran, Shaninuga, Preeti, Geetanjali, Ambika and Shalima was invaluable.

The close and warm association I had with Dr. Biswas (Biswasda) and his family (our universal Didi), Amar, Rinni (Amar's family), Keya (Pavan's family) made

my non-academic life enjoyable and mitigated my home sickness. Thank you, Didi, Rinni and Keya for the lavish food I used to enjoy often with you all and your constant encouragement. The rejuvenation I derived by playing with young Priya, Megha and Srijita is unforgettable.

I am lucky to have found a perfect roomie in the guise of Atish Dipankar Jana, your hard work and sincerity in many things had guided me through on numerous issues. I have always been an admirer of your wit and spirit of doing science for what it offers mankind. The friendship I had with Pavan, a person who shares many of my interests about life, is rare.

I thank Prof. Parthasarathy of our institute, Prof. Lambert of University of Texas, Austin, Prof. Anil Pradhan of Ohio State Univ., Prof. C. Froese Fischer of Vanderbilt Univ., Dr. Farid Parpia of IBM, Prof. C.D. Lin of Kansas State Univ., Mr. Sandeep Koheli of CDAC for the help during the course of thesis work.

Wherever I go and wherever I will be, babu, maa, mama, Haru-jyatha, dida I will keep in my mind your words to do my best in whatever I do. I have tried it many a times but I have failed. Still that does not stop me from trying once more. The solace you gave for my being away from you encouraged me over the years. Munna, my young niece, your smiles and prank behaviour are always in my mind, though I am mostly away from you. My dear Bhai, Bardi and Bon, Jamaibabu, Dhiraj, Masi, Meso, Biplab, Raja, Gora all of you have always been a cause to look forward to tomorrows tiding with hope. I love you all, I am proud and lucky to have been among you.

Abstract

Atomic and molecular processes in astronomical objects have profound implications. Many of those objects in which certain atomic and molecular species have been detected are the sites for evolution of stellar envelopes and star formations. Measurements of atomic and molecular line intensities are powerful diagnostic tools for the exploration of many astrophysical processes. Accurate calculations of energy levels, lifetimes of states, oscillator strengths and shapes of the atomic and molecular transition lines are often necessary to understand those processes. Rigorous treatments of atomic and molecular many-body effects are necessary for accurate calculations of these quantities. Such calculations have become important with the advent of high resolution spectrographs used in several ongoing missions for solar and stellar projects. Even improved experimental data are not adequate for them. Forbidden lines, which is one of the important features in this thesis work, are difficult to measure. Here we have employed various many-body approaches to calculate electronic properties of some atoms, ions and molecules which have astrophysical importance. Both non-relativistic and relativistic studies have been performed using perturbative and non-perturbative approaches.

Effective valence shell Hamiltonian (H^v) theory, one of the most advanced non-relativistic approaches to multireference many-body perturbation theory (MBPT) is used to calculate binding energies (energy relative to first ionization threshold), excitation energies, oscillator strengths and transition probabilities of neutral carbon and calcium. The same method is used for calculating ground state energy difference between the cyclic and linear isomers of propynlidyne (C_3H), as well as their harmonic vibrational frequencies, ionization potentials, electron affinities, excited state energies, dipole moments and oscillator strengths, some of which have not been reported before. One of the most important forbidden transitions, magnetic quadrupole transitions for Be-like ions are calculated using the multiconfiguration Dirac-Fock method, which is a self consistent variational relativistic many-body method. The leading relativistic correction to the Coulomb interaction known as the Breit interaction is included in these calculations using first-order perturbation theory. The weak allowed transitions of Mg II are accurately computed using one of

the most powerful non-perturbative size-extensive approaches, the coupled cluster (CC) method. A new approach to generate the Dirac-Fock (DF) orbitals using finite basis set expansions is developed. These DF orbitals are used in the CC calculations to achieve high accuracies for various electronic properties of atoms.

List of Publications

List of Publications, Presentations and Posters based on the work reported in this Thesis.

Publications

1. Sonjoy Majumder, B. P. Das and Rajat K. Chaudhuri, 1999.
Excitation Energies and Oscillator Strengths of Ca I using
Multireference Many-body Perturbation Theory :
Physical Review A., **59**, 3432
2. Sonjoy Majumder and B. P. Das, 2000.
Relativistic Magnetic Quadrupole Transitions in Be-like Ions :
Physical Review A., **62**, 0420508-1
3. Rajat K. Chaudhuri, Sonjoy Majumder and Karl Freed, 2000.
Determination of Conformational Energy Differences of C_3H Isomers
using the Effective Valence Shell Hamiltonian Method:
Journal of Chemical Physics, **112**, 9301
4. Sonjoy Majumder, B. P. Das and Rajat K. Chaudhuri, 1998.
Excitation Energies and Oscillator Strengths of Ca I and Cl :
*Proceedings of Sixth International Colloquium on Atomic Spectra and Oscilla-
tor Strengths for Astrophysical and Laboratory Plasmas*, pp. 99
5. Sonjoy Majumder, Geetha Gopakumar, Holger Merlitz and B.P. Das, 2001.
A new approach to generate relativistic basis :
(submitted to *Physical Review A.*),

6. Sonjoy Majumder, Holger Merlitz, Geetha Gopakumar, B.P.Das, U.S. Mahapatra and Debasish Mukherjee, 2001.

Accurate Calculations of Allowed transitions of Mg^+ ion using relativistic coupled cluster method:

(submitted to *Physical Review A.*),

Presentations

1. Sonjoy Majumder

Excitation Energies and Oscillator Strengths of Ca I and Ca II :

An oral presentation at the Sixth International Colloquium on Atomic Spectra and Oscillator Strengths for Astrophysical and Laboratory Plasmas,

at University of Victoria, Victoria, B.C., Canada, August 9-13, 1998

Posters

1. Sonjoy Majumder, Rajat K. Chaudhuri and Karl Freed,

Theoretical studies on the interstellar propynylidyne isomers :

IAU symposium 197 on Astrochemistry: from molecular clouds to planetary systems

Swagipo, Cheju Island, South Korea, August 22-26, 1999

2. Sonjoy Majumder, Holger Merlitz, K.P. Geetha, B.P.Das, U.S. Mahapatra and Debasish Mukherjee,

Accurate Calculations of Allowed transitions of Mg^+ ion using relativistic coupled cluster method:

National Conference on Atomic and Molecular Physics, Indian Association for the Cultivation of Science, Jadavpur, Calcutta, India. January 16-20, 2001.

Acronyms

Acronyms Used In this Thesis

au	:	Atomic unit
BWPT	:	Brillouin-Wigner Perturbation Theory
CASSCF	:	Complete Active Space SCF
CC	:	Coupled Cluster
CCSD	:	Single and Double CC
CGTO	:	Contracted Gaussian Type Orbital
CI	:	Configuration Interaction
CIS	:	Single CI
CSF	:	Configuartion State Function
DF	:	Dirac-Fock
DHF	:	Dirac-Hartree-Fock
DPT	:	Degenerate Perturbation Theory
EE	:	Excitation Energy
EOL	:	Extended Optimal Level
EOMCC	:	Equation OF Motion CC
EOMIP	:	Equation OF Motion IP
EPC	:	Even-parity Pair Channel
FBSE	:	Finite Basis Set Expansion
FUBSE	:	Finite Universal Basis Set Expansion
GTO	:	Gaussian Type Orbital
HAAR	:	Hydrogen Atoms Abstraction Reaction
HF	:	Hartree-Fock

HST	:	Hubble Space Telescope
IP	:	Ionization Potential
IPM	:	Independent Particle Model
ISM	:	Interstellar Medium
IVO	:	Improved Virtual Orbital
JLV	:	Jucys, Levinson and Vanagas
MBPT	:	Many-Body Perturbation Theory
MCDF	:	Multiconfiguration Dirac-Fock
MCHF	:	Multiconfiguration Hartree-Fock
MCSCF	:	Multiconfiguration SCF
MP	:	Möller-Plesset
MRCI	:	Multi-reference CI
NIST	:	National Institute of Standard and Technology
OL	:	Optimal Level
OPC	:	Odd-parity Pair Channel
OSCC	:	Open-Shell CC
PN	:	Planetary Nebula
QDPT	:	Quasi-Degenerate Perturbation Theory
RCI	:	Relativistic CI
ROHF	:	Restricted Open-Shell HF
RSPT	:	Rayleigh-Schrödinger Perturbation Theory
SCF	:	Self-Consistent Field
SG	:	Spline-Galerkin
SS	:	Superstructure
STEOM	:	Similarity Transformed Equation of Motion
STO	:	Slater Type Orbital
TMC	:	Taurus Molecular Cloud
UV	:	Ultra-Violet

Contents

List of Figures	xiv
List of Tables	xvi
1 Introduction	1
1.1 Atomic and Molecular Processes in Astrophysics	1
1.2 Many-Body Theory of Atoms and Molecules	5
1.3 Organization of Thesis	9
2 Non-relativistic Many-Body Calculations of Atomic Properties of Astrophysical Interest	13
2.1 Introduction	13
2.2 Theory	16
2.3 Properties of neutral carbon	19
2.3.1 Basis set and reference space	20
2.3.2 Results	22
2.4 Properties of Neutral Calcium	27
2.4.1 Computational Details	28
2.4.2 Results and Discussions :	33
2.5 Conclusion	42
3 <i>ab initio</i> Relativistic Studies of Excitation Energies and Oscillator Strengths in Atomic Systems	48
3.1 Introduction	48

3.2	Magnetic Quadrupole transitions for ions of Be-sequence using the MCDF Approach	52
3.2.1	Theory (MCDF-EOL)	54
3.2.2	Results and Discussions	58
3.3	Relativistic DF orbitals generation: A new approach using finite basis set expansion	65
3.3.1	Method of Calculation	66
3.3.2	Results and Discussion	69
3.4	Properties of Mg II using the Coupled Cluster Approach	78
3.4.1	Theory (Coupled Cluster Method)	80
3.4.2	Results and Discussions	85
3.5	Conclusion	91
4	Applications of Molecular Studies to Astrophysics	97
4.1	Introduction	97
4.2	Determination of Properties of Propynlidyne Isomers using the H^v Method	101
4.2.1	Computational Details	104
4.2.2	Results and Discussion	107
4.2.2.1	Cyclic C_3H	107
4.2.2.2	Linear C_3H radical	110
4.2.2.3	Conformational energy difference	112
4.3	Conclusion	113
5	Conclusion and Future Directions	122
5.1	Conclusion	122
5.2	Future Directions	126
	Appendix:A	128
A.1	Rayleigh-Ritz Variational Principle	129
A.2	Dirac-Fock equation for Atoms	129
A.3	Multiconfiguration Dirac-Fock Equations for Atoms :	132

List of Figures

2.1	<i>Typical one and two body H^v dipole diagrams. Here, the line going up (down) refers to virtual (core) orbital. The valence orbitals are represented by a line with a double arrow and a line with an arrow inside a circle, can be a valence or virtual orbital.</i>	19
2.2	<i>Variation of third order H^v (with 14V reference space) correlation energy as a function of basis set.</i>	30
2.3	<i>Variation of third order H^v (with 14V reference space) $4s^2 \rightarrow 4s5s(^1S)$ transition energy as a function of number of valence orbitals in the reference space.</i>	32
2.4	<i>Variation of third order H^v (with 14V reference space) $4s^2 \rightarrow 4s4p(^1P)$ oscillator as a function of number of valence orbitals in the reference space.</i>	33
3.1	<i>The effect of Breit interaction on the excitation energies</i>	60
3.2	<i>Percentage of error in IP results of valence orbitals of MgII obtained using analytical Gaussian basis (solid line) and new basis (dashed line) 75</i>	75
3.3	<i>Percentage of error in EE results of among the excited states of MgII obtained using analytical Gaussian basis (solid line) and from new basis (dashed line). (i) $3s-3p(1/2)$, (ii) $3s-3p(3/2)$, (iii) $3s-5p(1/1)$, (iv) $3s-5p(3/2)$, (v) $3p(1/2)-3d(3/2)$, (vi) $3p(1/2)-5d(3/2)$, (vii) $3d(3/2)-5p(1/2)$, (viii) $4p(1/2)-4d(3/2)$, (ix) $3d(3/2)-4f(5/2)$ and (x) $3d(3/2)-5f(5/2)$. . .</i>	77
3.4	<i>Empirical curve of growth for the ion states expected to be most populated in H I regions (taken from reference [58])</i>	80

4.1 Calculated *ab initio* structures and relative energies of triplet C_3H_2 and doublet C_3H isomers. Filled circles are carbon atoms and void circles are hydrogen atoms. Figure taken from Kaiser's article [13] . . 102

List of Tables

2.1	<i>Excitation energies (in Rydberg) of C I.</i>	24
2.2	<i>Oscillator strengths of C I for the ground $2p^2(^3P) \rightarrow$ excited $2p3s(^3P)$ and $2p4s(^3P)$ transitions.</i>	24
2.3	<i>Oscillator strengths of C I for the ground \rightarrow excited states and excited states \rightarrow excited states transitions.</i>	25
2.4	<i>Low-lying binding energies (in cm^{-1}) of Ca I.</i>	35
2.5	<i>Third order H^v excitation energies (in Rydberg) for S, P, D and F multiplets of Ca I.</i>	37
2.6	<i>Transition energies (in Rydberg) for S multiplets of Ca I, obtained from third order H^v method using 13V (4s, 5s, 6s, 7s, 4p, 5p, 6p) valence space.</i>	38
2.7	<i>Third order H^v Oscillator Strengths for S, P, D and F multiplets of Ca I.</i>	39
2.8	<i>Transition probabilities (in $10^8 sec^{-1}$) computed through third H^v method for S, P, D and F multiplets of Ca I.</i>	40
2.9	<i>Variation of third order ground state correlation energy (in a.u.) as a function of reference space.</i>	40
3.1	<i>Selection rules for allowed electric dipole (E1) transition and forbidden magnetic quadrupole (M2) transition</i>	50
3.2	<i>Comparison of the percentage of differences of calculated excitation energies from experimental values between the MCHF+BP and MCDF+B (first order correction) methods</i>	61
3.3	<i>Contributions of the Breit interaction to the excitation energies (in cm^{-1})</i>	62

3.4	Excitation Energies (in cm^{-1}) from the ground state.	63
3.5	$\langle 1s2s3s3p_{\frac{1}{2}}(^3P_2) M_2 1s2s3p_{\frac{1}{2}}3p_{\frac{3}{2}}(^1S_0) \rangle$ matrix element values for different Z	63
3.6	Transition rate (in sec^{-1}) from $2s2p(^3P_2)$ to the ground state.	64
3.7	Number of basis used for each symmetry to calculate DF energies and wavefunctions of Mg^+ and Ca^+	69
3.8	The comparison of DF bound orbitals' energies for Mg^+ calculated by using the new method and the analytical method.	71
3.9	The comparison of DF bound orbitals' energies for Ca^+ calculated by using the new method and the analytical method.	72
3.10	Number of orbitals used in CCSD(T) calculation.	73
3.11	IP got using nonlinear CCSD in units of (cm^{-1}):	74
3.12	EE of Mg II got using nonlinear CCSD in units of (au)	76
3.13	Comparison of some oscillator strength results of Mg II	76
3.14	Excitation Energies from the ground state in cm^{-1}	86
3.15	Oscillator Strengths of $3s - 3p$ and $3s - 4p$ transitions	87
3.16	Oscillator Strengths of various transitions	88
4.1	Structural data for the C_3H isomers.	114
4.2	Vertical excitation energies (in eV) and oscillator strengths (in parentheses) of the $c\text{-C}_3\text{H}$ radical.	114
4.3	Vertical ionization potentials and electron affinities (in eV) of the $c\text{-C}_3\text{H}$ radical.	115
4.4	Dipole moments (in Debye) of the $c\text{-C}_3\text{H}$ radicals	115
4.5	Vibrational frequencies (in cm^{-1}) of the $c\text{-C}_3\text{H}$ radical.	115
4.6	Vertical excitation energies (in eV) and oscillator strengths (in parentheses) of the $l\text{-C}_3\text{H}$ radical.	116
4.7	Dipole moments (in Debye) of the $l\text{-C}_3\text{H}$ radical.	116
4.8	Vertical ionization potentials and electron affinities (in eV) of the $l\text{-C}_3\text{H}$ radicals.	116
4.9	Vibrational frequencies (in cm^{-1}) of the $l\text{-C}_3\text{H}$ radical.	117

4.10 Energy difference (in KJ mole^{-1}) between the $c\text{-C}_3\text{H}$ and $l\text{-C}_3\text{H}$ radicals.	117
--	-----

Chapter 1

Introduction

1.1 Atomic and Molecular Processes in Astrophysics

Almost all of our knowledge of the distant universe reaches us in the form of photons. Therefore, atomic and molecular spectroscopic data are essential components of research in astronomy and astrophysics. There has been a long history of intimate connections between astrophysics and atomic/molecular spectroscopy. Prior to 1962, *The Astrophysical Journal* was explicitly subtitled “An International Review of Spectroscopy and Astronomical Physics”. The accuracy with which physical conditions in objects studied by astronomers can be inferred from spectroscopic observations depends directly on the breadth and precision of the data available for atomic and molecular processes. In addition, reliable spectroscopic data are required for models of photon driven physical and chemical processes; and models of the steady state properties of astronomical objects that absorb and emit photons [1, 2, 3]. The increasing astronomical techniques and theoretical models in astrophysics continually create new demands for important data on atomic and molecular properties.

The quantitative distribution of the atomic and molecular elements in the universe is a classical problem in cosmochemistry [4] and astronomy. As far as it was possible

to test the hypothesis, the chemical composition of our part of the galaxy seems to be representative of that of the observable part of the astronomical universe [5]. Given an equivalent width, an oscillator strength value of the transition line of a particular element and an astrophysical model in a certain astronomical region, one can derive an abundance of that element in that region [6, 7]. Abundances derived from the technique of spectral synthesis can no more be accurate than the system of physical inputs used in the theoretical calculation, like oscillator strengths. At the outset, let us enumerate the reasons why we are interested in the abundances of the atomic and molecular elements:

1. We would like to know the primordial composition of the solar system and its relation to the present composition of the Earth and other planets. Such data might throw some light on vexing problems connected with the origin and chemical history of the Earth [8].
2. A knowledge of the composition of the local part of our galaxy is needed for the construction of models of the Sun and stars, and for a complete understanding of physical and chemical processes taking place in the stellar atmospheres and the interstellar medium (ISM) [9].
3. The observed abundance distribution of elements, and particularly of the individual nuclides, enable us to test the hypotheses that have been proposed for element formation.

Quantitative analysis of the spectra of the astronomical sources and of the processes that populate the atomic and molecular energy levels that give rise to emission and absorption by these sources, require accurate data on transition frequencies (or differences of energies of initial and final states of the transitions) and probabilities, ionization cross sections, electron impact excitations, deactivation, photoionization and photodetachment cross sections, radiative and dielectronic recombination and radiative attachment rate coefficients and cross sections for heavy particle collisions involving charge transfer. For molecules, processes such as radiative association, rotational and vibrational excitation, ion-molecule and neutral-particle chemical reactions, dissociative recombination, photodissociation and collision induced ab-

sorption must be quantitatively described. Much of these data are not available in literature [3].

The resonance lines of neutral and singly ionized lighter atoms are possible to observe through the earth's atmosphere, but for most of the abundant atoms and ions the first excited level with different parity from the ground state lies above 33000 cm^{-1} . Therefore, their resonance lines occur at wavelengths $\lambda < 3000 \text{ \AA}$. This large separation of the lowest levels also means that many of the strongest permitted lines in the spectra of planetary nebula and diffuse nebulae occur at ultraviolet (UV) wavelengths.

Therefore, in the last one decade we have seen the deployment of powerful new satellite instruments for astronomical UV spectroscopy and unprecedented concomitant growth in the quality and variety of astronomical spectroscopic data [10]. Because space astrophysics missions are conspicuous engineering efforts, instrument signals are sometimes equated with scientific success. However, critical attention to the scientific data is needed. Robust experimental and theoretical programmes in laboratory astrophysics are required to optimize mission planning and, ultimately, to transform returned spectroscopic data into scientific knowledge through calibration, analysis and interpretation.

The far UV line spectra of stars were observed first with rockets. But the equivalent widths were rather large, probably because of blending with stellar lines. Now with Hubble Space Telescope (HST) and Far Ultraviolet Spectroscopic Explorer (FUSE) operating in orbit, we have new source of high quality spectroscopic data [11, 12, 13, 14]. The actual ranges are 1090 to 1700 \AA for Echelle-A and 1700 to 3100 \AA for Echelle-B of HST spectrographs. But below 1150 \AA the sensitivity is low. FUSE complements HST spectrograph in UV range. Certainly the sorting of interstellar lines which overlap in velocity is done best with a small aperture.

The identification of molecules in interstellar space has profound implications. Many of the clouds in which molecules have been detected are the sites of star formation. The measurements of molecular line intensities are powerful diagnostic tools for the exploration of the physics of gravitationally collapsing interstellar clouds [15]. The energy and ionization balance of an interstellar cloud are significantly modified

by the presence of molecules and the chemical evolution of the cloud affects in an essential way the dynamical history of the collapse.

Fortunately, many of the analyses of laboratory spectra now provide more than adequate accuracy on wavelengths for the investigation of the best possible HST data. In most modern work physicists and chemists have calculated wavelengths from the energy levels, which have been derived from the measurements of many different transitions. But, accuracy is not much adequate in the far ultraviolet region where FUSE yields best data.

A reasonable goal for interstellar abundances is 1σ uncertainties within ± 0.1 dex so that it is desirable to know oscillator strengths (f-values) to ± 0.03 dex. Accurate f-values particularly important when one combines lines of different strengths from the same ion to obtain the curve of growth of the interstellar cloud or compares profiles to determine the amount of saturation. The f-values for many resonance lines now have this accuracy, but numerous important ones still have only poor measurements or rough theoretical estimates available and a few do not have even these.

In brief, we can list why accurate wavelength, energy level and oscillator strength data are needed for astrophysical studies:

1. Identification of overlapping weak lines in astronomical spectra and disentanglement of their blends;
2. To study stellar convection, macro- and micro-turbulence, rotation, supernovae and nebulae;
3. To correct and improve the accuracies of known atomic and molecular energy levels and find previously unknown atomic energy levels;
4. Important predictions of forbidden transitions which are the best source to study nebulae, circumstellar and supernova remnants;
5. To support stellar atmospheric models, where millions of atomic and molecular lines of thousands of species are used.

In order to calculate excitation energies and oscillator strengths for atomic and molecular systems, it is necessary to use many-body theory.

1.2 Many-Body Theory of Atoms and Molecules

The development in modern many-body theory based on quantum mechanics took place in the early 1950's. The stimulus for this was provided by the training of numerous theorists in the techniques of field theory. In this area, the theorists had become familiar with high order perturbation methods, handling of divergences, renormalization and Feynman diagrams.

Many-body theory probably has had its greatest success in applications to atoms. Molecular calculations are much more difficult, because in molecules one not only takes into account interactions among electrons of a particular atom, but also interactions of the electron-electron, electron-nucleus and nucleus-nucleus of different atoms.

In atoms, the electron densities and kinetic energies are large, particularly in heavy atoms, as a result of the dominance of the nuclear field. The simple atomic or molecular picture, that physicists and chemists have of electrons occupying orbitals is in reality an approximation, sometimes a very good one but nevertheless, an approximation – the independent particle model (IPM) (also called Hartree-Fock (HF) approximation). In this model electrons are assumed to move independently of each other in an average field due to the nucleus and the other electrons. The IPM and the variational principle then lead to the (unrestricted) Hartree-Fock equation. The HF approximation is important not only for its own right but also as a starting point for more accurate approximations, which include the effects of electron correlation. A few of the computational methods of atomic and molecular processes bypass the HF approximation, but most do not. All the methods, described in this thesis use the HF approximation as the starting point.

The study of atomic and molecular structure has been traditionally divided into two separate approaches : a) *ab initio* and b) semiempirical. In this thesis, we have employed various many-body *ab initio* methods to calculate electronic properties of some atoms, ions and molecules which are of astrophysical importance.

The first quantitative application of the many-body perturbation theory (MBPT) to atomic structure was by Kelly in 1963-64 who calculated properties of ground and excited states of several light atoms [16, 17, 18]. Such calculations were probably not

feasible much earlier because of large computational requirements. Kelly found that perturbation methods usually converged rather slowly even in atoms of simple structure unless selective diagrams whose summation was used to obtain energy shifts and the excited orbitals were optimally chosen. The following non-relativistic and relativistic studies have been performed using perturbative and non-perturbative approaches.

Effective valence shell Hamiltonian (H^v) theory is one of the most advanced non-relativistic approaches to *ab initio* multireference many-body perturbation theory (MR-MBPT) [19]. Given a set of one-electron orbitals which is partitioned into core, valence and excited orbitals, it is possible to transform the original Schrödinger equation for the effective valence shell Hamiltonian. H^v is defined in such a way that it depends explicitly only upon the valence orbitals. However, since H^v is formally exact, its diagonalization reproduces the same valence state energies which result from the solution of the full Schrödinger equation for those states within the given orbital basis.

H^v is a novel alternative to configuration interaction (CI) calculations for studying the role of electron correlation. It combines the most desirable features of the MBPT and the multiconfigurational self-consistent field (MCSCF) approaches. The second order H^v calculations have demonstrated the remarkable fact that it is possible to use the same H^v effective integrals for all charged species of the same valence system simultaneously. Third order calculations provide accurate results for a variety of atomic and molecular properties. We shall employ the H^v method to calculate various electronic properties of neutral open shell carbon and closed shell calcium. We shall investigate the effectiveness of the multireference structure and the method of tackling non-dynamical correlations of the H^v method by applying to astrophysically important C_3H radicals.

A relativistic theory is required for the description of atoms and molecules whenever their orbital electrons probe regions of space with high potential energy near the atomic nuclei. Primary effects of a relativistic description include changes to spatial and momentum distributions, spin-orbit interactions, quantum electrodynamic corrections such as the Lamb shift and vacuum polarization. Secondary effects in

many-electron systems arise from shielding of the outer electrons by the distributions of electrons in penetrating orbitals; they change orbital binding energies and dimensions and so modify the order in which atomic shells are filled in the lower rows of the Periodic Table. Relativistic atomic and molecular structure theory can be regarded as a simplification of the fundamental description of quantum electrodynamics (QED). An understanding of the Dirac equation, its solutions and their numerical approximation, are essential material for studying many-electron systems here.

Non-relativistic theories are appropriate for light atoms or ions. Due to various nuclear processes (like the r process) heavier elements become abundant in the astronomical objects. Also, only allowed transitions can be calculated with the non-relativistic theory. Extremely hot environments of the stars (for instances, corona of the Sun, planetary nebulae etc) show abundances of highly stripped ions. With the advent of many high resolution spectrographs, observations of weak or forbidden transition lines become possible and they are of great astrophysical interest. Many astrophysical phenomena like, coronal heating, evolution of many chemical compositions on the stellar envelope, determination of the type of chemistry in the planetary nebulae precursor's envelope are believed to be explained largely by these forbidden lines. There are some approaches based on the relativistic corrections to the non-relativistic Hamiltonian that are available in the literature, have been extensively used. Full fledged relativistic approaches are being used by various research groups [20].

The multiconfiguration Dirac-Fock (MCDF) approach [21] is the relativistic counterpart of the multiconfiguration Hartree-Fock (MCHF) method [22]. This is a self-consistent variational many-body method which takes into account the electron correlation to a large extent with a rather small number of orbitals. In the MCDF method there is a choice of optimization procedures. There are in principle two different ways of allowing the calculation to minimize energy. The average level type calculations use the weighted sum of the diagonal Hamiltonian matrix elements for the energy state specified. The optimal level (OL) scheme minimizes the energy for one state (level). The OL scheme can be extended to include several levels in an

energy functional that contains weights for the states under consideration, this is referred to as an extended optimal level (EOL) calculation. The latter method is computationally preferable. The relativistic two-electron operator cannot be written down in closed form. In Quantum Electrodynamics (QED), the interaction between two electrons can be expressed as a series expansion. The leading correction to the Coulomb interaction is known as the Breit interaction. This corrections of the energies of the atomic states can be included using first-order perturbation theory. The magnetic quadrupole transition of Beryllium-like ions, which were calculated earlier for a few ions with low atomic number using relativistic correction methods, will be calculated in this thesis with MCDF-EOL approach to investigate the implications of the method described above.

The most common type of configuration interaction (CI) calculation includes all singly and doubly excited configurations with respect to a reference configuration. These CI calculations are sometimes supplemented by a Davidson correction [23] for the fact that the variational treatment with singles and doubles is not size consistent. Couple Cluster (CC) theories provide an alternative means for incorporating single and double excitations, but, at the expense of more involved computations, they are explicitly size consistent and do not require Davidson type corrections. This method is one of the successful many-body non-perturbative approaches for quantitative studies on atomic systems. It was developed by Coester and Kümmel [24, 25] in 1958-60 and adopted a form which is useful for quantum chemistry by Cizek, Paldus and co-workers [26, 27, 28, 29]. It can be viewed as a closed-form set of equations which may be used to sum certain categories of MBPT diagrams to all orders [30]. This has the advantage that order dependence is removed from the computation and certain invariance properties are present which are not normally applied to a finite-order method. This method has been extended to the relativistic regime in the last decade. The cluster expansion of the wave functions in the CC representation provides the size-extensivity of the computed energies in a straight forward manner. The non-relativistic CC has been applied with great success to a wide variety of problems including a host of molecular systems. The relativistic version of the CC has become practical only recently [31]. That is because the angular

reduction of the CC equations is rather complex, and the number of cluster amplitudes and the computational effort are several times larger than in the corresponding non-relativistic approximation. Therefore, the most sought improved *ab initio* calculations for the unexpectedly weak $3s - 4p$ doublet transitions of Mg^+ system can be investigated with this fully *ab initio* non-perturbative relativistic approach.

1.3 Organization of Thesis

In this thesis, we have employed various many-body approaches to calculate electronic properties of some atoms, ions and molecules which are of astrophysical importance. Both non-relativistic and relativistic studies have been performed using perturbative and non-perturbative approaches. In Chapter 2, we discuss the non-relativistic perturbative H^v approach to calculate various electronic properties of neutral carbon and calcium. Both the above mentioned neutral atoms have immense astrophysical importance and have strongly interacting configurations. In our work we show how the multireference H^v approach handles these configurations and yields accurate results of their electronic properties.

Relativistic effects are prominent for heavier elements. The MCDF is discussed in the first section of Chapter 3. In this chapter, we calculate magnetic quadrupole transitions for beryllium-like ions for which accurate transition probability calculations are extremely useful in astrophysical interpretations. Finite basis set expansions can be used to solve the single particle Dirac-Fock equations. The conventional approach using the Gaussian-type orbitals (GTOs) is tedious and does not always produce results of desired accuracy. In the next section of Chapter 3, we develop a new approach using the numerical wavefunctions (obtained from Dirac-Fock (DF) calculations in the MCDF framework) for occupied and a few low lying unoccupied orbitals; and GTOs for remaining high lying orbitals. This approach has large implications, specially, for the highly correlated methods, like, coupled cluster (CC) method which we will be using to investigate the electronic properties of singly ionized magnesium atom. Also this new method of generating orbitals will be useful to calculate electronic properties like hyperfine transitions, where the accuracy of the core orbital wavefunctions is very important. The unexpectedly low strength

of $3s - 4p$ doublet transitions of Mg^+ in various calculations has compelled us to calculate these transitions using the *ab initio* powerful non-perturbative many-body approach, the CC method. In last section of Chapter 3, we will investigate how all order perturbation nature of the method yields accurate electronic properties and the effect of highly excited reference space on them.

The understanding of hydrocarbon synthesis in interstellar clouds provides a stimulus for studying the hydrocarbon radical C_3H and its isomers. Here the ground and excited state properties of the *l*- and *c*- C_3H radicals are computed through the third order H^v method for both H^v optimized geometries, as well as for the experimental and MP2/6-31G(d,p) optimized geometries for comparison discussed in Chapter 4. Several harmonic vibrational frequencies are obtained as a by-product of the optimization procedure.

In the last chapter, we summarize the important conclusions of this thesis and describe future work that may be beneficial for a deeper understanding of the nature of the methods we have used.

References

- [1] D. C. Morton, *Astroph. J. Suppl.*, **77**, 119 (1991)
- [2] A. Dalgarno and D. R. Layzer, *Spectroscopy of Astrophysical Plasmas*, Cambridge University Press, Cambridge, (1987)
- [3] T. Hartquist, *Molecular Astrophysics*, Cambridge University Press, Cambridge, (1990)
- [4] C.R.Cowley, *Introduction to Cosmochemistry*, Cambridge University press, Cambridge (1995)
- [5] L. H. Aller, *The abundance of the Elements*, Interscience Publishers Inc., NY(1961)
- [6] L. Spitzer, *Physical Processes in the Interstellar Medium*, Wiley, NY (1978)
- [7] D.E.Osterbrock, *Astrophysics of Gaseous nebulae and Active Galactic Nuclei*, University Science Books, Mill Valey, CA,(1989)

-
- [8] E. Anders and N. Grevesse, *Abundances of Elements : Meteoritic and Solar*, *Geochim. Cosmochim. Acta.*, **53**, 197 (1989)
- [9] C. R. Cowley, *The Theory of Stellar Spectra*, Gordon and Breach Science publishers, NY (1970)
- [10] P. L. Smith and W. L. Wiese, *Atomic and Molecular Data for Space Astronomy*, *Lecture Notes in Physics* 407, Springer-Verlag (1992)
- [11] <http://fuse.pha.jhu.edu/papers/papers.html>
- [12] J. A. Cardelli, B.D. Savage, F.C. Bruhweiler, A. M. Smith, D. C. Ebbets, K. R. Sembach, and U. J. Sofia, *Astro. Phys. J.*, **377**, L57 (1991)
- [13] B. D. Savage, J. A. Cardelli, F.C. Bruhweiler, A. M. Smith, D. C. Ebbets and K. R. Sembach, *Astrophys. J.*, **377**, L53 (1991)
- [14] A. M. Smith, F.C. Bruhweiler, D. L. Lambert, B. D. Savage, J. A. Cardelli, D. C. Ebbets, C-H Lyu and Y. Sheffer, *Astro. Phys. J.*, **377**, L64 (1991)
- [15] A. Dalgarno, F. Masnou-Seeuws, and R. W. P. McWhirter, *Atomic and Molecular Processes in Astrophysics*, Swiss Society of Astronomy and Astrophysics, Fifth Advances Course, Saas-Fee (1975)
- [16] H.P. Kelly, *Phys. Rev.*, **131**, 684 (1963)
- [17] H.P. Kelly, *Phys. Rev. A*, **134**, 1450 (1964)
- [18] H.P. Kelly, *Phys. Rev. B*, **136**, 896 (1964)
- [19] K.F. Freed, in *Lecture Notes in Chemistry*, edited by U. Kaldor, **52**, 1, Springer, Berlin, (1989)
- [20] I. P. Grant, *Atomic, Molecular, and Optical Physics Handbook*, ed. G.W.F. Drake, pp 258 (1996)
- [21] I. P. Grant, B.J. McKenzie, P.H. Norrington, D.F. Mayers, and N. C. Pyper, *Comput. Phys. Commun.*, **21**, 207 (1980)

-
- [22] C. Froese Fischer, *The Hartree-Fock Method for Atoms*, John Wiley & Sons, NY (1976)
- [23] S. R. Langhoff and E. R. Davidson, *Int. J. Quant. Chem.*, **8**,61 (1974)
- [24] F. Coester, *Nucl. Phys.*, **1**, 421 (1958)
- [25] F. Coester and H Kümmel, *Nucl. Phys.*, **17**, 477 (1960)
- [26] J. Cizek, *J. Chem. Phys.*, **45**, 4256 (1966); *Adv. Chem. Phys.*, **14**, 35 (1969)
- [27] J. Cizek, J. Paldus and Sroubkova, *Int. J. Quantum Chem.*, **3**, 149 (1969)
- [28] J. Paldus, J. Cizek and I Shavitt, *Phys. Rev. A*, **5**, 50 (1972)
- [29] J. Paldus, and J. Cizek, in *Energy, Structure and Reactivity*, ed. D.W. Smith and W. B. McRae, Wiley, NY, p. 389 (1973)
- [30] R. J. Bartlett and G. D. Purvis, *Int. J. Quantum Chem.*, **14**, 561 (1978)
- [31] I. Lindgren, *Physica Scripta*, **36**,591 (1987)

Chapter 2

Non-relativistic Many-Body Calculations of Atomic Properties of Astrophysical Interest

2.1 Introduction

Two widely used perturbative methods to obtain accurate solutions of the time independent Schrödinger equation are Rayleigh-Schrödinger (RSPT) and Brillouin-Wigner (BWPT) perturbation theories. They have been applied quite successfully to the calculation of energy levels in many systems for which a reasonable zeroth order approximation is provided by a single reference function. Examples of such applications to ordinary (non-many-body) systems are well known and can be found in textbooks [1]. On the other hand, many-body systems, such as open shell ground and excited states of atoms, finite nuclei with particles beyond a doubly magic core, transition states on potential surfaces, and excited states of molecular systems, have degenerate or quasi-degenerate zeroth order states which must be described with multireference determinantal wave functions. Generalizations of perturbation theory to these cases are known as degenerate perturbation theory (DPT) and quasi-degenerate perturbation theory (QDPT). Some theories [2, 3, 4, 5, 6] are developed as perturbation expansions for the eigenfunctions and eigenvalues of the Hamiltonian

H , and others [7, 8, 9, 10] are formulated in terms of an effective Hamiltonian H_{eff} , where the total eigenspace of unperturbed Hamiltonian is divided into model space (P -space) and complementary space (Q -space). Here we discuss the H_{eff} method. The dimension d of the space P in which H_{eff} is defined is small, in general and the d eigenvalues of H_{eff} are identical to the d eigenvalues of H . Thus, the effective Hamiltonian calculations offer an interesting alternative to variational calculations because they avoid the problem of diagonalizing large matrices and d energies are obtained simultaneously from a single calculation. Since order by order expansions may not always converge well and sometimes may even diverge, effective Hamiltonian methods also been formulated using methods that are, in principle, exact; for example, iterative schemes [11, 12, 13].

Similar transformations may also be applied to an arbitrary time-independent operator \mathbf{A} , producing an effective operator \mathbf{A}_{eff} in the model space P . \mathbf{A}_{eff} gives exact expectation values and transition moments of \mathbf{A} between the eigenfunctions of H corresponding to those of H_{eff} . In the effective Hamiltonian formalism, the model space is chosen to include the required configurations and other configurations which are strongly interacting with them to obtain good convergence in *ab initio* calculations of atomic energy levels and molecular potential surfaces [14, 15, 16], for instance. Two general categories of partitioning are called Möller-Plesset (MP) and Epstein-Nesbet (EN) partitionings. The generalized MP partitioning utilizes a “sum over orbitals” treatment, whereas the generalized EN partitioning pursues a “sum over states” formulation in constructing the unperturbed Hamiltonian, H_0 . Different potentials may be utilized to construct H_0 , and a wide range of potentials have been chosen [17, 18] with varying degrees of success. Unfortunately, both MP and EN partitionings are unsuitable for multireference MBPT (MR-MBPT) computations, as they often generate divergent perturbative expansions for reasons explained by Chaudhuri and Freed [19].

To improve both the perturbative convergence and the serious intruder state problems in several MR-MBPT methods, Freed and co-workers [20, 21, 22] use multiple Fock operators to obtain the valence orbitals. All reference space orbitals and orbital energies are obtained from $V^{(N-1)}$ potentials, thereby providing a good first

order approximation to the low lying excited states and thus minimizing the work left for the perturbation expansion. When applied to larger reference spaces, the valence orbital energies are then forced to be degenerate. The form of the diagonal H_0 in the forced degeneracy the H^v method is given by

$$H_0 = \sum_c^{N_c} \epsilon_c a_c^\dagger a_c + \bar{\epsilon}_v \sum_v^{N_v} a_v^\dagger a_v + \sum_e^{N_e} \epsilon_e a_e^\dagger a_e \quad (2.1)$$

where c , v and e stand for core, valence and excited orbitals. The average valence orbital energy $\bar{\epsilon}_v$ is obtained from the original set of valence orbital energies by the democratic averaging,

$$\bar{\epsilon}_v = \frac{\sum_i^{N_v} \epsilon_v}{N_v} \quad (2.2)$$

with N_v the number of valence orbitals defining the complete reference space. The forced degeneracy condition introduces a diagonal perturbation $\delta V = \epsilon_v - \bar{\epsilon}_v$ that starts to contribute in third order. The magnitude of δV directly depends upon the spread of the original valence orbital energies ϵ_v before averaging. In fact, some third order computations with small, quasi-degenerate valence spaces do not require valence orbital energy averaging.

Effective Hamiltonians and effective operators are used to provide a theoretical justification and, when necessary, corrections to the semi-empirical Hamiltonians and operators of many fields. In such applications, H_0 may, but does not necessarily, correspond to a well defined model. When the effective Hamiltonian formulation is applied to many-body problems, the zeroth order Hamiltonian H_0 is usually represented as a sum of one-particle operators that are defined in terms of a set of one-particle functions. These functions are called spin-orbitals or simply orbitals in atomic and molecular physics. The orbitals are divided into core, valence or active, and excited orbitals. The model space configurations are characterized by having all core orbitals occupied and all excited orbitals empty. If these model space configurations include all possible ways of distributing the active electrons into the valence orbitals, the model space is called “complete”. Proofs have been given for the existence of a fully linked perturbation expansion for some types of effective Hamiltonian in a complete model space [9, 23, 24]. However, some model space configurations can cause a wide spread in the eigenvalues of H_0 , potentially leading

to serious convergence problems. In many cases the number of configurations in a complete model space can be prohibitively large. To alleviate these problems, Hose and Kaldor have suggested the use of an “incomplete” model space defined by retaining only the “important” configurations of the complete model space [25]. Much work has been done using incomplete model space, and there are now several different schemes for selecting the configurations. Many of these alternatives are computationally convenient [26]. In this part of the thesis work we employ the third order H^v method to calculate the various electronic properties of neutral carbon and calcium.

2.2 Theory

Perturbative methods proceed by first partitioning the exact Hamiltonian H into a zeroth order part H_0 and the perturbation V ,

$$H = H_0 + V, \quad (2.3)$$

where H_0 contains all one-electron Fock operators. The Schrödinger equation for the unperturbed Hamiltonian (H_0) is taken as providing a complete set of eigenfunctions $|\Phi_i\rangle$ with corresponding eigenvalues E_i^0 , i.e., the unperturbed eigenfunctions satisfy the zeroth order equation,

$$H_0|\Phi_i\rangle = E_i^0|\Phi_i\rangle. \quad (2.4)$$

The eigenfunctions of H_0 can be divided into two complementary subspaces, defined by two projectors P and Q , where the reference space projector is

$$P = \sum_{i=1}^d |\Phi_i\rangle\langle\Phi_i| = \sum_i P_i \quad (2.5)$$

and the projector for the orthogonal complement of P is

$$Q = 1 - P = \sum_{j=d+1}^{\infty} |\Phi_j\rangle\langle\Phi_j| = \sum_j Q_j \quad (2.6)$$

The subspace P of dimension d is variously called the *reference or model* space, while its orthogonal complement is formed from the remaining zeroth order eigenvectors and is called the *complementary or virtual* space.

The reference space functions $|\Psi_i^0\rangle$ are defined as the projections of the exact eigenfunctions $|\Psi_i\rangle$ on the reference space,

$$|\Psi_i^0\rangle = P|\Psi_i\rangle. \quad (2.7)$$

Alternatively, the exact eigenfunctions $|\Psi_i\rangle$ may be determined from the model space functions $|\Psi_i^0\rangle$ with the aid of the wave operator Ω_k ,

$$|\Psi_k\rangle = \Omega_k|\Psi_k^0\rangle \quad (2.8)$$

Using the definitions of P , Q and Ω , the exact Schrödinger equation can be expressed as

$$H_{eff}|\Psi_i^0\rangle = E_i|\Psi_i^0\rangle, \quad (2.9)$$

where the effective Hamiltonian H_{eff} is given by

$$H_{eff} = PH\Omega P. \quad (2.10)$$

An expression for Ω is obtained by projecting the Bloch equation ($H\Omega = \Omega PH_{eff}P$) on the virtual space (Q) from left

$$Q[\Omega, H_0]P = Q[V\Omega - \Omega V]P. \quad (2.11)$$

An order by order expression for Ω (and hence H_{eff}) can be derived by expanding Ω as

$$\Omega = 1 + \Omega^{(1)} + \Omega^{(2)} + \dots \quad (2.12)$$

and then substituting Ω into Eq. (2.11), yielding

$$[\Omega^{(n)}, H_0]P = (V\Omega^{(n-1)} - \sum_{m=1}^{n-1} \Omega^{(m)}V\Omega^{(n-m-1)})P, \quad (2.13)$$

where $\Omega^{(n)}$ is the n th order contribution to the wave operator. The matrix element of the $(n+1)$ st order contribution to the effective Hamiltonian H_{eff} is then obtained by inserting $\Omega^{(n)}$ into Eq. (2.13) to produce

$$\langle \Phi_i^0 | H_{eff}^{(n+1)} | \Phi_j^0 \rangle = \langle \Phi_i^0 | PV\Omega^{(n)}P | \Phi_j^0 \rangle. \quad (2.14)$$

The wave operator Ω in the equations above depends upon the model function on which it operates, i.e., Ω is a state or ket dependent wave operator. Further, the

above derivation of H_{eff} assumes that Ω satisfies intermediate normalization (i.e., $P\Omega P = P$), which, in fact, is not mandatory [27, 28].

The H^v method gives the unique lowest-order approximation of H_{eff} ,

$$H^v = PHP + \frac{1}{2} \sum_{\phi, \phi'} [P(\phi)VQ(E_\phi - H_0)^{-1}QVP(\phi') + h.c.] \quad (2.15)$$

where $P(\phi)$ is the projector onto the valence space basis function ϕ and $h.c.$ denotes the Hermitian conjugate of the preceding term. The computations of excitation energies proceed to the next order (third) in V .

The matrix elements of an operator D are transformed by the H^v theory into

$$\langle \Psi_i | D | \Psi_j \rangle \rightarrow \langle \Psi_i^v | D^v | \Psi_j^v \rangle \quad (2.16)$$

where D^v is effective valence shell operator which is computed from D by

$$D^v = PDP + \frac{1}{2} \sum_{\phi, \phi'} [P(\phi)VQ(E_\phi - H_0)^{-1}QDP(\phi') + h.c.] \quad (2.17)$$

Many body theory techniques can be applied to reduce the above expressions (2.16) and (2.17) to represent the matrix elements of D^v in the valence orbital basis. The resulting equations may be written alternatively in terms of core-, one-, two-, \dots electron valence shell operators D_c^v , D_i^v , D_{ij}^v , \dots , respectively, in the operator representation,

$$D^v = D_c^v + \sum_i D_i^v + \frac{1}{2} \sum_{i,j} D_{ij}^v + \dots, \quad (2.18)$$

where D is a dipole operator, D^v is an effective dipole operator that acts only on the P -space. It should be noted that although dipole operator is a one-electron operator, two-electron effective terms D_{ij}^v appear in the nontrivial lowest order perturbation expansion of Eq. (2.17). This non-classical two electron term is necessary to obtain accurate dipole transition moments. Fig. 2.1 shows typical one- and two-body diagrams that are zeroth and first order in V .

In the actual computation, the effective Hamiltonian H^v is first diagonalized to obtain the desired eigenvalues and eigenfunctions. The latter are then used to compute expectation values and transition moments of some operator D . In the length gauge, the absorption oscillator strength (f) is defined as:

$$f_{i \rightarrow f} = \frac{2\Delta E}{3} |\langle \Psi_f | \sum_k \mathbf{r}_k | \Psi_i \rangle|^2 \quad (2.19)$$

where $\Delta E = E_f - E_i$ is the transition energy, $\langle \Psi_f | \mathbf{r} | \Psi_i \rangle$ is the transition moment.

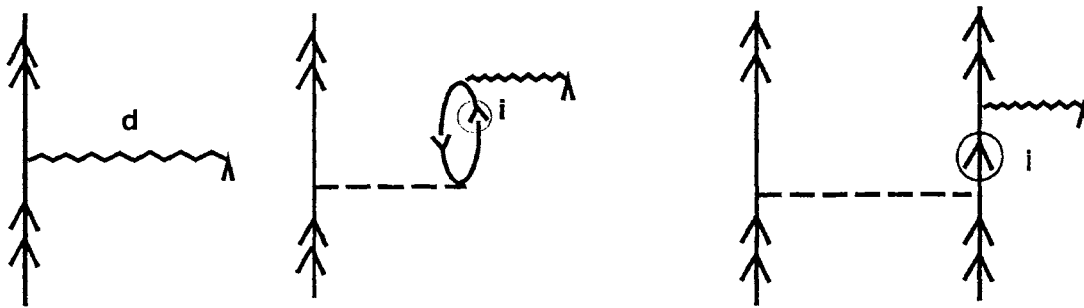


Figure 2.1: Typical one and two body H^v dipole diagrams. Here, the line going up (down) refers to virtual (core) orbital. The valence orbitals are represented by a line with a double arrow and a line with an arrow inside a circle, can be a valence or virtual orbital.

2.3 Properties of neutral carbon

Atomic data of neutral carbon are one of the most important set of parameters in the area of observational astronomy because of the ample abundances of carbon throughout the universe. Moreover, the determination of the relative population of carbon atoms provides one of the best tools for studying solar phenomena, stellar atmospheres and interstellar media. The inability of experimentalists to produce some of the requisite high resolution data has inspired theoretical computations to fill the void. Over the past few years, considerable effort has been devoted to reduce the discrepancies between the experimental and the theoretically predicted transition energies and oscillator strengths. Notably, Nussbaumer *et al* [29] were quite successful in reducing the error of the predicted transition energies from few thousand cm^{-1} to a few hundred cm^{-1} . However, their estimated oscillator strengths for the most important $2p \rightarrow 3s$ and $2p \rightarrow 4s$ transitions are unacceptably low compare to the empirical values [30].

The difficulty in accurately estimating transition energies and oscillator strengths of the atom arises mainly due to the following reasons: (a) the precise computation of transition energies and oscillator strengths requires a balanced description of the ground and excited states, (b) the use of inadequate basis leads to difficulties in describing the excited states and an unbalanced treatment of dynamical correlation

and polarization effects. The problems due to basis set inadequacy can be removed partially by increasing the basis for small and moderate sized atomic and molecular systems. Here, size-consistency [48] of the theory plays an important role in handling the proper treatment of electron correlation and by that way it treats properly the differential correlation energies of the interacting (initial and final states) zeroth order states. It ensures that the state energies scale linearly with the number of electrons in a rigorous way.

Many correlated many-body methods, including coupled cluster theory [31], generally treat the excited state of neutral carbon as a double electron attachment to the closed shell doubly ionized atom ($M^{+2} + 2e \rightarrow M$). Such approaches use overly contracted atomic orbitals from positive ions for computing the transition moment of the neutral system. These orbitals yield an incorrect description of the excited state of neutral carbon atom.

We have improved the reliability of the theoretically predicted neutral carbon excitation energies and oscillator strengths (for non-relativistically allowed transition) for a wide range of configurations. The computations are performed employing the effective valence shell Hamiltonian (H^v) method, proposed by Freed and collaborators [32]. The H^v method has been found to be quite successful in accurately assigning the electronic spectrum of atomic and complex molecular systems, such as conjugated polyenes and inorganic molecules [33, 34, 35, 36]. By virtue of being a multireference configuration approach, the H^v method incorporates the non-dynamical correlation (correlation internal to the valence orbitals) necessary to describe open-shells and, hence, the method possesses distinct advantages over the traditional single reference many-body perturbation theory. The present computations for neutral carbon reinforce our prior assertions that the H^v method provides a useful alternative scheme for the calculations of atomic properties.

2.3.1 Basis set and reference space

The appropriate selection of the basis set, orbitals and the model space are difficult but most essential task in all *ab initio* many body methods, because the perturbative convergence of a finite order calculation strongly depends upon these factors. A

prior knowledge of the system of interest may reduce the computational effort to find an optimal basis set and reference space, otherwise some trial and error is required to achieve this goal. The present computations use a rather large basis for carbon atom constructed from the $(12s6p3d2f)/[5s4p3d2f]$ PVQZ correlation consistent set of Dunning [37], augmented by one polarized d -function ($\zeta_d = 0.75$) and two s - ($\zeta_s = 0.0230$ and 0.0055), two p - ($\zeta_p = 0.0210$ and 0.0049) and two d diffuse functions ($\zeta_d = 0.0150$ and 0.0032), yielding a 81-contracted Gaussian type orbitals (CGTO). Although Slater type orbitals (STO) are more appropriate for atomic calculations, the CGTOs are more convenient and compensated for the inadequacy by the addition of more basis functions. Here we have used D_{2h} symmetry.

The reference space of multireference many-body perturbation theory (MR-MBPT), is constructed as follows: First, the orbital space is divided into “core” (doubly occupied in all reference space configurations), “valence” (partially occupied in the reference space configurations) and “virtual” orbitals (unoccupied in all reference space configurations). The electrons present in the valence orbitals are distributed over the valence orbitals in all possible ways to generate complete reference space and thereby to ensure the size-extensivity of the computations. An obvious choice of the occupied valence orbitals for atomic carbon is the $2s$ and $2p$ orbitals since these are the outermost orbitals that have same principal quantum number. However, in the perturbative computation of some high lying Rydberg states of interest, the inclusion of $2s$ orbital in the valence space introduces numerical instabilities of the perturbative expansion because of the wide zeroth order energy gap between the $2s$ and $2p$ orbitals and the forced degeneracy imposed in H_0 upon the reference space. The forced degeneracy for a $\{2s, 2p\}$ valence space would produce a large diagonal perturbation in V that disrupts the convergence of the perturbative expansion. To avoid this numerical instability, we consider $2p$ as the only valence orbital that is occupied (partially) in the single determinantal approximation in the ground state. This choice of reference space precludes transitions involving excitations from $2s$ orbitals, but our focus here is upon generating accurate estimation of oscillator strengths for $2p \rightarrow kv$ transitions where k designates orbitals with principal quantum number 3 or 4 and v indicates symmetries. The excited kv orbitals are unoccupied

in the ground state configuration and retermed as *unoccupied valence orbitals*. The inclusion of both $2s$ and kv Rydberg orbitals in the reference space would lead to numerical instability due to the presence of intruder states.

The selection of the unoccupied valence orbitals is based on the excited state(s) of interest. For example, the $3s$, $3p$, $4s$ and $4p$ unoccupied valence orbitals are included in the reference space designed for computing the $2p^2$, $2p3s$, $2p3p$, $2p4s$ and $2p4p$ excitation energies. (Although the $3d$ orbital is nearly degenerate with $3p$ and $4s$ orbitals, and it contributes to the ground state, but the contribution of the $3d$ orbital is insignificant for the $2p3p$ and $2p4p$ excited states). On the other hand, the computation of the $2p3d$ excited states requires the inclusion of the $3d$ orbital in the valence space. However, in this case, $4p$ orbital is not retained in the valence space (i) to reduce the size of the reference space and (ii) to minimize the computation labor. The omission of the $4p$ orbital from the latter reference space is permissible because the contribution of the $4p$ orbital to the $2p3d$ excited state is negligible.

2.3.2 Results

Table 2.1 compares selected excitation energies, computed by the H^v method with experiment [38] and with other correlated *ab initio* calculations [29, 31]. It includes a series of $1s^22s^22p4p$ Rydberg states that have not been treated previously by accurate *ab initio* methods. This table clearly demonstrates that both superstructure (SS) and coupled cluster based on similarity transformed equation of motion (STEOM-CC) method overestimate the excited state energies to a greater extent than the close coupling and the H^v method. Both the STEOM-CC and SS calculations exhibit deviations from experiment that steadily increases with the energies of the excited states. However, the relative performance of STEOM-CC approach far surpasses that of the SS method, even though both treatments use C^{+2} orbitals instead of neutral orbitals which are more appropriate for these calculation. [The C^{+2} orbitals are used in the STEOM-CC and SS approach for convenience.] The STEOM-CC scheme begins with the closed coupling calculation for the closed shell Be-like configuration ($1s^22s^2$) of C^{+2} and then two electrons are added to com-

pute the excitation energies of neutral carbon [the STEOM-CC calculations employ contracted Gaussian type orbitals (CGTO) [39]]. Hence, it is not surprising that STEOM-CC provides a poorer estimate of the excited state energies as compared to the H^v calculations which uses neutral carbon orbitals for treating all the excited states. The overall accuracy of the closed coupling and H^v excitation energies are roughly similar, although majority of the low lying and some of the high lying states are better estimated by the H^v method, wherever comparisons are available (like $2p4p$ states are not calculated by Nussbaumer *et al* [29]).

Table 2.2 displays the oscillator strengths for $2p \rightarrow 3s$ and $2p \rightarrow 4s$ transitions as obtained from the experiment, observed as well as from the H^v , closed coupling and SS calculations [29]. Also we present the same transitions reported by Luo and Pradhan [40] in the framework of the opacity project [41] using closed coupling method and the SS method [42] based on CI *ab initio* calculation for comparison. We find that both the closed coupling and the SS schemes underestimate the observed oscillator strengths. The SS method offers better estimate to the observed value of the oscillator strengths for the $2p \rightarrow 3s$ transition than the other approaches, but for $2p \rightarrow 4s$ transition is underestimated. [Note that, oscillator strength is a product of transition energy and the square of the transition moment (see Eq. 2.19). Since, the transition energy of $2p \rightarrow 3s$, produced from the closed coupling method, is close to the experiment, its small computed oscillator strength compared to the observed value probably indicates an underestimate in the $2p \rightarrow 3s$ transition moment.]. The H^v computation provides closer to observed oscillator strengths for both the $2p \rightarrow 3s$ and $2p \rightarrow 4s$ transitions probably indicating that the $2p \rightarrow 3s$ and $2p \rightarrow 4s$ H^v transition moments may be more accurate than those from the CC, SS and other techniques.

Table 2.3 displays our computed oscillator strengths for the transitions from ground (3P) state and excited states to excited states transitions and compares with the calculations of Nussbaumer *et al* [29] and with experiment. We have found that our H^v f-values for the transitions $2p3s \rightarrow 2p4p$ are in excellent agreement with the experimental values, and also we do not find the constant difference in f-values between the theoretical values and experimental measurements as mentioned by

Table 2.1: Excitation energies (in Rydberg) of C I.

Terms	State	Labs. ^a	Closed	SS	STEOM-CC	H^v
Coupling						
$2s^22p^2$	3P	0.0000	0.0000	0.0000	0.0000	0.0000
	1D	0.0926	0.0953	0.1057	0.0992	0.0930
	1S	0.1970	0.2101	0.2479	0.2036	0.2034
$2s^22p3s$	3P	0.5499	0.5457	0.5896	0.5498	0.5545
	1P	0.5646	0.5613	0.6075	0.5659	0.5644
$2s^22p3p$	1P	0.6272	0.6256	0.6659	0.6174	0.6271
	3D	0.6351	0.6335	0.6733	0.6365	0.6346
	3S	0.6444	0.6427	0.6830	0.6512	0.6450
	3P	0.6501	0.6489	0.6899	0.6527	0.6504
	1D	0.6614	0.6603	0.7024	0.6784	0.6636
	1S	0.6739	0.6727	0.7155	0.7019	0.6662
	3P	0.7117	0.7081	0.7495		0.7094
$2s^22p4s$	1P	0.7136	0.7097	0.7522		0.7120
	1D	0.7076	0.7052	0.7454		0.7126
$2s^22p3d$	3D	0.7133	0.7108	0.7513		0.7132
	1F	0.7153	0.7127	0.7541		0.7149
	1P	0.7172	0.7143	0.7563		0.7154
	3P	0.7225	0.7214	0.7609		0.7156
	1P	0.7338				0.7319
$2s^22p4p$	3D	0.7361				0.7340
	3S	0.7391				0.7366
	3P	0.7411				0.7402
	1D	0.7451				0.7448
	1S	0.7495				0.7467

a : [38], b : [29], c : [31]

Table 2.2: Oscillator strengths of C I for the ground $2p^2(^3P) \rightarrow$ excited $2p3s(^3P)$ and $2p4s(^3P)$ transitions.

Terms	Lab.	Observed ^c	Nussbaumer <i>et al</i> ^d		LP ^e	Hibbert ^f	H^v
			CC	SS			
$2p^2(^3P) \rightarrow 2p3s(^3P)$	0.14 ^a	0.191	0.139	0.162	0.147	0.118	0.165
$2p^2(^3P) \rightarrow 2p4s(^3P)$	0.049 ^b	0.035	0.022	0.019	0.022	0.022	0.023

a : [43], b : [44], c : [30],

d : [29], e : [40] f : [42]

Table 2.3: Oscillator strengths of $C I$ for the ground \rightarrow excited states and excited states \rightarrow excited states transitions.

Initial state	State Multi.	Final state	State Multi.	$\lambda(\text{\AA})$	Labs.	CC	SS	H^v
$2s^22p^2$								
	3P	$2s^22p3s$	3P	1657.2	0.14	0.139	0.162	0.165
	1D	$2s^22p3s$	1P	1930.1	0.123	0.114	0.111	0.145
	1S	$2s^22p3s$	1P	2478.6	0.050	0.086	0.085	0.072
	3P	$2s^22p4s$	3P	1280.4	0.049	0.022	0.019	0.023
	1D	$2s^22p4s$	1P	1467.4		0.014	0.010	0.023
	1S	$2s^22p4s$	1P	1763.9		0.003	0.010	0.008
$2s^22p3s$								
	1P	$2s^22p3p$	1P	14542.5		0.267	0.278	0.402
	3P	$2s^22p3p$	3D	10693.4	0.677	0.507	0.526	0.535
	3P	$2s^22p3p$	3S	9639.7	0.141	0.107	0.111	0.336
	3P	$2s^22p3p$	3P	9086.8	0.712	0.356	0.374	0.460
	1P	$2s^22p3p$	1D	9405.7	0.391	0.624	0.657	0.527
	1P	$2s^22p3p$	1S	8335.1	0.103	0.117	0.122	0.475
$2s^22p3p$								
	1P	$2s^22p4s$	1P	10541.2	0.135	0.051	0.011	0.126
	3D	$2s^22p4s$	3P	11886.1		0.161	0.159	0.205
	1D	$2s^22p4s$	1P	17448.6		0.250	0.226	0.325
	1S	$2s^22p4s$	1P	22906.6		0.515	0.690	0.400
$2s^22p3s$								
	3P	$2s^22p4p$	3P	4771.0	0.013			0.013
	3P	$2s^22p4p$	3D	4892.4				0.005
	3P	$2s^22p4p$	3S	4832.5				0.007
	1P	$2s^22p4p$	1S	4933.7	0.004			0.070
	1P	$2s^22p4p$	1D	5053.6	0.008			0.018
	1P	$2s^22p4p$	1P	5381.9	0.006			0.002

a : References are in Nussbaumer & Storey(1984) for excitation from ground states and in Lambert(1968) for excitation from excited states b : Nussbaumer & Storey(1984)

(Continued from the previous page)

Initial state	State Multi.	Final state	State Multi.	$\lambda(\text{\AA})$	Labs.	CC	SS	H^v
<i>2s²2p4s</i>								
	³ P	2s ² 2p4p	³ P	31250.5				0.501
	³ P	2s ² 2p4p	³ D	37316.4				0.592
	³ P	2s ² 2p4p	³ S	33650.9				0.934
	¹ P	2s ² 2p4p	¹ S	25568.6				0.956
	¹ P	2s ² 2p4p	¹ D	29151.3				0.679
	¹ P	2s ² 2p4p	¹ P	44978.6				0.481
<i>2s²2p²</i>								
	³ P	2s ² 2p3d	³ D	1277.5	0.090	0.094	0.094	0.040
	¹ D	2s ² 2p3d	¹ D	1481.8		0.013	0.012	0.011
	¹ D	2s ² 2p3d	¹ P	1459.0		0.006	0.010	0.006
	¹ S	2s ² 2p3d	¹ P	1751.8	0.078	0.132	0.132	0.030
<i>2s²2p3p</i>								
	¹ P	2s ² 2p3d	¹ D	11330.3		0.671	0.678	0.957
	¹ P	2s ² 2p3d	¹ P	10123.9		0.300	0.331	0.339
	³ D	2s ² 2p3d	³ D	11641.3		0.143	0.141	0.191
	³ D	2s ² 2p3d	³ P	10421.6		0.0003	0.00003	0.043
	³ S	2s ² 2p3d	³ P	11664.2		0.463	0.564	0.571
	³ P	2s ² 2p3d	³ D	14416.0		0.687	0.694	0.706
	³ P	2s ² 2p3d	³ P	12591.1		0.265	0.304	0.319
	¹ D	2s ² 2p3d	¹ D	19722.0		0.114	0.112	0.174
	¹ D	2s ² 2p3d	¹ P	16333.9		0.001	0.013	0.002
	¹ S	2s ² 2p3d	¹ P	21023.2		0.591	0.380	0.386

a : References are in Nussbaumer & Storey(1984) for excitation from ground states and in Lambert(1968) for excitation from excited states *b* : Nussbaumer & Storey(1984)

Lambert [45] earlier.

Although experimental data are not available for most of the transitions from ground to excited states and for the excited to excited states. We strongly hope our predicted values will aid in observing those transitions.

2.4 Properties of Neutral Calcium

Atomic transition lines of neutral calcium were first found in solar spectrum as early as the middle of the nineteenth century, when the 4227Å line was identified along with the famous singly ionized H and K lines [46]. Neutral calcium lines have also been observed in all types of stellar and interstellar spectra, even like late-type of dwarf stars. The crude abundance of Ca I ($\lambda 6717.7\text{\AA}$) has been observed in Am Binaries [47]. To confirm those identifications and to find new lines one has to depend on atomic experimental data or computational data based on theoretical models of the calcium atom. The abundances of neutral calcium in these astronomical bodies depend on the oscillator strengths of those lines, which come from the excitation energies of various levels and transition moments among those levels.

The accuracy of the computed excitation energy depends mostly upon the quality of the unoccupied valence orbitals to which excitation occurs. The traditional choice of some unoccupied valence orbitals from a ground state self-consistent field (SCF) computation introduces V^N orbitals that are best suited for describing negative ions and not the low-lying excited states. Thus, the valence orbitals those are not occupied in the ground state SCF should be taken as more representative orbitals suitable for the excited states. One possible choice emerges from restricted single excitation configuration interaction (CIS) procedure [49], where excitations are only permitted from the highest occupied orbitals. A simpler and often equivalent approach involves using improved virtual orbitals (IVOs) [32] in the H^v valence space or reference space. Here, the IVOs are generated by single orbital SCF optimization in which the Fock operator is defined by promoting an electron from the highest occupied orbital to the orbital being optimized, while all the previously determined orbitals are kept frozen. Alternatively this can be accomplished by a unitary transformation [50]. The IVO orbital energies obtained through this way are lower than

those evaluated from the traditional SCF procedure due to the absence of an extra coulomb operator in the former one. For example, H^v calculation for neutral calcium atom, the two-orbital ($4s, 4p$) minimal reference space is produced by the sequence

$$\begin{aligned} (1) & 1s^2 2s^2 2p^6 3s^2 3p^6 4s^2 && 1^1S_0 \\ (2) & [1s^2 2s^2 2p^6 3s^2 3p^6 4s^1] 4p^1 && 1^3P_1 \end{aligned}$$

The first step is a SCF calculation for the ground state and step two requires only a single orbital optimization in which the orbitals shown in square brackets are frozen as those determined in the previous steps i.e. in step (1). The excited orbitals are then obtained by diagonalizing the 1^1S_0 state Fock operator in the orbital space complementary to the union of the core and reference spaces.

Successful H^v computations for Mg-like ions [51] and neutral carbon have stimulated us to try this scheme for neutral calcium atom (Ca I) and, in this section, we present the theoretically computed excitation energies, binding energies (energy relative to first ionization threshold) and oscillator strengths and transition probabilities of Ca I for a wide range of configurations (non-relativistically allowed transitions). Section 2.4.1 briefly describe the computational details. The computed results and discussions are presented in Section. 2.4.2.

2.4.1 Computational Details

The method of the selection of basis set and the valence space is same as discussed in Section 2.3.1 for neutral carbon. We employ a variety of basis sets and reference spaces to study their effect on the computed excitation energies through the third order H^v method.

We emphasize that there exist a significant difference in the choice of both orbitals and orbital energies between the H^v method and the traditional MR-MBPT scheme [1, 9, 18, 32, 53, 54, 55, 56]. In MR-MBPT method all orbitals and orbital energies are obtained from a single V^N Fock operator (the ground state Fock operator), and, therefore all orbitals (core, valence and excited) and their energies are evaluated from a V^N potential. The unoccupied reference orbitals are, therefore, more appropriate for describing negative ion states than for low lying excited states of interest. On

the other hand, the H^v method determines the unoccupied reference space orbitals and their energies as improved virtual orbitals (IVOs) from a V^{N-1} potential. The unoccupied reference space orbital energies are much lower than those evaluated from V^N potential due to the absence of an extra coulomb operator in the former. After the H^v valence orbital energies are computed in this above mentioned fashion, the reference space orbitals are replaced by their democratic average to eliminate (or reduce) the convergence difficulties. The valence orbital energy averaging process introduces an additional diagonal perturbation [32] which appears in the perturbation expansion from third order onwards discussed in section 2.1.

Fig. 2.2 plots the variation of the correlation energy ($E^{third} - E_{HF}$) as a function of basis set obtained from 14V reference space computation (described later), where we find that the correlation energy decreases substantially as the number of basis function increases from 49 to 73. The variation in correlation energy then slows down with further increase in the basis set. Here, we employ a moderate size Calcium basis (to reduce the computational effort without sacrificing the accuracy) which is constructed from the (12s9p5d/5s4p1d) contracted Gaussian basis of Dobbs and Hehre [57], augmented by one polarized d -function ($\zeta_d = 0.100$) and two s ($\zeta_s = 0.011, 0.0056$), one d ($\zeta_d = 0.0416$) and three f ($\zeta_f = 3.0, 1.5$ and 0.75) diffused functions and this yields a 73 contracted Gaussian type orbitals (CGTO). [Some third order H^v calculations have also been performed with 87 CGTO (generated by adding few s, p and d functions to 73 basis set). Here we have used D_{2h} symmetry. Since the perturbative convergence of the computed excitation energies and oscillator strengths for this set are close to the smaller one (73 CGTO), we only report the smaller basis set (73 CGTO) H^v results.]

The valence orbitals are selected on the basis of their orbital energies (to avoid the near degeneracies among the reference and virtual space states) and on their relative importance in properly describing the excited states of interest, i.e, in providing an accurate first order description to minimize the perturbative corrections. This selection is almost mandatory in all MR-MBPT method to mitigate the so called *intruder-state* problem [58] that arises due to the near degeneracy of the reference and virtual space states and their relative ordering [59]. The reference space must

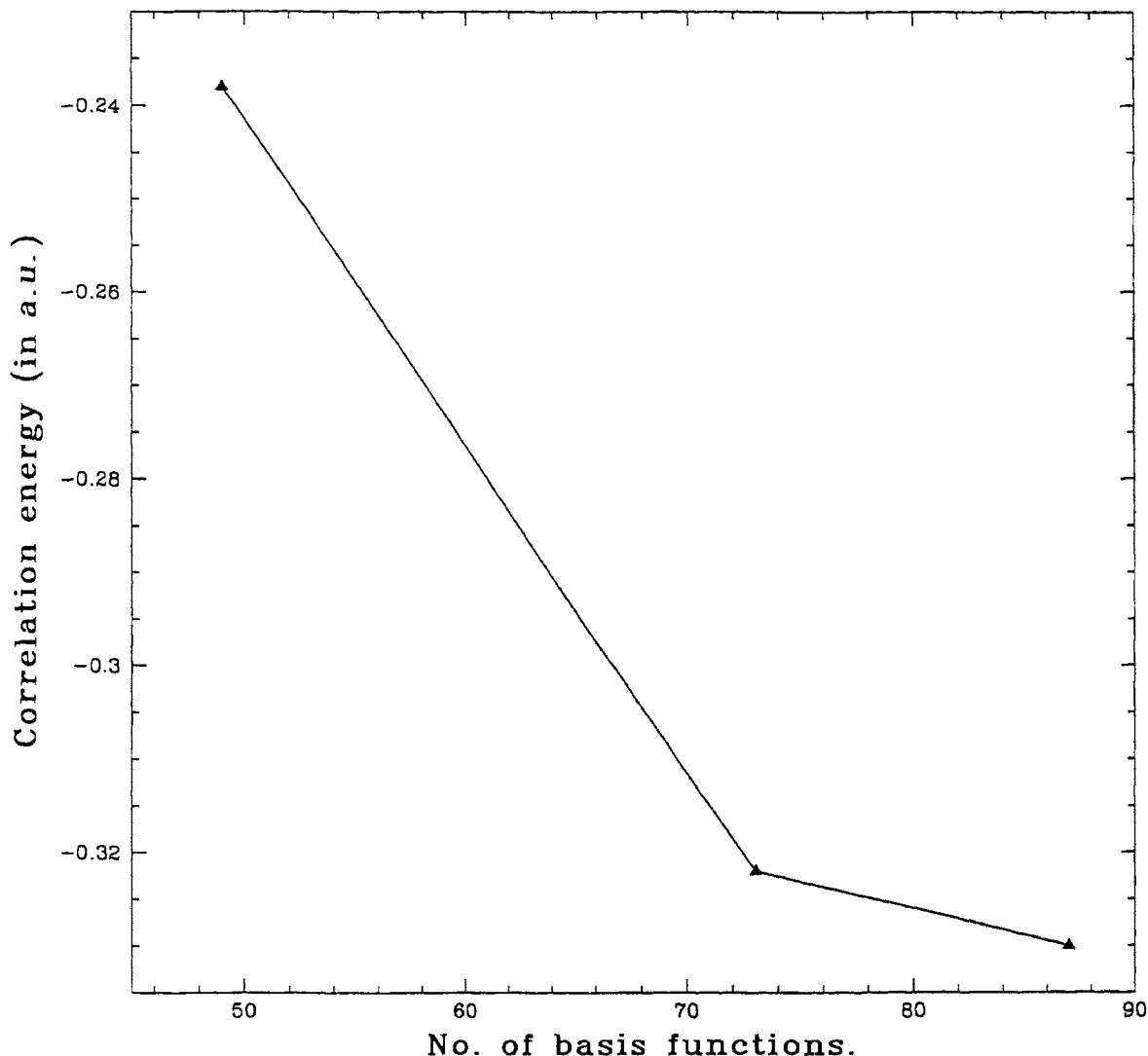


Figure 2.2: Variation of third order H^v (with $14V$ reference space) correlation energy as a function of basis set.

include the $4s$ (the outermost occupied orbital) and the $4p$ (lowest lying unoccupied orbital) for describing the lowest lying states of S and P multiplets which arises from $4s \rightarrow 4p$ transition. [Note that the ground state (1S_0) of neutral Calcium atom is mostly dominated by $[\text{Ar}]4s^2$ (91%) and $[\text{Ar}]4p^2$ configuration state functions (CSFs) [60].] Therefore, the minimal reference space contains only the $4s$ and $4p$ orbitals with two active electrons in the active space. Since, a minimal reference space $\{4s, 4p\}$ provides an inadequate description of excited states (CSFs $[\text{Ar}]4s4p$ (80%) and $[\text{Ar}]4p3d$ (16%) contribute 96% to the first excited singlet state of P symmetry [60]) and, moreover, since our states of interest are not only the lowest lying but the higher lying too, we extend the valence space carefully to avoid the near-degeneracy

of the reference and virtual space states as much as possible in order to reduce the perturbative convergence problem. Thus, our first extended valence space is made of 4s, 4p, 5s and 5p orbitals (called 8V, according to D_{2h} symmetry p orbitals has symmetry with respect to three axis, i.e., p_x , p_y and p_z). Although the computed transition energies obtained from 8V reference space matches favorably well with the experiment and other correlated calculations for the low lying excited states of S and P multiplets, it fails to provide an acceptable transition energies for D multiplets as well as the high lying excited states of S and P multiplets, e.g., $3^1S_0, 4^1S_0, 2^1P$ etc. The origin of this discrepancy can be traced back from the earlier work of Vaeck *et al* [60] who showed that the 3^1S_0 excited states of neutral Calcium is mainly described by the CSF [Ar]4s6s (94%) whereas for 4^1S_0 excited state the major contribution comes from the CSFs [Ar]4s7s (10%), [Ar]4p² (45%) and [Ar]3d² (38%), respectively. Since, the orbitals 3d, 6s and 7s are not included in 8V H^v reference space, it is expected that these excited states will be poorly described in H^v method and so their transition energies. Similar arguments also apply to the transition energies of D and F multiplets. Therefore, in order to improve the accuracy of the above mentioned problematic excited states it is necessary to include the 3d, 6s and 7s orbitals. Unfortunately, little leeway exists in extending the valence space by including the 7s orbital alone because these orbitals are near degenerate to 4d, 4f, 6p and 7p orbitals, respectively. Inclusion of 4d, 4f, 6s, 6p, 7s and 7p orbitals in the reference space will, of course, improve the first order description of the excited states, but it will severely affect the perturbative convergence due to the presence of *intruder states* and large diagonal perturbation that appears from third order onwards due to the valence orbital degeneracy condition. [Note that, as the number of valence space orbitals increases, the quasi-degeneracy among the valence orbitals decreases sharply with a consequent increase in the diagonal perturbation.] Moreover, the presence of large number of valence orbitals in the reference space will reduce the computational efficiency of the post Hartree-Fock calculation. Therefore, an optimal set of valence orbital space is required which will neither reduces the computational efficiency of the post- Hartree Fock calculation nor introduces serious convergence problem *at least* at low order. Based on the earlier work of Vaeck *et al* on neutral Calcium atom,

we construct the complete active H^v reference space (to ensure the size-extensivity) by allocating the two-active electrons of $4s$ orbitals among $4s, 4p, 3d, 5s, 5p$ and $6s$ ($14V$) in all possible way. Some typical results obtained from a series of third order H^v calculations with varying reference are depicted in Figs. 2.3 and 2.4 which display the variation of third order H^v excitation energies and oscillator strengths as a function of the valence space, respectively. Figs. 2.3 and 2.4 indicates that the accuracy of the computed transition energies and oscillator strengths sharply increases with the increasing size of the valence space.

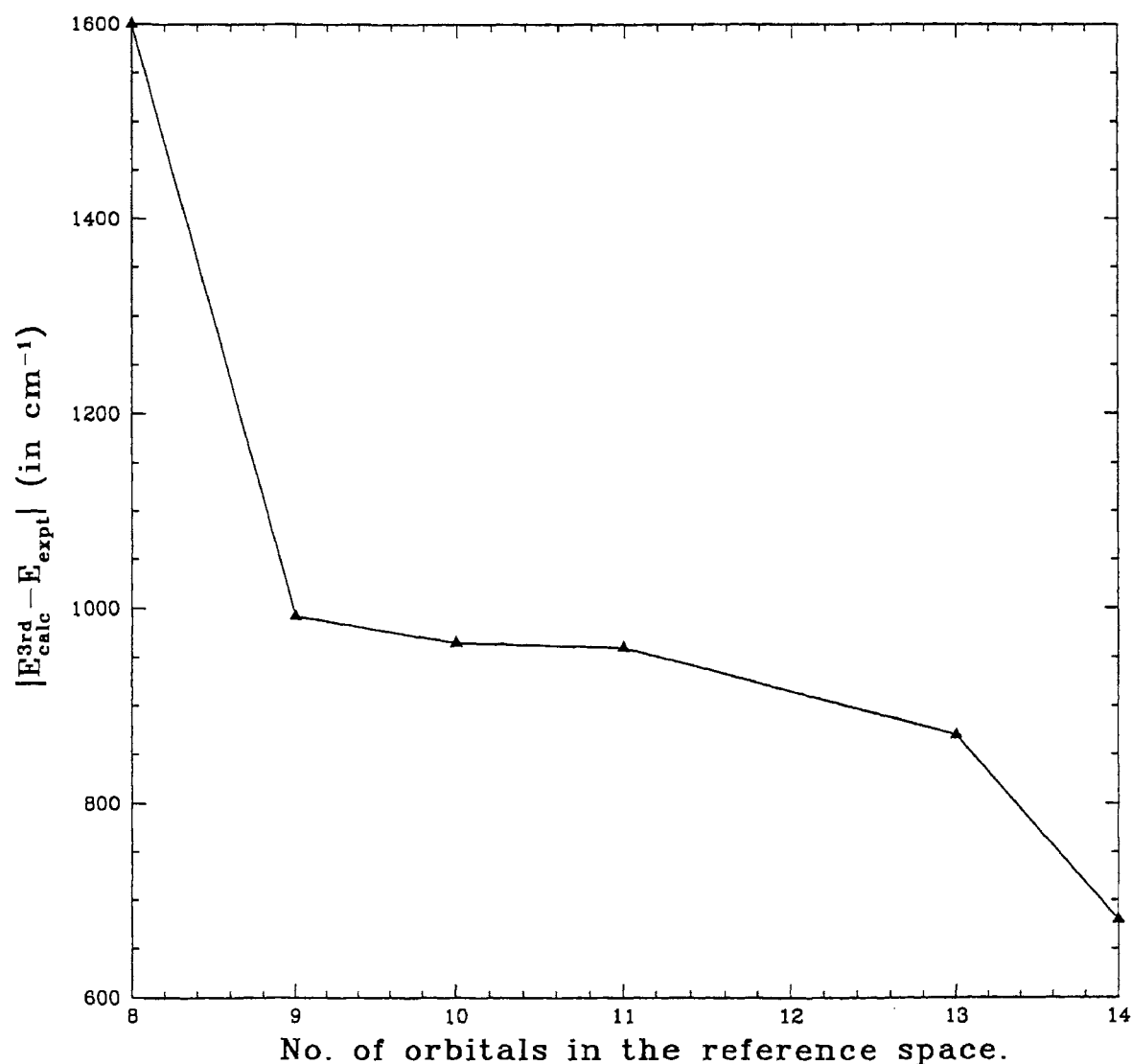


Figure 2.3: Variation of third order H^v (with $14V$ reference space) $4s^2 \rightarrow 4s5s(^1S)$ transition energy as a function of number of valence orbitals in the reference space.

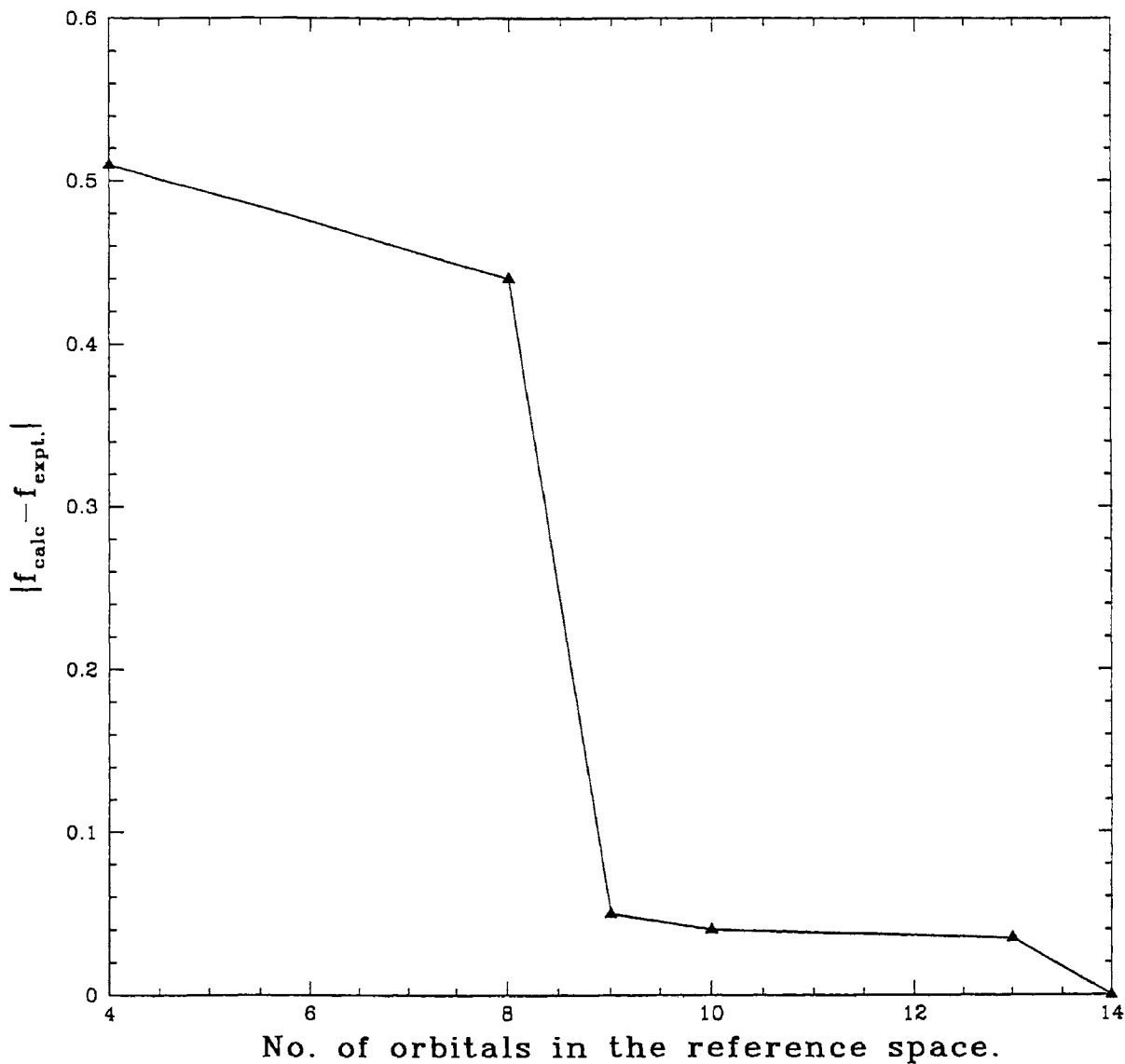


Figure 2.4: Variation of third order H^{ν} (with $14V$ reference space) $4s^2 \rightarrow 4s4p(^1P)$ oscillator as a function of number of valence orbitals in the reference space.

2.4.2 Results and Discussions :

The third order H^{ν} binding energies (energy relative to the first ionization potential) are compared with the experimental data and with other theoretical values which were obtained by using multiconfiguration Hartree-Fock (MCHF) [60], CI [61], Spline-Galerkin (SG) [62] and model-potential (MP) methods [63] in Table 2.4. This table clearly demonstrates that the accuracies of our calculations of the third order H^{ν} binding energies for singlets (average deviation $\approx 855 \text{ cm}^{-1}$) are better than those of the MCHF (average deviation $\approx 1027 \text{ cm}^{-1}$) and CI calculations

(average deviation $\approx 1103 \text{ cm}^{-1}$) though the number of configurations used in the latter calculations are much larger than ours. This demonstrates the power of the MR-MBPT approach in general and the H^v method in particular. This approach is computationally more efficient than the MCHF and CI methods, since it includes strongly interacting configurations in the model space and relating weakly interacting configurations which lie in the complementary space are treated perturbatively. The SG and MP calculations for the binding energies are in general in better agreement with experimental than ours. Table 2.4 clearly indicates that our results are consistently better than those obtained by the CI method. For example, for the triplet states the average deviation for our calculations is 1061 cm^{-1} while for the CI calculations it is 2026 cm^{-1} . This suggests that the H^v method treats the differential correlation more accurately than the MCHF and CI methods. Despite the fact that the H^v method provides accurate estimate of the binding energies for most of the excited states, it fails to produce accurate binding energy for the 4^1S excited states (deviates by 2711.5 cm^{-1} from experiment). The underlying reason for this large deviation in the estimated binding energy of the 4^1S excited state becomes transparent when we analyze the composition of the 4^1S excited state in terms of CSFs. The MCHF calculation of Vaeck *et al* and other calculations show that this particular singlet excited state is multiconfiguration in nature, where the major contribution comes from the CSFs $[\text{Ar}]4p^2$ (46%), $[\text{Ar}]3d^2$ (39%), $[\text{Ar}]4s7s$ (10%), $[\text{Ar}]4s^2$ (1.9%) and $[\text{Ar}]4d^2$ (1.6%). Since $4d$ and $7s$ orbitals are not included in the H^v reference space in order to maintain the quasi-degeneracy of the valence orbital and enhance the perturbative convergence rate, this particular excited state (4^1S) is inaccurately described in the H^v method, and hence, is poorly estimated. Inclusion of $4d$, $4f$, $6p$, $7s$ and $7p$ orbital in the valence space will definitely improved the first order description of the 4^1S excited state, but the perturbative convergence and the accuracy of high order MBPT (third order) may deteriorate due the presence of large number of intruder states and huge diagonal perturbation which exerts an opposing force to the perturbative convergence.

Table 2.4: Low-lying binding energies (in cm^{-1}) of Ca I.

Terms	States	Expt.[1]	MCHF[2]	CI[3]	SG[4]	MP[5]	H^v
Singlet States							
$4s^2$	1S	49306.0	47649.0	47600.5	48930.31	49278.3	48420.28
$4s5s$	1S	15988.7	15729.3	15720.5	15935.28	15966.5	15989.32
$4s6s$	1S	8615.5	8277.6	8270.5	8599.40	8536.0	7625.89
$4p^2$	1S	7519.7	6709.7	6585.1	7887.13	7606.2	10231.19
$4s4p$	1P	25653.7	24689.2	24667.6	25472.25		25720.66
$4s5p$	1P	12574.3	12160.1	12143.3	12683.80		12127.36
$4s3d$	1D	27456.3	24869.2	24404.7	27478.99	27365.8	26123.48
$4p^2$	1D	8586.1	7402.9		8802.75		8992.11
Triplet States							
$4s5s$	3S	17766.0		17461.4		17765.7	17590.5
$4s6s$	3S	8831.2		8714.0		8831.1	8355.2
$4s4p$	3P	34042.5		34076.7	34851.67		33986.6
$4s5p$	3P	12740.3		12570.2	12899.61		12334.3
$4p^2$	3P	10797.7		11120.1			11675.8
$3d^2$	3F	5811.7		835.7		5811.6	5381.1
$3d4p$	3F	13474.2		10797.9	14032.06		12244.7
$4s3d$	3D	28948.9		24293.0	28096.19		27413.2
$3d4p$	3P	9967.6		7148.3	9866.51		7392.3
$3d4p$	3D	11073.1		6881.8			8218.1

[1]Reference [67], [2] Reference [60], [3] Reference [61], [4] Reference [62], [5] Reference [63]

Table 2.5 compares the first few excitation energies obtained through third order H^v calculation with MCHF and CI values as well as experimental data. Like binding energies, here, we also find that all the low lying excited states transition energies are in excellent agreement with experiment while there exists a small but non-negligible error in the estimation of the high lying states. We do expect this trend from the binding energy calculation as well as from previous H^v computation on Mg-like ions [51]. As explained before, it is the $4d, 7s$ orbitals whose absence in the

valence orbital space inaccurately describes the 4^1S excited states and, hence, poorly estimates this transition energy. Likewise, absence of $4d$, $4f$, $6p$ and $7p$ orbitals affect the computation of high lying excited states for P , D and F multiplets. For instance, it is shown by Vaeck *et al* that the major contribution to the 2^1D and 3^1D excited states comes from the CSF $[\text{Ar}]4s4d$, while CSF $[\text{Ar}]4s4f$ contributes about 80% to the 1^1F excited state. Since, we have not included these orbitals ($4d$, $4f$ and $7s$) in our reference space, the above mentioned excited states are expected to be poorly described and so their state energies. We have also estimated excitation energy for $3d^2(^1G)$ state (46422.8 cm^{-1}). There is no experimental data available for that, but our result is in fair agreement with Brage and Fischer's [62] result (46164.24 cm^{-1}), and Laughlin and Hansen's result (46075.4 cm^{-1}) [63].

Since a wide variety of reference space are used in the present calculation, it is important to study the low order convergence behavior of the different choices. We have demonstrated the importance of $3d$ orbital in the calculation. In table 2.6, we present the results obtained from a typical 13V (defined below) third order H^v computations where the computed transition energies are close to the experiment but the relative order of the singlet and triplet excited states are incorrect.

As pointed out by Vaeck *et al* that the low-lying excited S multiplet states of Ca I are dominated by the CSFs $[\text{Ar}]4sns$, we construct a H^v reference space by allocating two active electrons of $4s$ orbital among $4s$, $4p$, $5s$, $5p$, $6s$, $6p$ and $7s$ (13V) orbitals. The computed third order H^v transition energies are collected in Table 2.6 and compared with experimental data. From Table 2.6 we find that the $E_{2^3S} > E_{3^1S}$ and $E_{3^3S} > E_{4^1S}$ instead of $E_{2^3S} < E_{3^1S}$ and $E_{3^3S} < E_{4^1S}$. This incorrect ordering of the excited states of S multiplets most probably arises due to absence of the $3d$ orbital in valence space, because this peculiar problem does not arise in our 14V H^v calculation where orbital $3d$ is included in the valence space.

Table 2.5: Third order H^v excitation energies (in Rydberg) for S, P, D and F multiplets of $Ca I$.

Terms	State	Expt.[1]	δE [2]	δE [3]	$\delta E(H^v)$
<i>S</i> -multiplets					
$4s^2$	1S	0.000	0.000	0.00000	0.00000
$4s5s$	3S	0.28741		0.01276	0.00646
$4s5s$	1S	0.30361	0.01289	0.01310	0.00807
$4s6s$	3S	0.36883		0.01447	0.00373
$4s6s$	1S	0.37079	0.01218	0.01239	0.00095
$4p^2$	1S	0.38078	0.00733	0.00702	0.03298
<i>P</i> -multiplets					
$4s4p$	3P	0.13813		0.01489	0.00620
$4s4p$	1P	0.21553	0.00651	0.00655	0.00867
$4s5p$	3P	0.33305		0.01377	0.00421
$4s5p$	1P	0.33711	0.01398	0.01400	0.00638
$4p^2$	3P	0.35052		0.01808	0.01567
$3d^2$	3P	0.44231		0.02162	0.00266
$3d4p$	3P	0.35845		0.01018	0.01542
$3d4p$	1P	0.33472		0.05740	0.09362
<i>D</i> -multiplets					
$3d4s$	3D	0.18543		0.02696	0.00600
$3d4s$	1D	0.19911	0.01155	0.01226	0.00407
$3d5s$	3D	0.43264			0.01491
$4p^2$	1D	0.37106			0.01176
$3d4p$	3D	0.34864			0.01770
$3d4p$	1D	0.32655			0.00464
<i>F</i> -multiplets					
$3d4p$	3F	0.32637			0.00328
$3d4p$	1F	0.36941			0.04254
$3d^2$	3F	0.39630			0.00409

$$\Delta = |E_{calc.} - E_{expt.}|$$

[1] Reference [38], [2] Reference [60], [3] Reference [61]

Table 2.6: Transition energies (in Rydberg) for S multiplets of Ca I, obtained from third order H^v method using $13V$ ($4s, 5s, 6s, 7s, 4p, 5p, 6p$) valence space.

Terms	State	Expt.	H^v
4s6s	3S	0.36883	0.368218
4s6s	1S	0.37079	0.368004
4s7s	3S	0.40078	0.400079
4s7s	1S	0.40348	0.396437

Effective dipole operator calculations have also been performed to compute the transition probability and oscillator strengths of states. These calculations take the matrix element of the second-order effective dipole operator between the H^v eigenvectors as determined by the third order calculations. While our estimated oscillator strengths and transition probabilities for ground \rightarrow excited states (low-lying) are reasonably close to the MCHF, CI and experimental data, oscillator strengths for the excited \rightarrow excited state transition are somewhat off (see Table 2.7 and 2.8). The inferior quality of the oscillator strengths and probabilities for the ground to high-lying excited state and excited \rightarrow excited state can be anticipated because the reference space lacks important configurations like $[\text{Ar}]4s7s$, $[\text{Ar}]4s4d$ etc., that not only contributes to energies but also exert a strong influence on dipole properties [51]. [Note that oscillator strength and transition probability depends upon the transition energy and transition moment. Therefore, an error in the estimation of either of the two can yield a poor value for transition probability and oscillator strength.] The accuracy of the transition energies, oscillator strengths and transition probabilities for the ground to high-lying excited states and excited to excited states may be enhanced by including important CSFs in the reference space, and, research in this direction is in progress.

We have seen that our result for the λ 6717.7 Å line (i.e., $4s3d$ (1D) to $4s5p$ (1P) transition) is in good agreement with the experimental values for both the excitation energy and the transition dipole moment. So the observed crude abundances of neutral calcium [47] arise most probably because of some other property of the Am binaries which is presently not well understood.

Table 2.7: Third order H^v Oscillator Strengths for S, P, D and F multiplets of $C_{\infty} I$.

Transition	Multi-plet	Wave-length	Expt.[1]	MCHF[2]	CI[3]	H^v
$2 \rightarrow 4s4p$	$1S - 1P$	4227.9	1.75	1.89	1.820	1.74824
$2 \rightarrow 4s5p$	$1S - 1P$	2722.5	0.0009	0.0174	0.00101	0.00734
$5s \rightarrow 4s5p$	$1S - 1P$	29288.1		0.9968	0.926	1.03968
$4p \rightarrow 4s5s$	$1P - 1S$	10346.6		0.3975	0.118	0.34376
$4p \rightarrow 4s6s$	$1P - 1S$	5869.2		0.0029	0.0009	0.07591
$5p \rightarrow 4s6s$	$1P - 1S$	25260.0		0.6567	0.168	0.93595
$4p \rightarrow 4p^2$	$1P - 1S$	5514.5	0.17	0.4449	0.120	0.25685
$5p \rightarrow 4p^2$	$1P - 1S$	19783.7		0.0211	0.0153	0.02999
$4p \rightarrow 4s5s$	$3P - 3S$	6123.9	0.121		0.156	0.4508
$4p \rightarrow 4s6s$	$3P - 3S$	3958.2	0.0248		0.187	0.0524
$3d \rightarrow 4s5p$	$3D - 3P$	6163.1	0.076		0.0407	0.030
$3d \rightarrow 4s4p$	$1D - 1P$	55473.3		0.0007	0.0014	0.00017
$3d \rightarrow 4s5p$	$1D - 1P$	6717.7	0.049	0.0916	0.0585	0.04237
$3d \rightarrow 4p3d$	$3D - 3P$	5271.7	0.15		0.201	0.46996
$3d \rightarrow 4p3d$	$3D - 3D$	5596.0	0.23		0.346	0.36092
$3d \rightarrow 4p3d$	$3D - 3F$	6465.6	0.42		0.364	0.29119
$3d \rightarrow 4p3d$	$1D - 1P$	4526.9	0.075		0.0585	0.28348
$3d \rightarrow 4p3d$	$1D - 1F$	5350.9		0.1087	0.0925	0.08844
$4p \rightarrow 4p^2$	$3P - 3P$	4303.7	0.377		0.529	0.4756
$4p \rightarrow 4p^2$	$1P - 1D$	5859.1	0.57	0.4706	0.550	0.31677
$2 \rightarrow 3d4p$	$1D - 1F$			0.4998	0.00008	0.05281

Compiled by Wiese *et al* [68]. [Estimated uncertainty is $\approx 10-50\%$.], [2]Reference
, [3] Reference [61],

Table 2.8: Transition probabilities (in 10^8sec^{-1}) computed through third H^v method for S, P, D and F multiplets of Ca I .

Transition	Multi-plet	Wave-length	Expt.[1]	H^v
$4s^2 \rightarrow 4s4p$	$^1S - ^1P$	4227.9	2.18	2.011
$4s^2 \rightarrow 4s5p$	$^1S - ^1P$	2722.5	0.0027	0.022
$4s4p \rightarrow 4p^2$	$^1P - ^1S$	5514.5	1.1	2.64
$4s4p \rightarrow 4s5s$	$^3P - ^3S$	6123.9	0.354	1.452
$4s4p \rightarrow 4s6s$	$^3P - ^3S$	3958.2	0.175	0.392
$4s3d \rightarrow 4s5p$	$^3D - ^3P$	6163.1	0.19	0.698
$4s3d \rightarrow 4s5p$	$^1D - ^1P$	6717.7	0.12	0.102
$4s3d \rightarrow 4p3d$	$^3D - ^3P$	5271.7	0.50	1.758
$4s3d \rightarrow 4p3d$	$^3D - ^3D$	5596.0	0.49	0.886
$4s3d \rightarrow 4p3d$	$^3D - ^3F$	6465.6	0.53	0.348
$4s3d \rightarrow 4p3d$	$^1D - ^1P$	4526.9	0.41	1.923
$4s4p \rightarrow 4p^2$	$^3P - ^3P$	4303.7	1.36	1.586
$4s4p \rightarrow 4p^2$	$^1P - ^1D$	5859.1	0.66	0.353

[1] Compiled by Wiese *et al* [68]. [Estimated uncertainty is $\approx 10\text{-}50\%$.]

Table 2.9: Variation of third order ground state correlation energy (in a.u.) as a function of reference space.

Correlation contribution from	No. Reference space orbitals			
	SR-MBPT(0V)	4V	10V	14V
Core-Core	-0.27166	-0.27166	-0.27166	-0.27166
All Electron	-0.33179	-0.32201	-0.31174	-0.30808
Core-Valence + Valence-Valence	0.0	-0.05034	-0.04200	-0.03664

[1] Approximate contribution of 4s valence orbital to the ground state correlation energy is -0.060128 a.u.

Table 2.9 displays the contribution to the correlation energy arising from the core-core, core-valence plus valence-valence and all-electron interactions. Unlike the core-core correlation energy computation, it is not straight forward in our MR-MBPT approach to separate out the core-valence and valence-valence contributions and we therefore only quote the sum total of those two contributions which can also be obtained by subtracting the core-core contribution from the all-electron correlation energy. It is evident from Table 2.9 that the correlation contribution from core-valence and valence-valence decreases with the increasing dimension of the reference space. This variation in the correlation energy (core-valence plus valence-valence) is simply a consequence of the imposition of the valence orbital degeneracy condition. It can be easily shown that the forced valence orbital degeneracy condition enlarges the gap between the core and valence orbital energies which increases with the increasing size of the non-degenerate reference space [59, 64]. Consequently, the correlation contribution from core-valence and valence-valence interactions decreases with increasing size of the reference space.

It has been observed that the second order H^v computations often overestimate/ underestimate the state energies, and this eventually is counterbalanced by the third order H^v contributions. Thus, the low order perturbative convergence of the H^v method sometimes exhibits an oscillatory pattern that arises mainly because of the valence orbital energy averaging procedure, especially when the zeroth order orbital eigenspectrum is highly non-quasidegenerate. For example, the error in the computed $4s \rightarrow 4p$ resonant transition energy rapidly drops from 35% \rightarrow 2.5% as the perturbation order increases from 1 \rightarrow 3. But for non-resonant transition the perturbative convergence shows somewhat oscillatory behavior. This type of convergence pattern is quite common and has also been observed in earlier calculations where the triplet state is described more accurately than the singlet state with a minimal reference space H^v computation. Systematic increase of the valence space, for instance, the inclusion of the $3d$ and $6s$ orbitals in the reference, improves the low order perturbative convergence of the H^v method and that way it reduces the error in the computed third order excitation energy from 8.5% to 3.5% for resonance transition and from 10.7% to 3.17% for non-resonant transition without sacrificing

the second order accuracy of transition energy, which is small compared to the above. The inclusion of the $3d$ and $6s$ orbitals not only improves the accuracy of H^v transition energies but also improves the oscillator strengths.

We reiterate that the use of large valence space may provide a very good first order description for excited states of interests but eventually it may destroy the perturbative convergence because it involves a trade-off. The success of the H^v method largely depends upon the relative importance of the competing factors. The large reference space provides a better first order description of the state of interest, and, thereby accelerates convergence rate, while the diagonal perturbation that rises from the orbital averaging procedure destroy the perturbative convergence. Thus, care should taken during the selection of the reference space. In fact, the success of the H^v scheme lies largely on the appropriate selection of the valence space, a process that requires some trial and searching and *priori* knowledge of the most important configurations.

2.5 Conclusion

The effective valence shell Hamiltonian method is applied to compute the excitation energies and oscillator strengths for C I and Ca I. The H^v energies and wavefunctions are computed through third order and the effective dipole operator, μ^v , evaluated through second order. The accuracy of the computed low-lying and some high-lying excited state energies, binding energies, oscillator strengths, first ionization potential calculated for Ca I demonstrate the power of the method. Many excitation energies and oscillator strengths are in agreement with experiment for C I (some have good agreement with observations) and other highly correlated theoretical calculations. The present H^v computations for C I strongly suggest the use of multiple reference spaces for the excited states computations because of the different nature of correlation in various classes of excited states. This work highlights a number of unique and desirable features of the H^v method. For instance, the H^v calculations for Ca I provide uniform accuracy for most excited states than is obtained with some other schemes, such as the MCHF and CI methods.

The present calculations suggest that a minimal reference space is sufficient for the

accurate estimation of the excitation energies of the triplet states, while a large reference space is necessary to treat the singlet states. Since our computations have covered a wide range of reference spaces, it might be possible to use different set of reference spaces for excited states of different symmetry. This kind of approach has been found to be quite successful in generating potential energy surfaces [65].

On the whole the H^v method improves the agreement between theory and experiment, but a number of problem still remain. It has been argued over the past few years that the ever present intruder states can affect the numerical stabilities of the large scale H^v calculations. However, this assumption has been dispelled by the extensive studies of the convergence behavior [64, 65, 66]. It should be emphasized that a large (complete) reference invariably leads to the situation where the zeroth order eigenspectrum of the reference space overlaps with that of the virtual space states, i.e., the large (complete) reference space MR-MBPT computations must ultimately become plagued by the intruder states, and, consequently yield divergent perturbative expansion. However, when pursuing a large scale low order perturbative computation, we generally neither know nor care whether the series is truly convergent or not, since this information has no practical value. The H^v approach uses physical and mathematical consideration to produce acceptable accurate results in low order. The present computations for neutral carbon and calcium reinforces our prior assertions that this method can be used as a useful alternative scheme for the calculations of atomic properties.

References

- [1] I. Lindgren and J. Morrison, *Atomic Many-Body Theory*, Springer-Verlag, NY (1982)
- [2] A. Messiah, *Quantum Mechanics*, (Wiley, NY, 1962), Vol. II, pp. 698-700.
- [3] J. O. Hirschfelder, *Int. J. Quantum Chem.*, **3**, 731 (1969).
- [4] H. J. Silverstone, *J. Chem. Phys.*, **54**, 2325 (1971)
- [5] J. O. Hirschfelder and P. R. Certain, *J. Chem. Phys.*, **60**, 1118 (1974)

- [6] H. J. Silverstone and R. K. Moats, Phys. Rev. A, **23**, 1645 (1981)
- [7] C. Bloch, Nucl. Phys., **6**, 329 (1958)
- [8] J. des Cloizeaux, Nucl. Phys., **20**, 321 (1960)
- [9] B. H. Brandow, Rev. Mod. Phys., **39**, 771 (1967)
- [10] V. Kvanisčka, Czech. J. Phys., **B24**, 605 (1974)
- [11] Y.S. Lee and K. Suzuki, Phys. Lett., **91B**, 173 (1980)
- [12] K. Suzuki and S. Y. Lee, Prog. Theory. Phys., **64**, 2091 (1980)
- [13] Ph. Durand, J. Phys. Lett., **43**, L461 (1982)
- [14] U. Kaldor, Phys. Rev. A, **38**, 6013 (1988)
- [15] Ph. Durand and J. P. Malrieu, Adv. Chem. Phys., **67**, 321 (1987)
- [16] G. Jolicard and M. Y. Perrin, Chem. Phys., **123**, 249 (1988)
- [17] D. M. Silver and R.J. Bartlett, Phys. Rev. A.,**13**, 1 (1976)
- [18] D. M. Silver, S. Wilson and R.J. Bartlett, Phys. Rev. A.,**16**, 477 (1977)
- [19] R. K. Chaudhuri and Karl F. Freed, J. Chem. Phys., **107**, 6699 (1997)
- [20] X.-C. Wang and K. F. freed, J. Chem. Phys., **86**, 2899 (1987)
- [21] R. L. Graham and K. F. Freed, J. Chem. Phys., **96**, 1304 (1992)
- [22] J. P. Finley and K. F. Freed, J. Chem. Phys., **102**, 1306 (1995)
- [23] I. Lindgren, J. Phys. B, **7**, 2441 (1974)
- [24] P. Westhaus, Int. J. Quantum chem., **S7**, 463 (1973)
- [25] G. Hose and U. Kaldor, J. Phys. B, **12**, 3827 (1979); Phys. Scripta, **21**, 357 (1980), Chem. Phys. **62**, 469 (1981), J. Phys. Chem., **86**, 2133 (1982)
- [26] G. Hose, in: *Many-body Methods in Quantum Chamistru*, U. Kaldor(ed.) (Springer-verlag, Berlin) p.43 (1989)

- [27] D. Mukherjee, Proc. Ind. Acad. Sci., **96**, 145 (1986)
- [28] D. Mukherjee, Chem. Phys. Lett., **125**, 207 (1986)
- [29] H. Nussbaumer and P.J. Storey, *Astron. & Astrophys.*, **140**, 383 (1984).
- [30] K.S. de Boer and D.C. Morton, *Astron. Astrophys.*, **71**, 141 (1979)
- [31] M. Nooijen and R.J. Bartlett, *J. Chem. Phys.*, **107**, 6812 (1997)
- [32] K. F. Freed, in *Lecture Notes in Chemistry*, edited by U. Kaldor (Springer, Berlin, 1989), Vol. 52, p. 1, and references therein.
- [33] Chaudhuri R.K., Mudholkar A., Freed K.F., Martin C.H. and Sun H., *J. Chem. Phys.* **106**, (1997), 9252 and references therein.
- [34] Lee Y. S., Sun H., Sheppard M.G. and Freed K. F., *J. Chem. Phys.* **73**, (1980), 1472.
- [35] Lee Y.S., Sun H., Freed K.F. and Hagstrom S.A., *Bull. Korean Chem. Soc.* **7**, (1986), 262.
- [36] Sun H. and Freed K.F., *J. Chem. Phys.* **88**, (1988), 2659.
- [37] T.H. Dunning(Jr.), *J. Chem. Phys.*, **90**, 1007 (1989)
- [38] C. E. Moore, *Atomic Energy Levels (NSRDS-NBS(U.S.) 35)* (PUBLISHER, ADDRESS, 1971).
- [39] A. Sadlej, *Theor. Chim. Acta*, **79**, 123 (1991).
- [40] Luo D. and Pradhan A.K., 1989, *J. Phys. Mol. Opt. Phys.*, **22**, 3377.
- [41] M.J. Seaton, Y.Yu, Mihalas and A.K. Pradhan, *Mon. Notes R. Astron. Soc.*, **266**, 805 (1994)
- [42] Hibbert A., Biémont E., et al 1993, *A&AS*, **99**, 179.
- [43] J. Bromander, *Phys. Scr.*, **4**, 61 (1971)
- [44] M.-C. Poulizac, M. Druetta and P. Ceyzeriat, *J.Q.S.R.T.*, **11**, 1087 (1971)

- [45] Lambert D.L., 1968, MNRAS, **138**, 143.
- [46] E. Gibson, *The Quiet Sun* (NASA, Washington D.C., 1973).
- [47] I. K. Iliev and J. Budaj, ASP Conference Series, M.A.S.S. **108**, 283 (1996).
- [48] R. J. Bartlett, Ann. Rev. Phys. Chem. **32**, 359 (1981).
- [49] R. K. Chaudhuri and K. F. Freed (unpublished).
- [50] J. F. Finley and K. F. Freed, J. Chem. Phys. **102**, 1306 (1995).
- [51] R. K. Chaudhuri, B. P. Das, and K. F. Freed, J. Chem. Phys. **108**, 2556 (1998).
- [52] Sonjoy Majumder, R. K. Chaudhuri and B. P. Das, *proceed. of 6th Intl. Colloquium on Atomic Spectra and Oscillator Strengths for Astrophysical and Laboratory Plasmas*, Aug. 9-18, ed. J. Tatum, pp. 99 (1998).
- [53] M. A. Haque and D. Mukherjee, Pramana **23**, 651 (1980).
- [54] J. P. Malrieu, P. Durand, and J. P. Daudey, J. Phys. A **18**, 809 (1985).
- [55] B. O. Roos, K. Andersson, M. P. Fulscher, P. -A. Malmqvist, L. Seeeano-Anders, K. Pierloot and M. Merchan, Adv. Chem. Phys. **93**, 219 (1996) and references therein.
- [56] K. Hirao, Int. J. Quantum Chem. **S26**, 517 (1992).
- [57] K. D. Dobbs and W. J. Hehre, J. Comput. Chem. **7**, 359 (1986).
- [58] T. H. Schucan and H. A. Weidenmuller, Ann. Phys. (N.Y.) **73**, 108 (1972); *ibid* **76**, 483 (1973).
- [59] R. K. Chaudhuri and K. F. Freed, J. Chem. Phys. **107**, 6699 (1997), and references therein.
- [60] N. Vaeck, M. Godefroid, and J. E. Hansen, J. Phys. B **24**, 361 (1991).
- [61] J. Mitroy, J. Phys. B **26**, 3703 (1993).
- [62] T. Brage and C. F. Fischer, Physica Scripta **49**, 651 (1994).

-
- [63] C. Laughlin and J. E. Hansen, *J. Phys. B* **29**, L441 (1996).
- [64] J. P. Finley, R. K. Chaudhuri, and K. F. Freed, *Phys. Rev. A* **54**, 343 (1996).
- [65] R. K. Chaudhuri, J. P. Finley, and K. F. Freed, *J. Chem. Phys.* **106**, 4067 (1997).
- [66] J. P. Finley, R. K. Chaudhuri, and K. F. Freed, *J. Chem. Phys.* **103**, 4990 (1995).
- [67] J. Sugar and C. Corliss, *J. Phys. Chem. Ref. Data* **14 Suppl. 2**, 51 (1985).
- [68] W. L. Wiese, M. W. Smith, and B. M. Glennon, *Atomic Transition Probabilities (NBS NSRD-22)* (U.S. Govt. Printing Office, Washington, DC, 1966), Vol. 2.

Chapter 3

ab initio Relativistic Studies of Excitation Energies and Oscillator Strengths in Atomic Systems

3.1 Introduction

Various nuclear processes (like the r process) in astronomical objects are responsible for acquiring an abundance of heavier atoms and ions in their envelope and the ISM as mentioned in chapter 1. For most of these systems, the low lying orbitals probe regions of space with high potential energy near the atomic nuclei. Relativistic theory is required for the description of the electronic structure of these systems. Relativistic many-body theory is more complex than non-relativistic theory as it is inherently an infinite-body system, since one has to consider different quantum electrodynamic effects. There is an added difficulty because the relativistic many-body problem is also a multi-time problem. Each particle must have its proper time, and thus a Hamiltonian formalism is *a priori* not possible. This is the cause of the retardation effect, due to the finiteness of the speed of light. However, it is only in the case of a Hamiltonian formalism that powerful many-body methods have been developed. To solve this problem there are in general two possibilities. One can handle the full problem of bound states Quantum Electrodynamics (QED), write

all possible Feynman diagrams to a given order in the perturbation expansion and evaluate the energy shift that will include some correlation, relativistic effects and radiative corrections, if one goes at least to second order in fine structure constant. The problem is that such an approach is too complex and difficult, except for high-Z two-electron ions. Another, less rigorous, approach is to derive an effective no-pair Hamiltonian where retardation effects are taken into account and pair creation is suppressed to avoid including effects that can be handled, only in proper QED [1, 2]. One can use this Hamiltonian, which is however not Hermitian because of the retardation term, for calculating correlation and relativistic effects. QED corrections can then be introduced with care, to avoid counting some terms twice. Such a program has been partly carried for few-electron systems, using the Multiconfiguration Dirac-Fock method (MCDF), which is the exact analogue of the Multiconfiguration Hartree-Fock method, using the relativistic, no-pair Hamiltonian as a starting point, in place of the Breit-Pauli Schrödinger equation. Also, the spin-orbit interaction Hamiltonian which is responsible for the intermediate coupling transitions is in-built in the Dirac-Fock Hamiltonian, unlike in the non-relativistic case, where one has to consider relativistic correction as a perturbation.

The idea of forbidden transitions has its root in the concept of the Ritz combination principle, which states that the measured frequencies of all observed spectral lines can be expressed as the difference of two term frequencies. The fact that for any system not all the possible differences of the known terms are observed initially led to a separation of the possible radiative transitions into allowed and forbidden types. The following well-known selection rules for electro-magnetic decay, which provide a time-tested basis for this separation, predate quantum mechanics and were originally based on the classical electromagnetic theory applied to the vector model of the atom. In the table below, we have shown the selection rules for electric dipole and magnetic quadrupole (M2) transitions which we have used for our calculations in this chapter.

Because of the low transition rate associated with the M2 radiative decay, such a transition is generally observed only in an environment of ultralow density, where the collision rate is comparably low. But, activity in these transitions, especially

Table 3.1: Selection rules for allowed electric dipole (E1) transition and forbidden magnetic quadrupole (M2) transition

Electric Dipole (E1)	Magnetic Quadrupole (M2)
$\Delta J = 0, \pm 1$ ($0 \not\leftrightarrow 0$)	$\Delta J = 0, \pm 1, \pm 2$ ($0 \not\leftrightarrow 0,$ $1/2 \not\leftrightarrow 1/2, 0 \not\leftrightarrow 1$)
$\Delta M = 0, \pm 1$ ($0 \not\leftrightarrow 0$ when $\Delta J = 0$)	$\Delta M = 0, \pm 1, \pm 2$
Parity Change One electron jumping, with $\Delta l = \pm 1$ $\Delta S = 0$	Parity Change $\Delta l = 0, \pm 1$ ($0 \not\leftrightarrow 0$) $\Delta S = \pm 1$

emission from the low levels, has been stimulated by two developments. First, the realization that along the isoelectronic sequence, there is a very rapid increase with the atomic number Z of the rate associated with the forbidden transition. Hence, the need for a collision-free environment becomes much less critical at high Z . Second, the proliferation of devices capable of producing highly ionized heavy atoms. Examples of such devices are the low-inductance vacuum spark, high-power lasers, plasma sources and heavy-ion accelerators. The beam-foil technique has been of particular value in these studies, since transition rates can easily be measured by time-of-flight techniques.

To a good approximation, the free electrons form a Maxwellian distribution of energies, characterized by an electron temperature T_e . The electron temperature is insensitive to density, but sensitive to excitation of these forbidden lines as it is the most important thermal balance mechanism (in particular energy loss) in nebulae [3]. An immediate question is why these forbidden lines attain great strength in gaseous nebulae as compared with permitted lines, particularly those of H and He.

The answer lies partly in the vast extent of a nebular plasma and partly in the structures of energy level diagrams.

First, we must know how the lines are produced. Recombination and cascade certainly will not suffice as then we would observe lines arising from high levels as well as these low levels. Note that the metastable levels lie a few eV above the ground level. The energy of the average electron in the plasma is of the order of an eV. Some electron will have energies of 2 to 4 eV, a few may have energies to 5 or 7 eV, but none will have energies of, say, 20 eV. Hence, there will be a supply of electrons capable of exciting atoms to the metastable levels. Once in an excited level, they may escape by superelastic collisions or by the emission of a forbidden line. The total number of emissions per second will be $N_n A$, where N_n is the occupancy number in the upper level and $A = \sum_n A_{nn}$ is the sum of Einstein coefficients to the lower levels. In the first part of this chapter we consider an important but rarely touched forbidden transition, i.e. magnetic quadrupole transition for ions of beryllium isoelectronic sequence using the MCDF method.

The Dirac-Coulomb or Dirac-Coulomb-Breit equation may be solved to a good approximation by the coupled cluster (CC) method delineated in following sections. Approximate one-electron solutions to these equations, known as Dirac-Fock (DF) or Dirac-Fock-Breit equations may be obtained by the self-consistent-field(SCF) procedure or by matrix mechanics using particular type of basis. The very important correlation part in the relativistic regime may be calculated by coupled cluster (CC) method described in section 3.4. In that section we have calculated various allowed transitions among the doublet states of Mg^+ ion using the CC method. The solutions of the CC methods depend on the solutions of DF equations to a large extent. In section 3.3 we shall develop a new basis set expansion approach to calculate the DF orbitals in the framework of GTO with the same accuracy of the numerical solutions of them at least for occupied and low lying virtual orbitals.

3.2 Magnetic Quadrupole transitions for ions of Be-sequence using the MCDF Approach

The possibility that magnetic quadrupole radiation might have astrophysical significance for atomic transitions, which satisfy the selection rule $\Delta S = 1$, was first pointed out by Mizushima [4]. Ions of the beryllium isoelectronic sequence, in particular, ions with low atomic number, have proved to be rich resources for studying the low solar transition region. The diagnostic possibilities of this sequence were first noted by Munro *et al.* [5] and Jordan [6], and they have been investigated in subsequent studies [7, 8, 9, 10, 11, 12]. The presence of strong lines that yield a density diagnostic, coupled with many experimental measures or theoretical estimations of their intensities in the sun, has provided an impetus to both atomic and solar studies. One or more of the ultraviolet transitions of this sequence have been observed as well in the spectra of planetary nebulae [13, 14], quasi-stellar objects [15] and both hot and cool stars [16, 17, 18, 19]. These lines are useful in the spectral diagnostics of those astronomical objects (for example, the ratio of C/O for most of the PN can be safely approximated by CIII/OIII [20]). There is no question that density variations are observed on the surface of the sun, but the determination of the absolute values of these variations requires atomic parameters with more accuracy than available, specially, where experimental results are absent. The abundance of carbon and oxygen also determines the type of chemistry in the PN precursor's envelope, whether carbon-rich or oxygen-rich. Because of the lack of data about the properties of the forbidden lines of highly ionized atoms, insufficient attention was given to their applications to astronomical objects, like hot stars or nebulae etc. A comprehensive modeling of a star's internal structure needs a precise estimate of the radiative transitions of atoms and ions. The evolution of these ions on the stellar surface could have an influence on the evolution of the star. PN and low-density interstellar medium (ISM) exhibit many of the forbidden lines in emission, which infer the abundances of these ions [14]. Even if, in dense ISM, these forbidden lines are seen for highly ionized atoms. In a way these tell about the abundances of these elements in galaxies, which helps the study of galactic chemical evolution. M2 transitions in highly ionized systems occur in ultraviolet and visible

emission band. Therefore, high resolution spectrographs of satellites can observe these lines and they need these data as precisely as possible.

Since the strengths of the forbidden transitions are rather weak, it is difficult to determine their rates accurately. The accuracies of the computed excitation energies and transition rates depend largely on a balanced treatment of the correlation effects, an adequate size of the orbital basis and the quality of the valence orbitals. The Multiconfiguration Dirac-Fock (MCDF) method is the relativistic counterpart of Multiconfiguration Hartree-Fock (MCHF) theory. Our calculations of the magnetic quadrupole transition probabilities of the beryllium-like ions are calculated with the MCDF method based on the extended optimal level (EOL) approximation described in the next subsection. In those calculations, the corrections of the energies of the atomic states due to the Breit interaction are included using first-order perturbation theory.

Jönsson and Froese Fischer [21] have done calculations for doubly ionized carbon with the MCDF-EOL method followed by relativistic-configuration-interaction (RCI) calculation. They have used a different set of orbitals for the initial and final states. There are a few other calculations for these transitions [22, 23, 24, 25]; the majority of those have used the intermediate coupling approach. Garstang has shown that in the non-relativistic limit the magnetic quadrupole transition probabilities are approximately proportional to the square of the electric dipole matrix element [22]. However, it was shown by Lin et al. [26] that this approximation is not quite accurate. They had calculated this line for a few ions of the Be-isoelectronic sequence using a semi-empirical model potential. The Z -expansion method used by Laughlin [27] appears to be a rough estimate, and its accuracy is uncertain. In the present work we have used a fully relativistic one-electron Hamiltonian and supplemented it by the two-electron Coulomb and Breit terms. To ensure the convergence for each of the applied models and to estimate the error, the calculation is performed stepwise. The strong Z -dependence (approximately $\propto Z^8$ [28]) of M2 transitions is known and also its relativistic nature becomes important near $Z = 17$ [22]. We have used the relativistic expression for the magnetic quadrupole moment and the General Relativistic Atomic Structure Package (GRASP) [29] for our computations.

3.2.1 Theory (MCDF-EOL)

The Hamiltonian for an N -electron atom is written in atomic units as

$$H = \sum_{i=1}^N H_i + \sum_{i,j;i < j}^N V(|r_i - r_j|) \quad (3.1)$$

where r_i 's are the positions of the i -th particle. H_i is the Dirac Hamiltonian of i -th particle defined as

$$H_i = c\boldsymbol{\alpha} \cdot \mathbf{p}_i + (\beta - 1)c^2 + V_{nuc}(r_i) \quad (3.2)$$

where V_{nuc} is the potential due to the nucleus. V is an operator representing the electron-electron interaction

$$V_{ij} = \Lambda_{ij}^{dag} V_{ij} \Lambda_{ij} \quad (3.3)$$

where

$$V_{ij} = \frac{1}{r_{ij}} - \frac{\boldsymbol{\alpha}_i \cdot \boldsymbol{\alpha}_j}{r_{ij}} - \frac{\boldsymbol{\alpha}_i \cdot \boldsymbol{\alpha}_j}{r_{ij}} (\cos(\omega_{ij} r_{ij}) - 1) - (\boldsymbol{\alpha}_i \cdot \boldsymbol{\Delta}_i)(\boldsymbol{\alpha}_j \cdot \boldsymbol{\Delta}_j) \frac{\cos(\omega_{ij} r_{ij}) - 1}{\omega_{ij}^2 r_{ij}} \quad (3.4)$$

and $\Lambda_{ij} = \Lambda_i \Lambda_j$ is an operator projecting onto the one-electron positive energy states, to avoid introducing unwanted pair creation effects. Here ω_{ij} is the energy of the photon exchanged between the electrons and α_i are Dirac matrices. The first term in the correction to the Coulomb interaction is the magnetic interaction and the rest represents retardation. Since this potential contains differences of electron binding energies (ω_{ij}) the Hamiltonian is no longer Hermitian. Those binding energies can easily be evaluated in the single-configuration case with the help of the Koopman's theorem, but are not defined for virtual orbitals in the MCDF case. More-over this potential is gauge dependent. Here it is written in the Coulomb gauge, which has been shown to be the best one because spurious contributions appears in other gauges can be canceled out only by re-summation of infinite classes of diagrams. There is also a debate on whether to use the full retardation term as in eq.(3.4) or the Breit interaction, which is truncated to contain only of the order up to (ω_{ij}^2) as the complete interaction seems to lead to larger QED corrections to the electron-electron interactions.

In the MCDF code only the first term of eq.(3.4) is taken for calculation. One can call it is a *Dirac-Coulomb Hamiltonian*. Later we will discuss how the Breit term is taken into account. The atomic wave function for N electrons is obtained by solving the equation

$$H\Psi(\Pi, J, M) = E\Psi(\Pi, J, M) \quad (3.5)$$

where Π is the parity, J is the total angular momentum eigenvalue and M is the eigenvalue of its projection on the z axis.

In the MCDF method, the trial wave function is taken to be a linear combination of configuration state functions (CSFs) :

$$|\Psi(\Pi, J, M)\rangle = \sum_{r=1}^n c_r \Phi_r(\Pi, J, M) \quad (3.6)$$

The CSFs are eigenfunctions of the parity, total angular momentum J^2 and J_z . The CSFs are expressed as a linear combination of Slater determinants of Dirac spinors,

$$\Phi_r(\Pi, J, M) = \sum_{i=1}^{N_r} d_i |D_i\rangle \quad (3.7)$$

where $|D_i\rangle$ is a determinantal wave function built from single particle states. and its coefficients, d_i 's are obtained by requiring that the CSFs are eigenstates of J^2 and its projection J_z . The variational principle is used to determine the radial wave functions and the mixing coefficients c_r self-consistently. The energy functional that is minimized is given by

$$E_\alpha = \int \Psi_\alpha^\dagger H \Psi_\alpha d\tau = \sum_{r,s} c_r^*(\alpha) H_{rs} c_s(\alpha) = c_\alpha^\dagger H c_\alpha \quad (3.8)$$

in the matrix notation where the Hamiltonian matrix element is defined by

$$H_{rs} = \langle \Phi_r | H | \Phi_s \rangle \quad (3.9)$$

Keeping the orbitals fixed, the variation of the energy functional E_α with respect to the mixing coefficients with the normalization condition $\langle \Psi_\alpha | \Psi_\alpha \rangle = 1$ yields

$$(H - E_\alpha I) c_\alpha = 0 \quad (3.10)$$

i.e. c_α is an eigenvector of the Hamiltonian with eigenvalue E_α .

Self-consistent field (SCF) equations are obtained by requiring that energy functional should be stationary when subject to variations in the radial functions (P_a, Q_a) such that the orbitals form an orthonormal set. Consider the energy functional :

$$E = E_{opt} + \sum_a \bar{q}_a \epsilon_a N(aa) + \sum_{a,b;a \neq b} \epsilon_{ab} N(ab) \quad (3.11)$$

with

$$E_{opt} = \sum_r d_r^2 H_{rr} + \sum_{r,s;r \neq s} d_{rs} H_{rs} \quad (3.12)$$

where $\bar{q}_a = \sum_r d_r^2 q_a(r)$ is the generalized occupation number for orbital a and d_r ($r = 1, \dots, n$), the real coefficients, depends on the configuration mixing coefficients, are chosen so that $\sum_r d_r^2 = 1$. The detailed descriptions of all the terms are given in the appendix following to this section. The Lagrange multipliers ϵ_a and ϵ_{ab} ensure the normalization and orthogonality conditions respectively.

The extended optimal level (EOL) approximation of the MCDF approach is an extension of the well known optimal level (OL) version [35]. For the latter case, $E_{opt} = E_\alpha$ yields $d_r = c_r(\alpha)$ and $d_{rs} = c_r(\alpha)c_s(\alpha)$ so that the wave function and mixing coefficients are optimum for the state α . In the EOL approach, optimization is done on a sum of energies $\sum_i E(\alpha_i)$, $i = 1, \dots, n_L$, where $n_L < n$, and for that case

$$E_{opt} = \frac{1}{n_L} \sum_{i=1}^{n_L} E_{\alpha_i} \quad (3.13)$$

so that

$$d_r = \left[\frac{1}{n_L} \sum_{i=1}^{n_L} c_r^2(\alpha_i) \right]^{\frac{1}{2}} \quad (3.14)$$

$$d_{rs} = \frac{1}{n_L} \sum_{i=1}^{n_L} c_r(\alpha_i)c_s(\alpha_i) \quad (3.15)$$

The relativistic two-electron operator is shown in eq.(3.4). As we see from that equation the interaction between two electrons can be expressed as a series expansion. The first term is the Coulomb interaction and the leading correction to it is known as the Breit interaction [30, 31, 32]. It is linear in the fine structure constant.

In the present work, we consider the Breit interaction as a first-order perturbation. We have used the expressions given by Grant and McKenzie to evaluate the Breit contributions [33]. The Hamiltonian matrix is constructed and diagonalized to estimate the mixing coefficients for the required atomic states (Eq. 3.10). Starting with these values of the mixing coefficients, the SCF equations are solved to obtain new estimates for the orbitals. This process is repeated until self-consistency is achieved. The eigenvalues and orbitals obtained in this way are used to calculate different atomic properties. The magnetic quadrupole emission coefficient is given by the expression [34]

$$A_{fi} = \frac{1}{[J_f]} \sum_{M_i, M_f} 2\pi |\langle \Psi_f | M2 | \Psi_i \rangle|^2 \quad (3.16)$$

where $[j] = 2j + 1$. The matrix element of the magnetic quadrupole operator, $M2$, with respect to initial ($|\Psi_i\rangle$) and final ($|\Psi_f\rangle$) wave functions can be written in terms of CSF as :

$$\langle \Psi_f | M2 | \Psi_i \rangle = \sum_{rs} c_{rf} c_{si} \langle \Phi_r | M2 | \Phi_s \rangle \quad (3.17)$$

where

$$\langle \Phi_r | M2 | \Phi_s \rangle = \sum_{ab} d_{rs}^k(ab) \langle \phi_b | M2 | \phi_a \rangle \quad (3.18)$$

The expression for this single matrix element is

$$\langle \phi_b | M2 | \phi_a \rangle = \left(\frac{\omega}{\pi c} \right)^{1/2} [j_b]^{1/2} (-1)^{(2j_a + j_b - 1/2)} |\bar{M}_{ab}| \begin{pmatrix} j_b & L & j_a \\ \frac{1}{2} & 0 & -\frac{1}{2} \end{pmatrix} \quad (3.19)$$

and

$$\bar{M}_{ab} = \frac{5}{\sqrt{6}} (\kappa_a + \kappa_b) I_L(\omega) \quad (3.20)$$

and

$$I_L(\omega) = \int_0^\infty (P_a Q_b + Q_a P_b) J_L \left(\frac{\omega r}{c} \right) dr \quad (3.21)$$

P and Q are the large and small components of the wavefunctions respectively and J_L is the spherical Bessel function of order L.

3.2.2 Results and Discussions

We have employed the MCDF approach in the EOL approximation to calculate excitation energies and the magnetic quadrupole transition rates for selected ions of the beryllium sequence. The advantage of this approach is that it is capable of taking into account a large class of electron correlation effects with a relatively small number of virtual orbitals. The intermediate coupling method was used to calculate magnetic quadrupole transition probabilities for a few Be-like ions [23, 24, 25]. In this method, different basis sets are used for the diagonalization of the different parts of the Hamiltonian. The Coulomb part is diagonalized with respect to the LS coupled basis, whereas the spin-orbital part with respect to JJ coupled basis. For $Z \leq 12$ Froese Fischer et al. [36] have used this approach in the framework of the multiconfiguration Hartree-Fock method supplemented by the Breit-Pauli corrections (MCHF+BP approach). There is a small difference between those results and ours, mainly because of the choice of the orbital basis and the incomplete treatment of the relativistic effects in their approaches. Our calculated excitation energies are in better agreement with the experimental values (wherever available) than the other calculations. The superiority of the MCDF-EOL method (with the Breit interaction) over the MCHF+BP method is obvious from table 3.2 (MCHF+BP excitation energies data are taken from Froese Fischer's web page : <http://www.vuse.vanderbilt.edu/cff/cff.html>). This table shows the percentage of the differences of the calculated excitation energies from the experimental values. The accuracy is much better in the case of the MCDF-EOL method and it steadily improves for higher Z values.

Our computations consist of several steps. We start with the Dirac-Fock (DF) calculation, and then optimize the two $2s^2 (^1S_0)$ and $2s2p(^3P_2)$ states (levels) with respect to stationary criteria (see Eq. 3.13). In each of the following steps, one new orbital (to avoid the problem of computational convergence) is added to the old set and optimization is done on the required sum of the state energies using that basis. In our EOL calculations we have optimized the lowest five energy states (i.e. $n_L=5$ in (3.13)).

Since we are interested in optimizing the $2s^2 (^1S_0)$ and $2s2p(^3P_2)$ states, we have

chosen CSFs which contribute to these two states. As the states are of opposite parities, only those CSFs will contribute which have the same parity and total angular momentum as either one of the above two states. Our orbital basis is constructed from 1s, 2s, 3s, 4s, 2p, 3p, 4p, 3d, 4d and 4f orbitals. The CSFs are constructed by taking all the possible excitations from the 1s and 2s orbitals to the other virtual orbitals apart from quadrupole excitations to the 4d and 4f orbitals. The convergence of the MCDF orbitals is significantly improved as the value of Z increases. In table 3.3, we give the contributions of the Breit interaction to the excitation energies. As expected they increase with Z . This leads to a significant change in the M2 transition rates as they are proportional to the fifth power of the excitation energies. The effect of Breit interaction on the excitation energies is plotted for various ionized atoms in figure 3.1. This figure shows that the calculation gives very good agreement with the NIST tabulated values for the excitation energies when the Breit interaction is taken into consideration.

In Table 3.4, we have presented the excitation energies of the $2s2p\ ^3P_2$ state from the ground states for different Z -values. The standard values are taken from NIST online database and in a few cases, where there are some differences between our calculated excitation energies and the standard values, we compare our results with the unpublished data of R.L.Kelly (indicated as †). For Z values of 35, 40, 45, 50 and 55 there is no data available in the literature. Table 3.4 shows excellent agreement between our calculations and the NIST data. For low Z ions, the difference between the standard values and our calculated values is on average $<50\text{ cm}^{-1}$, which is well within the limit of the former. We can improve these calculations, if we consider some more orbitals in the active space, but that is computationally expensive and can create convergence problems. In our calculation there is a change in the ordering of $1s^22p_{\frac{1}{2}}^2(^1S_0)$ and $1s^22s_{\frac{1}{2}}2p_{\frac{3}{2}}(^3P_2)$ states for highly ionized Be-like atoms ($Z=45, 50$ and 55). This is because of the rather large contraction of the $2p_{\frac{1}{2}}$ orbital for ions with large Z .

Unlike the allowed electric dipole transition between $1s^22s^2(^1S_0)$ and $1s^22s2p(^1P_1)$ states, the most important contributions to the M2 transition between $1s^22s^2(^1S_0)$ and $1s^22s2p(^3P_2)$ do not come from the Hartree-Fock configurations. In the latter

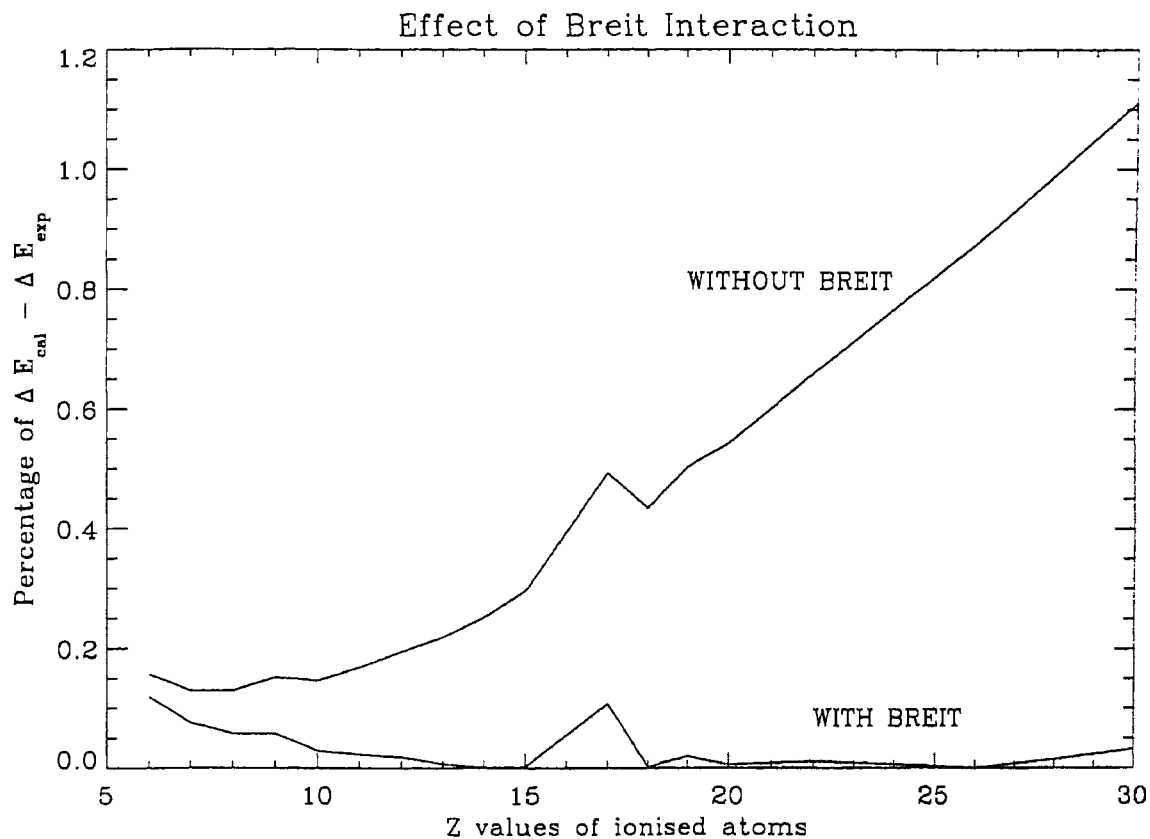


Figure 3.1: *The effect of Breit interaction on the excitation energies*

case one of the dominant contributions comes from the matrix element

$$\langle 1s2s3s3p_{\frac{1}{2}}(^3P_2) | M2 | 1s2s3p_{\frac{1}{2}}3p_{\frac{3}{2}}(^1S_0) \rangle$$

for all the ions. Table 3.5 shows how this contribution changes with the value of Z . This contribution decreases as the value of Z increases.

In Table 3.6, transition decay rates are given from $2s2p\ ^3P_2$ state to the ground state. It is clear that all the calculations are in fairly good agreement. The small discrepancies are due to the way in relativistic and the many-electron effects are incorporated in the different methods. Most of the other calculations have used relativistic corrections to the non-relativistic interaction Hamiltonian term to obtain the magnetic quadrupole moment operator. For doubly ionized carbon, Jönsson and Froese Fischer [21] have calculated the same transition probability with the MCDF-EOL+RCI method (with the Breit interaction and biorthogonal basis set). There is very good agreement between our result and theirs. Our result agrees with their

Table 3.2: Comparison of the percentage of differences of calculated excitation energies from experimental values between the MCHF+BP and MCDF+B (first order correction) methods

Z	MCHF+BP	MCDF+B
6	0.287	0.119
7	0.231	0.075
8	0.187	0.057
9	0.219	0.057
10	0.284	0.029

result (they also have calculated transition probability using the observed transition energy) if we use the standard excitation energy value for the M2 transition probability calculation. So, the small discrepancy is mainly due to the details of the optimization of the orbitals. As expected for low Z-ions, our results are not different from all the other results obtained using relativistic corrections. But for heavier ions the discrepancies are larger. M2 transition probabilities are not available for many of the highly ionized atoms.

Table 3.3: Contributions of the Breit interaction to the excitation energies (in cm^{-1})

Z	contributions to ΔE
6	19.84
7	35.93
8	59.11
9	91.28
10	131.67
11	185.67
12	253.70
13	340.02
14	443.40
15	570.07
17	895.77
18	1090.02
19	1322.64
20	1593.19
22	2247.92
26	4117.06
28	5363.68
30	6903.70
35	12047.52
40	19560.90
45	30095.86
50	44362.98
55	63024.75

Table 3.4: *Excitation Energies (in cm^{-1}) from the ground state.*

Z	2s2p (3P_2)	
	NIST	EOL
6	52447.11	52509.6
7	67416.3	67467.1
8	82385.3	82432.7
9	97437	97493.2
10	112704	112736.7
11	128218	128247.4
12	144091	144117.4
13	160429	160439.9
14	177318	177320.6
15	194856	194861.8
17	232660 [‡]	232410.5
18	252683	252688.1
19	274090 [‡]	274143.4
20	296950	296933.5
22	347240	347200.8
26	471780	471784.7
28	549500	549579.8
30	640470	640263.8
35		938933.4
40		1373896.5
45		1995158.4
50		2864042.8
55		4054174.1

[‡] From Kelly's unpublished work (<http://physics.nist.gov/cgi-bin/AtData/main-asd>)

Table 3.5: $\langle 1s2s3s3p_{\frac{1}{2}}(^3P_2) | M2 | 1s2s3p_{\frac{1}{2}}3p_{\frac{3}{2}}(^1S_0) \rangle$ matrix element values for different Z

Z	Value
6	1.15736 (-2) [‡]
16	4.12406 (-3)
28	2.23929 (-3)
40	1.50165 (-3)
50	1.17056 (-3)

[‡] The notation $\alpha(\beta)$ implies $\alpha \times 10^\beta$

Table 3.6: Transition rate (in sec^{-1}) from $2s2p(^3P_2)$ to the ground state.

Z	$\lambda(\text{\AA})$	EOL	MCHF +BP	Glass	Others
6	1906.7	5.176(-3)	5.193(-3)	5.261(-3)	5.139 ^a , 5.215(-3) ^b
7	1483.3	1.147(-2)	8.772(-3)	1.161(-2)	1.13(-2) ^c
8	1213.8	2.152(-2)	1.602(-2)	2.171(-2)	2.17(-2) ^c
9	1025.7	3.633(-2)	2.897(-2)	3.700(-2)	
10	887.0	5.720(-2)	5.235(-2)	5.838(-2)	5.76(-2) ^c
11	779.7	8.572(-2)	7.997(-2)		
12	693.9	1.239(-1)	1.177(-1)	1.269(-1)	1.25(-1) ^c
13	623.3	1.745(-1)			
14	563.9	2.410(-1)		2.460(-1)	4.8 ^d , 2.38(-1) ^c
15	513.2	3.281(-1)			
16	466.5	4.461(-1)			4.55(-1) ^c
17	430.3	5.906(-1)			
18	395.7	7.858(-1)		7.993(-1)	
19	364.8	1.0423			
20	336.8	1.3804		1.405	1.41 ^c
22	288.0	2.4234			
24	244.8	4.433			
26	211.9	7.6459		7.930	7.69 ^c , 10.2 ^d
28	181.9	1.3824(1)			13.8 ^c
30	156.2	2.5289(1)			
35	106.5	1.1899(2)			
40	72.8	5.8742(2)			
45	50.1	2.8789(3)			
50	34.9	1.3675(4)			
55	24.7	6.2006(4)			

a : [21], b : [25], c : [24], d : [27]

3.3 Relativistic DF orbitals generation: A new approach using finite basis set expansion

There has been an increased interest in solving the Dirac equation for many-electron atoms using the method of finite basis set expansion (FBSE) [37]. It has been found [38] that with kinetic balance condition imposed upon the basis set, Dirac-Fock self consistent field (DF-SCF) calculations can be performed on many-electron atoms using techniques similar to nonrelativistic methods. The imposition of the kinetic balance relation [39] between the large and the small components of the basis functions is one of the main features of the success of this approach, which in essence can be regarded as using the proper boundary condition for the orbitals. It was shown that Gaussian-type orbitals (GTOs) can give rise to a natural description of the relativistic wave functions within a finite nucleus [40].

A large number of atomic and molecular calculations adopt a pragmatic approach to the selection of basis sets. The quality of a particular basis set is determined by physical considerations and numerical tests. The accuracies of the orbital wavefunctions obtained from the numerical computations are rather high. Our aim is to obtain DF orbitals using FBSE approach atleast to that accuracies. The art of selecting the basis set lies in the experience gained in previous studies and the requirements of a particular property. Since it is beyond the scope of the present work to discuss this aspect, we refer the review article by Čársky and Urban [41] and the references therein. The most important feature of the FBSE method in the GTO framework is to determine the appropriate exponential parameter (exponent), which largely determines the quality of the wavefunctions.

Large basis sets can be efficiently generated by utilizing the concept of an even-tempered Gaussian basis set (ET-GTO)[42]. While Matsuoka and co-workers [43] used well-tempered finite Gaussian basis set in computing DF energies, Mohanty and Clementi [37] employed geometric-type exponent for the Gaussian primitives [44] with kinetic balance condition between the large and small component spinors and DF energies of orbitals are compared to the corresponding numerical DF values [45]. Chaudhuri and co-workers [46] have developed a numerical procedure to solve the atomic relativistic DF-SCF equations using the finite universal basis set

expansion (FUBSE) method. They generate the large- and small-component part of the radial wave functions on a grid using the FUBSE procedure. The one- and two-electron radial integrals are evaluated numerically to avoid the complicated analytical expressions of their direct and exchange radial integrals. This procedure provides an easy way to reduce the $n_b(n_b + 1)/2$ operations to n_c operations in DF-SCF computation (n_b and n_c correspond to the total number of basis functions and occupied orbitals, respectively) and thereby reduces the computational time of the relativistic self-consistent-field calculations for heavy atoms.

In our present work we have generated the orbitals using a hybrid approach. We use the above mentioned DF-SCF method through the finite universal or even-tempered basis set expansion to generate the wavefunctions of all the orbitals. Among those orbitals, all the occupied and a few low lying unoccupied single particle wave functions are replaced by the corresponding single particle wave functions obtained from the numerical procedure [45]. The details of this procedure are described in next section. In that section we explain how the remaining orbitals are constructed. The importance of this type of basis set is to achieve highly accurate wave functions for the orbitals of the atoms. For a complete basis set, it is immaterial how one generates them. But we will see in Section 3.3.2 that for a truncated finite basis set our approach generates better single particle wave functions. We have employed wavefunctions of the single particle orbitals obtained using the Gaussian basis and the new approach in the *ab initio* coupled-cluster (CC) method (explained in Section 3.4.1) to calculate IP, EE and a few oscillator strengths of Mg^+ and Ca^+ ions. The CC method is strongly dependent on the choice of basis set to calculate various electronic properties of atoms and ions. We compare these results in that section.

3.3.1 Method of Calculation

Relativistic Hartree-Fock calculations using the basis set expansion method on atoms was initiated by Kim [47] and followed by many investigators [48]. Since this method can be applied to heavy atoms and ions relativistic treatment is necessary for getting true energies and wavefunctions. So one starts with the Dirac Fock Hamilto-

nian given by

$$H = \sum_i c\alpha_i \cdot \mathbf{p}_i + (\beta_i - 1)mc^2 + V_N + V_{DF} \quad (3.22)$$

where V_{DF} is defined in appendix-A consisting of direct and exchange parts. To first approximation we write the general wavefunction $|\Psi\rangle$ to be single determinant $|\Phi\rangle$ can be expressed in terms of single particle orbitals $|\phi_i\rangle$ s by

$$|\Phi\rangle = \frac{1}{N!} \text{Det}\{\phi_1\phi_2\dots\phi_N\} \quad (3.23)$$

Here the single particle orbital is expressed in terms of spinors with P_i as large component and Q_i as small component,

$$\phi_i = \frac{1}{r} \begin{Bmatrix} P_i & \chi_{\kappa_i m_i} \\ iQ_i & \chi_{-\kappa_i m_i} \end{Bmatrix} \quad (3.24)$$

where P and Q are radial parts and χ 's are spin-angular parts of the components. These radial components are expanded in terms of Gaussian basis functions

$$P_i = \sum_n C_{in}^L g_n^L$$

$$Q_i = \sum_n C_{in}^S g_n^S$$

where C_{in}^L and C_{in}^S are the expansion coefficients of large and small components.

The above DHF orbitals are generated using a hybrid scheme [46] by solving the DF equation through pseudo-eigenvalue approach where basis functions are defined on a grid and the one- and two-electron radial integrals are evaluated numerically. The large and small components of the radial wavefunctions are expressed as the linear combination of Gaussian Type Orbitals (GTOs).

The GTOs are of the form given by

$$g_{i,k} = r^{k_i} \cdot e^{-\alpha_i r^2} \quad (3.25)$$

where $k_i=1,2,3,\dots$ for s,p,d,... type functions respectively. The even-tempered basis set has exponent of the form

$$\alpha_i = \alpha_{i-1} \cdot \beta, i = 1, \dots, N_{isym} \quad (3.26)$$

where N_{isym} is the number of basis functions for a given symmetry and α_0, β are the parameters specified for the Gaussian orbitals of the particular symmetry. The

large component g_n^L of the single particle basis is expanded as

$$g_n^L = C_N^L r^{k_n} \exp(-\alpha_n r^2)$$

and the small component g_n^S is related with g_n^L by the kinetic balance condition given by relation :

$$g_n^S = C_N^S \left(\frac{d}{dr} + \frac{\kappa}{r} \right) g_n^L \quad (3.27)$$

where C_N^L and C_N^S are the normalization constants of large and small components of the basis functions.

For a system with n_c closed shell occupied orbitals, we use a Gaussian basis to solve the DF equation for closed shell core, which can be written for single particle orbital $|\phi_i\rangle$ as

$$t|\phi_i\rangle + V_{DF}|\phi_i\rangle = \epsilon_i|\phi_i\rangle \quad (3.28)$$

where $t = \sum_i c\alpha_i \cdot \mathbf{p}_i + (\beta_i - 1)mc^2 + V_{nuc}$.

The solution of this eigen value equation produces occupied and unoccupied orbitals for each symmetry:

$$\{\phi_1, \phi_2, \dots, \phi_{n_c^{i\text{sym}}}, \phi_{n_c^{i\text{sym}}+1}, \dots, \phi_{N_{i\text{sym}}}\}.$$

where $n_c^{i\text{sym}}$ is number of occupied orbitals of the given symmetry.

In the present method, we obtain the occupied and a few low lying unoccupied orbitals of each symmetry as numerical orbitals generated from GRASP [49] code.

The numerical orbitals are denoted as

$$\{\psi_1, \psi_2, \dots, \psi_{n_c^{i\text{sym}}}, \dots, \psi_{N_{i\text{sym}}}\}$$

where $n_{i\text{sym}}$ is the number of numerical orbitals used for $i\text{sym}$ -th symmetry. Since part of the orbitals are got numerically and part are analytically using two different methods, the orbitals will not be orthogonal among these two partial sets. So one obtains new unoccupied orbitals $\{\psi_{n_{i\text{sym}}+1}, \dots, \psi_{N_{i\text{sym}}}\}$ by the Schmidt orthogonalization procedure as defined as

$$|\psi_{n_{i\text{sym}}+k}\rangle = |\phi_{n_{i\text{sym}}+k}\rangle - \sum_{m=1}^{n_{i\text{sym}}+k-1} |\psi_m\rangle \langle \psi_m | \phi_{n_{i\text{sym}}+k}\rangle \quad (3.29)$$

where, k goes from 1 to $(N_{i\text{sym}} - n_{i\text{sym}})$. By this procedure the new partial set of virtual orbitals are made orthogonal to the numerical orbitals and among each

other. It is not convenient to use this basis as such in certain types of many-body calculations, since the new virtual orbitals are not got by the diagonalization of the DF Hamiltonian and hence they are not DF orbitals.

The Hamiltonian given in eq. (3.22) is then diagonalized only in the unoccupied space $\{\psi_{n_{isy}m+1}, \dots, \psi_{N_{isy}m}\}$ where the unoccupied DF orbitals $\{\psi'_{n_{isy}m+1}, \dots, \psi'_{N_{isy}m}\}$ are expressed as a linear combination of the Schmidt orthogonalized unoccupied orbitals as given below.

$$|\psi'_k\rangle = \sum_{l=n+1}^N b_{kl} |\psi_l\rangle$$

The coefficients b_{kl} are obtained by the above mentioned diagonalization and they are used for the generating of the new unoccupied DF singles particle orbitals which are orthogonal to the numerical orbitals and to themselves. This method has been extended to the open shell atoms by starting with a open shell Gaussian code [50].

3.3.2 Results and Discussion

In this section we discuss our calculations of some of the properties of Mg^+ and Ca^+ using the new basis. We employ the coupled cluster calculations using orbitals obtained from the analytical FBSE method and our new approach; and compare the values of the IP, EE and oscillator strength properties obtained from these calculations with the corresponding experimental values. The basis is generated with a closed shell potential ($V^{(N-1)}$) and defined on a grid. The number of basis GTOs used in each symmetry for both the systems is given in table 3.7. Since we are using a finite basis set, in practice, by changing suitably the exponents of the GTOs and the number of basis in each symmetry, one tries to get the bound DF orbitals as close as possible to the numerical DF orbitals [43]. But it is difficult to satisfy that for all the bound orbitals obtained analytically by changing the parameters. So, one of the best approaches to achieve the above purpose for all the occupied and a few low lying virtual orbitals is to use the new method explained in section 3.3.1.

Table 3.7: Number of basis used for each symmetry to calculate DF energies and wavefunctions of Mg^+ and Ca^+ .

s(1/2)	p(1/2)	p(3/2)	d(3/2)	d(5/2)	f(5/2)	f(7/2)	g(7/2)	g(9/2)
30	25	25	25	25	20	20	15	15

We have used a large even-tempered Gaussian basis with $\alpha_0=0.01$ (for Mg^+), 0.00725 (for Ca^+) and $\beta=2.90$ (for Mg^+), 2.73 (for Ca^+) for all the symmetries and obtained wave functions of relativistic orbitals. Table 3.8 and 3.9 show the comparison between DF energies of the bound orbitals calculated using the analytical FBSE method with the corresponding values using the new approach for Mg^+ and Ca^+ systems. Only bound orbitals are given in these tables and they are the numerical orbitals for the new method (shown in table 3.10). The agreement between the occupied and a few low lying unoccupied orbital energies using two different methods are good. But as we see from table 3.8 and 3.9, some of the higher lying orbitals deviate considerably from numerical ones.

The above basis is employed to calculate the IP and EE of the above mentioned systems using the Coupled Cluster Singles and Doubles with partial triples (CCSD(T)) [51, 52] method. In order to reduce the amount of memory needed for the CCSD(T) calculations we restrict an upper bound in energy for all single particle orbitals of s-, $p_{1/2^-}$, $p_{3/2^-}$ symmetries by 1500 a.u., $d_{3/2^-}$, $d_{5/2^-}$, $f_{5/2^-}$, $f_{7/2^-}$ symmetries by 500 a.u. and $g_{7/2}$, $g_{9/2}$ symmetries by 5 a.u. for Mg^+ ; and for Ca^+ s-, $p_{1/2^-}$, $p_{3/2^-}$ symmetries by 1000 a.u., $d_{3/2^-}$, $d_{5/2^-}$, $f_{5/2^-}$, $f_{7/2^-}$, $g_{7/2}$, $g_{9/2}$ symmetries by 500 a.u.. This is done to reduce the memory used in these computations. All the core orbitals are excited for these calculations. The basis orbitals used for the coupled cluster calculation for each symmetry with the number of numerical orbitals used are given in Table 3.10. Using the coupled cluster wave functions the IP and EE for the low lying levels were calculated using the two bases.

Table 3.11 shows the IP values for Mg^+ and Ca^+ . Table 3.12 shows EE values for Mg^+ . It is clearly seen that the higher excited orbitals or states obtained by using analytical Gaussian basis do not have as good agreement with the experimental values as obtained from our new basis. This may be due to the fact that the higher excited orbitals were not generated that accurately using analytical Gaussian basis. The importance of the use the new approach is clear from figures fig. 3.2 and fig. 3.3. The percentage of errors of both the IP and EE of Mg II show the necessity of using new basis. If one adjusts the exponents of the basis functions, it is possible to generate better basis with better agreement with experimental IP

and EE values (this work will be easier, if one uses even-tempered basis). This is not very important if new method is used. In some cases both the approach show comparable accuracy. This may be mere coincidence, as the results obtained using new approach show uniform accuracy. If we look at the overall results, the calculated results obtained from the new basis generation method are in better agreement with experimental results than those obtained from analytical basis. This picture will be more convincing if we check properties of heavier atoms using both the approaches.

Table 3.8: *The comparison of DF bound orbitals' energies for Mg⁺ calculated by using the new method and the analytical method.*

Orbital	Orbital Energies(au)	
	(new method)	(analytical)
1s	-49.864752462	-49.870881301
2s	-4.4964660926	-4.4976610628
3s	-0.54140221084	-0.54136243689
4s	-0.23172649438	-0.23156611955
5s	-0.12864892397	-0.12788140758
2p(1/2)	-3.0133544114	-3.0135872135
3p(1/2)	-0.38407140353	-0.38397409949
4p(1/2)	-0.18339057979	-0.18292597631
5p(1/2)	-0.10769454545	-0.10561870733
2p(3/2)	-3.0017458178	-3.0020865461
3p(3/2)	-0.38365982565	-0.38356761821
4p(3/2)	-0.18325079248	-0.18278440143
5p(3/2)	-0.10763095091	-0.10553127977
3d(3/2)	-0.22481498153	-0.22459405689
4d(3/2)	-0.12647690494	-0.12516420657
5d(3/2)	-0.080845062906	-0.065246507339
3d(5/2)	-0.22481875059	-0.22459789211
4d(5/2)	-0.12647920923	-0.12516661214
5d(5/2)	-0.080846385635	-0.065251272585
4f(5/2)	-0.12501099191	-0.12474809116
5f(5/2)	-0.080008914239	-0.078323201197
4f(7/2)	-0.12501046628	-0.12474755971
5f(7/2)	-0.080008654577	-0.078322867613
5g(7/2)	-0.080000373656	-0.079628692742
6g(7/2)	-0.055555838092	-0.038809791027
5g(9/2)	-0.080000203355	-0.079628522041
6g(9/2)	-0.055555739590	-0.038809441027

Table 3.9: The comparison of DF bound orbitals' energies for Ca^+ calculated by using the new method and the analytical method.

Orbital	Orbital Energies(au)	
	(new method)	(analytical)
1s	-150.71745249	-150.74644702
2s	-17.51577683	-17.522504704
3s	-2.79674825	-2.798286073
4s	-0.41663114	-0.4166592736
5s	-0.193315777	-0.19323713874
6s	-0.112034147	-0.11190684897
2p(1/2)	-14.2827952	-14.2832660
3p(1/2)	-1.88735294	-1.88758357
4p(1/2)	-0.309998594	-0.30990627
5p(1/2)	-0.156765658	-0.156551816
6p(1/2)	-0.09519934	-0.0946946996
2p(3/2)	-14.1436158	-14.1447707
3p(3/2)	-1.8718453	-1.87218898
4p(3/2)	-0.3090889	-0.309005119
5p(3/2)	-0.1564329	-0.156218249
6p(3/2)	-0.095040588	-0.094515993
3d(3/2)	-0.330869481	-0.331085459
4d(3/2)	-0.168738372	-0.16852932
5d(3/2)	-0.101351306	-0.100124895
6d(3/2)	-0.067523464	-0.046470480
3d(5/2)	-0.3307596	-0.3309822
4d(5/2)	-0.168664166	-0.16845722
5d(5/2)	-0.101314806	-0.100090263
6d(5/2)	-0.067503287	-0.0463757676
4f(5/2)	-0.1251762324	-0.1250548669
5f(5/2)	-0.0801426261	-0.0795791414
6f(5/2)	-0.055655986	-0.0241280364
4f(7/2)	-0.125176566	-0.12505519
5f(7/2)	-0.080143031	-0.0795795336
6f(7/2)	-0.055656295	-0.0276054744
5g(7/2)	-0.080001362	-0.0797286629
6g(7/2)	-0.055556899	-0.05189128110
5g(9/2)	-0.080001198	-0.079728497
6g(9/2)	-0.055556807	-0.0518911151

Table 3.10: Number of orbitals used in CCSD(T) calculation.

Symmetry	No. of orbitals in each symmetry	numerical orbitals used in the calculation	Gaussian orbitals used in calculation
MgII			
s	11	1,2,..5s	6s,..11s
p(1/2)	11	2p,..5p	6p,..11p
p(3/2)	11	2p,..5p	6p,..11p
d(3/2)	11	3d,..5d	6d,..10d
d(5/2)	11	3d,..5d	6d,..10d
f(5/2)	11	4f,5f	6f,..10f
f(7/2)	11	4f,5f	6f,..10f
g(7/2)	11	5g,6g	7g,..9g
g(9/2)	11	5g,6g	7g,..9g
CaII			
s	12	1,2,..6s	8s,..12s
p(1/2)	11	2p,..6p	7p,..12p
p(3/2)	11	2p,..6p	7p,..12p
d(3/2)	11	3d,..6d	7d,..12d
d(5/2)	11	3d,..6d	7d,..12d
f(5/2)	11	4f,..6f	7f,..13f
f(7/2)	11	4f,..6f	7f,..13f
g(7/2)	11	5g,6g	7g,..9g
g(9/2)	11	5g,6g	7g,..9g

Table 3.11: IP got using nonlinear CCSD in units of (cm^{-1}):

orbital	Experiment	Analytical method	Error(%)	New method	Error (%)
MgII					
3s	-121267.41	-121146.11	0.10	-121146.11	0.10
3p(1/2)	-85597.99	-85516.94	0.09	-85493.85	0.12
3p(3/2)	-85506.44	-85422.94	0.09	-85400.10	0.12
4s	-51462.22	-51401.11	0.11	-51422.62	0.07
3d(3/2)	-49776.09	-49702.80	0.14	-49741.43	0.07
3d(5/2)	-49776.70	-49703.43	0.14	-49741.90	0.07
4p(1/2)	-40646.61	-40536.31	0.27	-40611.47	0.08
4p(3/2)	-40616.11	-40503.86	0.27	-40580.27	0.08
5s	-28481.21	-28331.64	0.52	-28457.77	0.08
4d(3/2)	-27955.31	-27658.29	1.06	-27937.82	0.06
4d(5/2)	-27955.31	-27658.64	1.06	-27938.15	0.06
4f(5/2)	-27467.41	-27409.90	0.21	-27464.47	0.01
4f(7/2)	-27467.41	-27409.78	0.21	-27464.35	0.01
5p(1/2)	-23812.51	-23408.87	1.69	-23793.95	0.07
5p(3/2)	-23798.41	-23389.57	1.71	-23779.82	0.07
CaII					
4s(1/2)	-95748.00	-95974.06	0.24	-95836.80	0.09
3d(3/2)	-82098.87	-82430.28	0.4	-81644.66	0.55
3d(5/2)	-82037.42	-82241.53	0.25	-81465.49	0.69
4p(1/2)	-70556.70	-70719.12	0.23	-70569.94	0.02
4p(3/2)	-70332.84	-70482.08	0.21	-70327.26	0.007
4d(3/2)	-38908.69	-38852.47	0.14	-38710.65	0.05
4d(5/2)	-38889.49	-38816.18	0.18	-38677.34	0.10
5p(1/2)	-35213.00	-35229.60	0.05	-35218.60	0.01
5p(3/2)	-35134.80	-35146.30	0.03	-35133.77	0.00
4f(5/2)	-27691.04	-27670.68	0.07	-27684.85	0.02
4f(7/2)	-27691.04	-27670.69	0.07	-27670.06	0.07

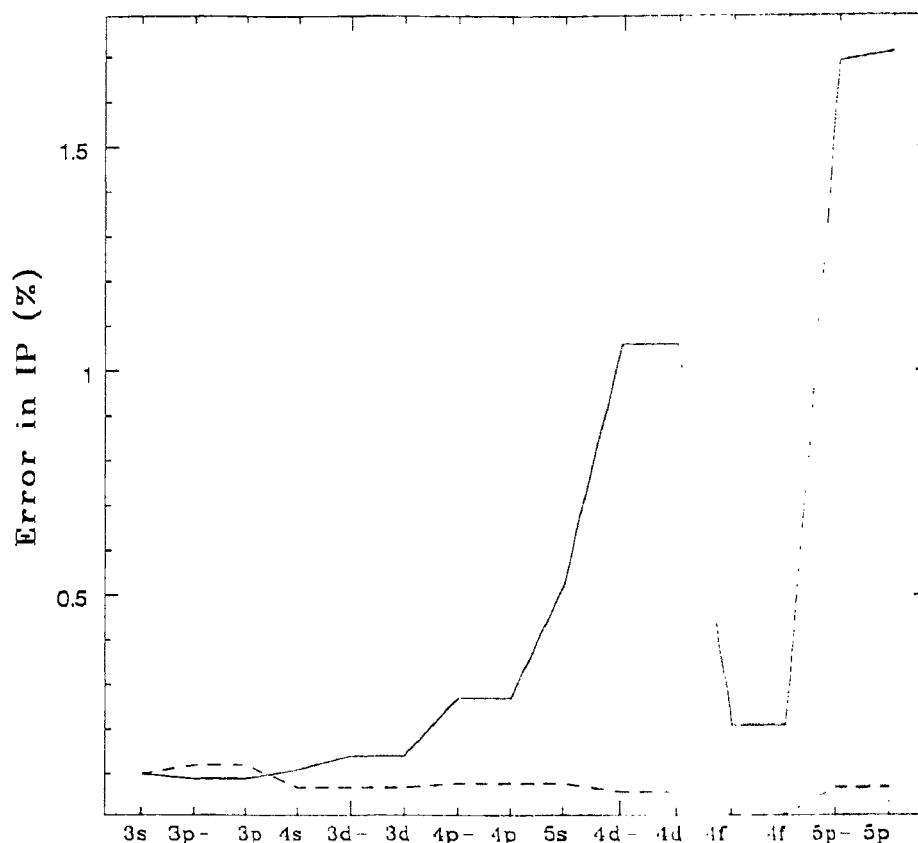


Figure 3.2: Percentage of error in IP results of valence orbitals of MgII obtained using analytical Gaussian basis (solid line) and new basis (dashed line)

Some of the other properties like dipole matrix elements, transition probabilities (which are dominated by the wavefunctions of core orbitals) etc. are more dependent on accurate wavefunctions than IP and EE. We have compared oscillator strength properties for transitions of Mg^+ , which is one of our motivations in this thesis work. Due to lack of accurate experiment on oscillator strengths of many transitions we could not quantify the accuracy all transitions. However, a comparison with the NIST and recent empirical values for a few transition is given in table 3.13 which does show the superiority of the new approach over the analytical one.

Table 3.12: *EE of Mg II got using nonlinear CCSD in units of (au)*

orbital	Experiment	Analytical method	Error(%)	New method	Error (%)
3s(1/2)-3p(1/2)	35669.42	35629.162	0.11	35652.26	0.05
3s(1/2)-3p(3/2)	35760.97	35723.170	0.10	35746.01	0.04
3s(1/2)-5p(1/2)	97454.90	97737.242	0.29	97352.16	0.10
3s(1/2)-5p(3/2)	97469.00	97756.539	0.29	97366.29	0.10
3p(1/2)-3d(3/2)	35821.90	35814.139	0.02	35752.42	0.19
3p(1/2)-5d(3/2)	67751.68	70877.636	4.61	67657.72	0.13
3d(3/2)-5p(1/2)	25963.58	26293.937	1.27	25947.47	0.06
4p(1/2)-4d(3/2)	12691.30	12878.022	1.47	12673.64	0.14
3d(3/2)-4f(5/2)	22308.70	22292.899	0.07	22276.95	0.14
3d(3/2)-5f(5/2)	32198.88	32490.301	0.90	32165.47	0.10

Table 3.13: *Comparison of some oscillator strength results of Mg II*

Transitions	NIST	Empirical	Analytical method	New Method
3s -3p(1/2)	0.313		0.30333	0.30365
3s -3p(3/2)	0.627		0.60845	0.60899
3s -4p(1/2)		3.2(-4)	3.04(-4)	3.32(-4)
3s -4p(3/2)		6.4(-4)	5.28(-4)	5.98(-4)
3d(3/2)-5p(1/2)	0.0039		0.0059	0.00385
4p(1/2)-5d(3/2)	0.083		0.12116	0.09368
3d(3/2)-5f(5/2)	0.165		0.23289	0.15924
4d(3/2)-5f(5/2)	0.80		1.23190	0.79511

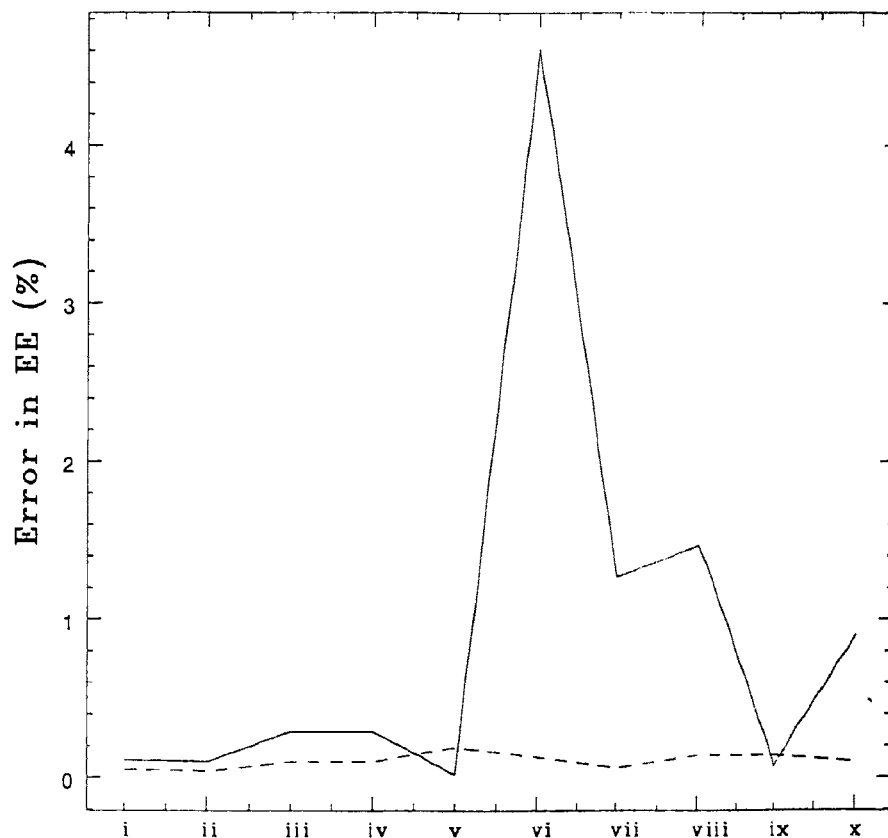


Figure 3.3: Percentage of error in EE results of among the excited states of MgII obtained using analytical Gaussian basis (solid line) and from new basis (dashed line). (i) $3s-3p(1/2)$, (ii) $3s-3p(3/2)$, (iii) $3s-5p(1/1)$, (iv) $3s-5p(3/2)$, (v) $3p(1/2)-3d(3/2)$, (vi) $3p(1/2)-5d(3/2)$, (vii) $3d(3/2)-5p(1/2)$, (viii) $4p(1/2)-4d(3/2)$, (ix) $3d(3/2)-4f(5/2)$ and (x) $3d(3/2)-5f(5/2)$

3.4 Properties of Mg II using the Coupled Cluster Approach

An alkali atom or ion can be treated as a one-electron system to a good approximation consisting of a single valence electron outside the closed shell core. Earlier works on the oscillator strength of the transitions from the valence electrons had been focussed primarily on the strong $ns \rightarrow np$ transitions. The intensity of successive lines $ns \rightarrow n'p$ decreases rapidly with increasing n' . Systematic calculations have shown this behaviour of alkali spectra to be only one example of a general feature of absorption spectra due to the non-hydrogenic character of realistic potentials $V(r)$ [54].

Interstellar ultraviolet lines of Mg II (λ 2796, λ 2803) have been observed as strong interstellar absorption lines in the spectra of early type stars like β , δ , τ Sco and β Cep [55]. The combination of high spectral resolution, photometric precision and sensitivity provided by many recent spectrographs has motivated the study of UV interstellar absorption lines. This study enables a detailed examination of individual absorbing regions in the interstellar medium (ISM). The potential precision of these measurements has also triggered new interest in the determination of atomic properties, particularly the oscillator strength (f-values), required to convert measured line strengths into gas-phase column density. The strong near-UV Mg II lines are generally highly saturated along most interstellar lines outside the local ISM and usually yield extremely uncertain estimates of Mg II column densities in interstellar gas. Since Mg^+ is the dominant form of Mg in the neutral ISM i.e. H I gas, and since Mg is expected to be a significant constituent of interstellar dust grains, the far-UV lines are critical for assessing the role of this important element in the ISM. Along the most interstellar lines -with the exception of those that pass only through the local ISM [56]- the near-UV Mg II $\lambda\lambda$ 2796,2803 lines are strongly saturated and yield limited column density information. The neutral source of accurate Mg II column densities is thus the other pair of observationally accessible Mg II lines, the intrinsically much weaker doublets around λ 1240 discussed below. The determination of column densities of any element in interstellar cloud is obtained from equivalent widths of the observed lines. The equivalent width is calculated from a

curve-of-growth analysis using suitable models for the velocity distribution of the absorbing gas element. Since Mg II is the main ionization stage in ISM, the column density of magnesium is relatively high among other cosmic abundance [55, 57].

Magnesium is one of the most abundant metals and, because it readily condenses into the solid form, it is also likely to be one of the main constituents of interstellar dust. In addition, Mg provides a diagnostic of electron density in the gas phase of the ISM, through the ionization ratio Mg/Mg^+ . An accurate assessment of the importance of Mg in both the gas and the dust must clearly start with accurate column densities.

Analogous to the above two strong lines $3s\ ^2S_{1/2} \rightarrow 4p\ ^2P_{1/2,3/2}$ transitions are also found in the ultraviolet region at approximately 1240 Å. As mentioned earlier this doublet transition is very weak. In 1975, Morton and Hu [58] had shown that with the theoretical value of the oscillator strength of these transitions provided by Black et al. [59] in 1972, the empirical curve of growth for the states of ions does not fit the equivalent widths that arise from the Mg^+ lines (see the figure 3.4). They claimed that the f-value should be a factor of 2.6 larger than the value calculated by Black et al.. But the oscillator strength calculated using various methods shows a steep drop. That is because of a cancellation of the positive and negative contributions to the radial integrals [54].

This part of the thesis is concerned with the calculations of allowed transitions for Mg^+ . We employ the coupled cluster method with singles, doubles and partial triples excitations (CCSD(T)) to calculate these transitions. For a few transitions, we calculate excitation energies and f-values using the MCDF-EOL method, and compare them with the corresponding values obtained using the CCSD(T) method. In recent years, many *ab initio*, semi-empirical and empirical calculations have been performed [60, 61, 62, 63]. The empirical investigation of f-values of Mg II λ , λ 1239, 1240 lines from the absorption towards the star ξ Persei [61] showed total inconsistency with *ab initio* calculations done by Hibbert et al. [60]. The improved *ab initio* calculations by Fleming et al. [63] are not in very good agreement with the recent empirical calculations by Fitzpatrick [62]. Our fully *ab initio*, highly correlated all order many body calculations, however, are consistent with Fitzpatrick's results and the relativistic

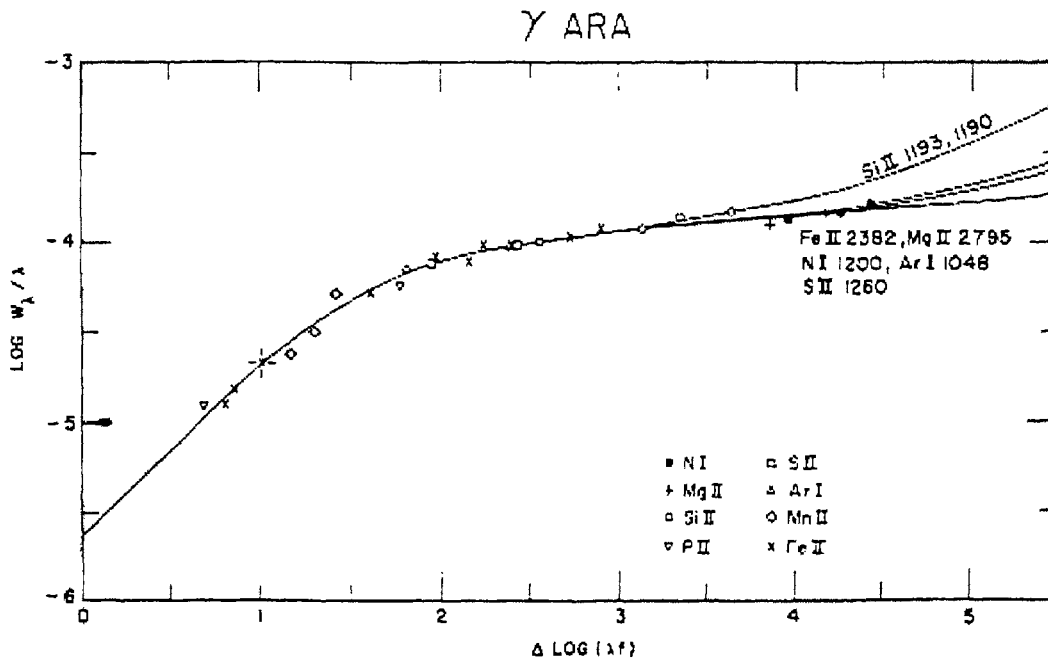


Figure 3.4: Empirical curve of growth for the ion states expected to be most populated in H I regions (taken from reference [58])

SD method [64]. We compare our results with the excitation energies and f-values provided in NIST database (ref: [http:// aeldata.phy.nist.gov/nist_beta.html](http://aeldata.phy.nist.gov/nist_beta.html)), wherever available.

3.4.1 Theory (Coupled Cluster Method)

We start with a N-electron closed shell Dirac-Fock (DF) reference state $|\Phi\rangle$ and write the closed shell ground state as

$$|\Psi\rangle = e^T |\Phi\rangle \quad (3.30)$$

where T is the core electron excitation operator. The Dirac-Coulomb equation

$$He^T |\Phi\rangle = Ee^T |\Phi\rangle \quad (3.31)$$

with

$$H = \sum_i c\alpha_i \cdot \mathbf{p}_i + (\beta_i - 1)mc^2 + V_N + \sum_{i<j} \frac{1}{r_{ij}}$$

leads to the exact ground state energy E of closed shell part of the system. Here α and β are Dirac matrices and V_N is the nuclear potential. However, it is technically

simpler to first define the normal ordered Hamiltonian

$$\tilde{H} \equiv H - \langle \Phi | H | \Phi \rangle = H - E_{DF}, \quad (3.32)$$

where $E_{DF} = \langle \Phi | H | \Phi \rangle$ and then solve the modified Dirac-Coulomb equation

$$\tilde{H}e^T|\Phi\rangle = (E - E_{DF})e^T|\Phi\rangle \equiv E_{corr}e^T|\Phi\rangle. \quad (3.33)$$

After projecting with $\langle \Phi | e^{-T}$ from the left we obtain the correlation energy

$$\langle \Phi | \tilde{H} | \Phi \rangle = E_{corr}, \quad (3.34)$$

where we have defined the dressed, normal ordered Hamiltonian

$$\bar{H} = e^{-T} \tilde{H} e^T. \quad (3.35)$$

If we project any of the excited determinants $\langle \Phi^* | e^{-T}$ from the left of eq. (3.34) we additionally get the set of equations,

$$\langle \Phi^* | \bar{H} | \Phi \rangle = 0. \quad (3.36)$$

Equations (3.34) and (3.36) are the coupled cluster equations. First, the set of equation (3.36) has to be solved to yield the cluster operator T , which then can be used to define the dressed Hamiltonian \bar{H} and to evaluate the correlation energy E_{corr} . In the CCSD (coupled cluster singles and doubles) approximation, the cluster operator T is composed of one- and two-body excitation operators, ie., $T = T_1 + T_2$, which are expressed in terms of second quantization,

$$T = T_1 + T_2 = \sum_{ap} a_p^\dagger a_a t_a^p + \sum_{abpq} a_p^\dagger a_q^\dagger a_b a_a t_{ab}^{pq}$$

After the contraction of the ladder operators [65] and rearranging the indices, eq. (3.36) can be expressed in the following matrix form :

$$A + B(T).T = 0, \quad (3.37)$$

where A is a constant vector which consists of the elements $\langle \Phi^* | \bar{H} | \Phi \rangle$ and the matrix $B(T)$ itself depends on the cluster amplitude so that Eq. (3.37) has to be solved in an iterative procedure.

Because of the spherical symmetry of atoms, the above derived equations can be separated into a radial and an angular part, which considerably reduces the numerical effort. The radial Coulomb integrals, which define the most time consuming part of the computation, can be stored in the computer's RAM, whereas the angular parts, which consist of much simpler algebraic expression, can be evaluated on the fly. The reduction of the angular part greatly simplifies the computational complexity of both DF and post-DF calculations. The corresponding angular factors have been derived by applying the graphical method of the angular momentum adaptation scheme, popularly known as the JLV scheme [66]. The multipole expansion of the Coulomb operator is given in many text books [67, 68, 69]. Similarly, in the $|jm\rangle$ basis, the one- and two-body cluster operator T_1 and T_2 can be expressed as

$$t_a^p = \langle p|T_1|a\rangle = \sum_{j_a m_a} T_1^0(p, a) \delta(j_a, j_p) \delta(m_a, m_p) \quad (3.38)$$

and

$$t_{ab}^{pq} = \langle pq|T_2|ab\rangle = \sum_{\substack{k, j_a m_a j_p m_p \\ j_b m_b j_q m_q}} T_2^k(p, q, a, b) (-1)^{(j_p - m_p + j_q - m_q)} \begin{pmatrix} j_p & k & j_a \\ -m_p & q & m_a \end{pmatrix} \begin{pmatrix} j_q & k & j_b \\ -m_q & q & m_b \end{pmatrix} \quad (3.39)$$

Here, $T_2^k(p, q, a, b)$ denotes the radial cluster operator, depending on the multipole k , the orbital indices a, b (occupied orbitals) and p, q (virtual orbitals), which is multiplied by a phase factor and the appropriate Wigner 3j-symbols. Applying the multipole expansion of the Coulomb operator and the cluster operator T together with the JLV scheme, the angular momentum reduction of the CC equations is straightforward.

In the multipole expansion of the Coulomb matrix element $\langle ab|\frac{1}{r_{12}}|cd\rangle$, only a subset of the multipoles of rank k leads to non-vanishing contributions. The triangular conditions for the angular momenta

$$|j_a - j_c| \leq k \leq j_a + j_c \text{ and } |j_b - j_d| \leq k \leq j_b + j_d \quad (3.40)$$

set the upper- and lower limit for the multipole moment k . Additionally, the overall

parity selection rule demands that the orbital angular momenta satisfy the relation

$$(-1)^{l_a+l_b+l_c+l_d} = 1 \quad (3.41)$$

and from the angular part of the Coulomb matrix element we can derive the additional constraints

$$(-1)^{l_a+l_c+k} = 1 \quad \text{and} \quad (-1)^{l_b+l_d+k} = 1 \quad (3.42)$$

Equations (3.41) and (3.42) imply that for a given set of orbitals $[a, b, c, d]$ either even or odd values for k lead to non-vanishing contributions.

In the case of the angular decomposition of the cluster operator T_2 , the triangular conditions (3.40) are still valid as well as the overall parity selection rule (3.41). Following Liu et al. [70], we call a certain set of allowed configurations $[a, p, q, b, k]$ in the angular decomposition of the two-body operator a *pair channel*.

The eq. (3.42) has to be satisfied only in the CC diagrams which contain the Coulomb integrations in less than third order, (i.e. during the first iteration: then the cluster operator itself represents one order in Coulomb interaction) whereas higher order Coulomb interactions (in latter iteration) lead to coupled angular momenta which violate Eq. (3.42). The excitations, which satisfy eq. (3.42), are called *even-parity pair channels* (EPC). Liu et al. [70] have argued that the EPC provide the dominant contribution to the CC equations and therefore it might be a valid approximation to discard the odd-parity pair channels (OPC) and in this way the number of cluster amplitudes and the computational effort reduces by a factor of half. We have followed this suggestion and applied the CC approach to only EPC cluster amplitudes, which we shall refer to as the CCSD-EPC approximation.

The ground state of Mg^+ contains only one valence electron in the $3s_{1/2}$ orbital. One way to evaluate the ground state energy of Mg^+ is to first compute the correlations within the closed shell system Mg^{++} using the closed shell CC approach and then add another electron to the $3s_{1/2}$ orbital with the help of the open shell CC (OSCC) technique [71]. Similarly, the valence electron can be added to any other orbital to yield excitation energies. In order to add an electron to the k 'th virtual orbital of the DF reference state we define

$$|\Phi_k^{n+1}\rangle \equiv a_k^\dagger |\Phi\rangle \quad (3.43)$$

with the particle creation operator a_k^\dagger . We now define the exact state using excitation operators for both, the core electrons and the valence electron, in the following way

$$|\Psi_k^{n+1}\rangle = e^T \{e^{S_k}\} |\Phi_k^{n+1}\rangle \quad (3.44)$$

where $\{S_k\}$ is the normal ordered valence electron excitation operator [69]. Since S_k has to contain the particle annihilation operator a_k , because of the normal ordering it cannot be connected to any other valence electron excitation operator so that $\{e^{S_k}\}$ reduces to $(1 + S_k)$ and we can write Eq. (3.44) as

$$|\Psi_k^{n+1}\rangle = e^T (1 + S_k) |\Phi_k^{n+1}\rangle \quad (3.45)$$

Following the same procedure as in the closed shell approach, we obtain a set of equations

$$\langle \Phi_k^{n+1} | \bar{H} (1 + S_k) | \Phi_k^{n+1} \rangle = \Delta E_k, \quad (3.46)$$

and

$$\langle \Phi_k^{*,n+1} | \bar{H} (1 + S_k) | \Phi_k^{n+1} \rangle = \Delta E_k \langle \Phi_k^{*,n+1} | S_k | \Phi_k^{n+1} \rangle \quad (3.47)$$

Here, ΔE_k is the difference between the energy of the single reference state $|\Psi_k^{n+1}\rangle$ and the closed shell state $|\Psi\rangle$. [The operators in left hand side of Eq. (3.46) and both sides of Eq. (3.47) are connected]. Eq. (3.47) is nonlinear in S_k because the energy difference ΔE_k itself is a function of S_k . To solve the set of equations, one has to start with an initial estimate for the S_k amplitudes, e.g. $S_1 = 0$ and $S_2 = \frac{\langle pq|v|ab\rangle}{(\epsilon_a + \epsilon_b - \epsilon_p - \epsilon_q)}$. Then one can evaluate the energy difference using Eq. (3.46) and put the result into Eq. (3.47) to solve the S_k amplitudes. This procedure has to be iterated and driven to self-consistency.

The next step in the calculation is the inclusion of the triple excitations in an approximate way shown as,

$$S_{abk}^{pqr} = \frac{\widehat{VT}_2 + \widehat{VS}_2}{\epsilon_a + \epsilon_b + \epsilon_k - \epsilon_p - \epsilon_q - \epsilon_r} \quad (3.48)$$

where S_{abk}^{pqr} is the amplitude corresponding to the simultaneous excitation of orbitals a, b, k to p, q, r ; $\widehat{VT}, \widehat{VS}$ are the contraction of all creation/annihilation operators; and ϵ_i is the orbital energy of the i -th orbital. This contribution is added to the energy obtained using singles and doubles.

The definition of the oscillator strength of a transition from $|\Psi_i\rangle$ to $|\Psi_f\rangle$ is

$$f_L = \frac{2}{3g_i}(\Delta_f - \Delta_i) \times |D_{fi}|^2 \quad (3.49)$$

where $(\Delta_f - \Delta_i)$ is the energy difference between final state and initial state, and the electric dipole moment matrix element D_{fi} is defined as

$$D_{fi} = \frac{\langle \Psi_f | \mathbf{d} | \Psi_i \rangle}{\sqrt{\langle \Psi_f | \Psi_f \rangle} \sqrt{\langle \Psi_i | \Psi_i \rangle}} \quad (3.50)$$

where,

$$\langle \Psi_f | \mathbf{d} | \Psi_i \rangle = \langle \Phi_f^{n+1} | \{e^{-S_f}\} \bar{d} \{e^{S_i}\} | \Phi_i^{n+1} \rangle \quad (3.51)$$

$\bar{d} = e^{-T} d e^T$ and d is the electric dipole moment operator. The connected parts of Eq. (3.50) and Eq. (3.51) will contribute and hence we only compute those parts in our dipole matrix element calculations.

3.4.2 Results and Discussions

The generation of single particle orbitals used in this calculations is discussed in the previous section (Sec. 3.3). The starting point of this calculation is the generation of DF orbitals for the Mg^{++} core. Though we have used a large basis space for the generation of the orbitals, we restrict the number of basis orbitals for the coupled cluster calculation by imposing an upper bound in energy for all single particle orbitals of s-, $p_{1/2}$ -, $p_{3/2}$ - symmetries by 1500 a.u., $d_{3/2}$ -, $d_{5/2}$ -, $f_{5/2}$ -, $f_{7/2}$ - symmetries by 500 a.u. and $g_{7/2}$, $g_{9/2}$ symmetries by 5 a.u.. This is done to reduce the huge memory required to store the matrix elements of the dressed operator \bar{H} and the two electron coulomb interaction in the main memory. We consider all the singles, doubles and partial triple excitations from the core in this calculations.

Our calculated ionization potential of the 3s orbital is $121117.91 \text{ cm}^{-1}$, which differs from the experimental value by 0.12%. In table 3.14 we present the excitation energies of the doublet states calculated using the CCSD(T) and the MCDF-EOL method, and compare them with the NIST data and values obtained from other calculations [60, 63, 64]. The accuracy of the results obtained using the MCDF-EOL and the all order relativistic SD method [64] are comparable with the CCSD(T) results. However, it is difficult to obtain convergence with the MCDF-EOL method

for more than a few states. Therefore, we were not able to calculate the electronic properties for higher excited states using that approach. Safronova et al. [64] have shown that the effect of Breit interaction is almost negligible. A moderate and large CI calculations were performed by Hibbert et al. [60] and Fleming et al. [63] respectively to calculate the excitation energies. However, the results of those calculations do not agree as well with the NIST data as our CCSD(T) calculations. This may be because of the advantages of the CCSD(T) method over the CI method as discussed in the review article by Bartlett [65]. Since single particle DF equations produce bound orbitals up to 6s, 6p, 5d, 5f and 6g for their respective symmetries, only the states made of those bound orbitals are presented in table 3.14.

Table 3.14: *Excitation Energies from the ground state in cm^{-1}*

States	multiplet	NIST	CCSD(T)	MCDF	Others
$2p^6 3p$	$^2P_{1/2}$	35669.31	35652.26	35673.05	35489.04 ^a , 35730.47 ^b , 35663.5 ^c
	$^2P_{3/2}$	35760.88	35746.01	35730.84	35754.8 ^c
$2p^6 4s$	$^2S_{1/2}$	69804.95	69723.49	69832.32	68827.24 ^a , 69804.4 ^c
$2p^6 3d$	$^2D_{3/2}$	71491.06	71404.68		71494.8 ^c
	$^2D_{5/2}$	71490.19	71404.21		71493.9 ^c
$2p^6 4p$	$^2P_{1/2}$	80619.50	80534.64	80492.37	79581.50 ^a , 80174.08 ^b
	$^2P_{3/2}$	80650.02	80565.83	80580.59	
$2p^6 5s$	$^2S_{1/2}$	92790.51	92688.34		91542.87 ^a
$2p^6 4d$	$^2D_{3/2}$	93311.11	93208.29		
	$^2D_{5/2}$	93310.59	93207.96		
$2p^6 4f$	$^2F_{5/2}$	93799.63	93681.63		
	$^2D_{7/2}$	93899.75	93681.76		
$2p^6 5p$	$^2P_{1/2}$	97455.12	97352.16		96195.73 ^a
	$^2P_{3/2}$	97468.92	97366.30		
$2p^6 6s$	$^2S_{1/2}$	103196.75	103108.93		101858.17 ^a
$2p^6 5d$	$^2D_{3/2}$	103420.00	103309.98		
	$^2D_{5/2}$	103419.70	103309.79		
$2p^6 5f$	$^2F_{5/2}$	103689.86	103570.15		
	$^2D_{7/2}$	103689.92	103570.21		
$2p^6 6p$	$^2P_{1/2}$	105622.34	105516.19		
	$^2P_{3/2}$	105629.72	105523.95		

a : Configuration method [60]; b : Superposition of configuration method [63]

c : Relativistic SD method [64]

One of the motivations of this work is to calculate $3s - 4p$ transitions with high accuracy. Fano and Cooper [54] argued that this transition amplitude should be small. Fleming et al. [63] have recently carried out a large scale non-relativistic CI calculation for this transition. They obtained a value of oscillator strength (8.33×10^{-4}); higher than their value calculated earlier (3.7×10^{-4}) [60]. In our calculation, we have obtained a better description of electron correlation by taking the excitations of all the electrons from the core into a large virtual space than them. Our results agrees very well with Fitzpatrick's [62] results obtained through an empirical method. But it smaller by about two and half times than Morton and Hu's [58] empirical value. This is shown in table 3.15 along with a comparison of oscillator strengths of $3s - 3p$ and $3s - 4p$ transitions with the values obtained from NIST database. Safronova et al. [64] have calculated $3s - 3p$ transitions by using a method which includes single and double excitations of the HF ground state to all orders in perturbation theory, which they called the relativistic SD method. Their calculated oscillator strengths are in good agreement with our.

Table 3.15: Oscillator Strengths of $3s - 3p$ and $3s - 4p$ transitions

Transitions	Multiplets	NIST	CCSD	Rel. SD	Empirical
$3s - 3p$	${}^2S_{1/2} - {}^2P_{1/2}$	0.306	0.30365	0.30403	
	${}^2S_{1/2} - {}^2P_{3/2}$	0.609	0.60899	0.60989	
$3s - 4p$	${}^2S_{1/2} - {}^2P_{1/2}$	7.7(-5)	3.322(-4)		3.2(-4)
	${}^2S_{1/2} - {}^2P_{3/2}$	1.5(-4)	5.980(-4)		6.4(-4)

In table 3.16, we give the oscillator strengths of all the possible doublet allowed transitions, $ms - np$, $mp - nd$ and $md - nf$ for various m and n calculated using the CCSD(T) method. A comparison is made with the NIST data, and a few MBPT [64], wherever available and MCDF data, wherever calculated. In this table we have presented the oscillator strengths of many transitions for which we do not find values in the literature to compare. Almost all the values obtained from NIST database shown here are compiled from the earlier non-relativistic semi-empirical calculations or relativistic HF type calculations (references are available in the web-site whose

address was given earlier). So there are small differences between all the f-values obtained from NIST database and our calculations using the CCSD(T) method. But there is good agreement between our results and those of relativistic SD [64] calculations, wherever available.

Table 3.16: Oscillator Strengths of various transitions

Transitions	Multiplets	NIST	CCSD	MCDF	Rel. SD
3s – 3p	$^2S_{1/2} - ^2P_{1/2}$	0.306	0.30365	0.30320	0.30403
	$^2S_{1/2} - ^2P_{3/2}$	0.609	0.60899	0.60952	0.60989
3s – 4p	$^2S_{1/2} - ^2P_{1/2}$	7.7(-5)	3.322(-4)		
	$^2S_{1/2} - ^2P_{3/2}$	1.5(-4)	5.980(-4)		
3s – 5p	$^2S_{1/2} - ^2P_{1/2}$	3.3(-3)	3.921(-4)		
	$^2S_{1/2} - ^2P_{3/2}$	6.6(-3)	7.427(-4)		
3s – 6p	$^2S_{1/2} - ^2P_{1/2}$		7.593(-6)		
	$^2S_{1/2} - ^2P_{3/2}$		1.953(-5)		
3p – 4s	$^2P_{1/2} - ^2S_{1/2}$	0.138	0.14561	0.1533	0.14427
	$^2P_{3/2} - ^2S_{1/2}$	0.139	0.14563	0.1595	0.14943
3p – 5s	$^2P_{1/2} - ^2S_{1/2}$		0.01763		
	$^2P_{3/2} - ^2S_{1/2}$		0.01767		
3p – 6s	$^2P_{1/2} - ^2S_{1/2}$		6.027(-3)		
	$^2P_{3/2} - ^2S_{1/2}$		6.066(-3)		
3p – 3d	$^2P_{1/2} - ^2D_{3/2}$	0.920	0.93669		0.94086
	$^2P_{3/2} - ^2D_{3/2}$	0.0919	0.09358		0.09409
	$^2P_{3/2} - ^2D_{5/2}$	0.828	0.84226		0.84716
3p – 4d	$^2P_{1/2} - ^2D_{3/2}$		3.8462(-2)		
	$^2P_{3/2} - ^2D_{3/2}$		3.844(-3)		
	$^2P_{3/2} - ^2D_{5/2}$		3.8463(-2)		
3p – 5d	$^2P_{1/2} - ^2D_{3/2}$		1.236(-2)		
	$^2P_{3/2} - ^2D_{3/2}$		1.265(-3)		
	$^2P_{3/2} - ^2D_{5/2}$		1.139(-2)		

(Continued from the previous page)

Transitions	Multiplets	NIST	CCSD	MCDF	Rel. SD
3d - 4p	$^2D_{3/2} - ^2P_{1/2}$	0.149	0.15131		
	$^2D_{3/2} - ^2P_{3/2}$	0.029	0.03034		
	$^2D_{5/2} - ^2P_{3/2}$	0.178	0.18105		
3d - 5p	$^2D_{3/2} - ^2P_{1/2}$	0.0039	3.886(-3)		
	$^2D_{3/2} - ^2P_{3/2}$	7.8(-4)	7.814(-4)		
	$^2D_{5/2} - ^2P_{3/2}$	0.0047	4.659(-3)		
3d - 4f	$^2D_{3/2} - ^2F_{5/2}$	0.95	0.97246		
	$^2D_{5/2} - ^2F_{5/2}$		0.04605		
	$^2D_{5/2} - ^2F_{7/2}$		0.92115		
3d - 5f	$^2D_{3/2} - ^2F_{5/2}$	0.164	0.15926		
	$^2D_{5/2} - ^2F_{5/2}$		7.542(-3)		
	$^2D_{5/2} - ^2F_{7/2}$		0.15085		
4s - 4p	$^2S_{1/2} - ^2P_{1/2}$	0.456	0.46478	0.442	
	$^2S_{1/2} - ^2P_{3/2}$	0.91	0.93224	0.843	
4s - 5p	$^2S_{1/2} - ^2P_{1/2}$	3.4(-4)	8.366(-4)		
	$^2S_{1/2} - ^2P_{3/2}$	6.9(-4)	1.745(-3)		
4s - 6p	$^2S_{1/2} - ^2P_{1/2}$		9.922(-5)		
	$^2S_{1/2} - ^2P_{3/2}$		2.237(-4)		
4p - 4d	$^2P_{1/2} - ^2D_{3/2}$	1.23	1.22868		
	$^2P_{3/2} - ^2D_{3/2}$	0.124	0.12285		
	$^2P_{3/2} - ^2D_{5/2}$	1.11	1.10562		
4p - 5s	$^2P_{1/2} - ^2S_{1/2}$	0.263	0.26105		
	$^2P_{3/2} - ^2S_{1/2}$	0.264	0.26108		
4p - 6s	$^2P_{1/2} - ^2S_{1/2}$	0.0315	0.02987		
	$^2P_{3/2} - ^2S_{1/2}$	0.0315	0.03002		
4p - 5d	$^2P_{1/2} - ^2D_{3/2}$	0.083	0.09699		
	$^2P_{3/2} - ^2D_{3/2}$	0.005	9.743(-3)		
	$^2P_{3/2} - ^2D_{5/2}$	0.074	0.08772		
4d - 4f	$^2D_{3/2} - ^2F_{5/2}$		0.05596		
	$^2D_{5/2} - ^2F_{5/2}$		2.654(-3)		
	$^2D_{5/2} - ^2F_{7/2}$		0.05309		

(Continued from the previous page)

Transitions	Multiplets	NIST	CCSD	MCDF	Rel. SD
4d - 5p	${}^2D_{3/2} - {}^2P_{1/2}$		0.30105		
	${}^2D_{3/2} - {}^2P_{3/2}$		0.06029		
	${}^2D_{5/2} - {}^2P_{3/2}$		0.36001		
4d - 6p	${}^2D_{3/2} - {}^2P_{1/2}$				
	${}^2D_{3/2} - {}^2P_{3/2}$				
	${}^2D_{5/2} - {}^2P_{3/2}$				
4d - 5f	${}^2D_{3/2} - {}^2F_{5/2}$	0.80	0.79765		
	${}^2D_{5/2} - {}^2F_{5/2}$		37782(-2)		
	${}^2D_{5/2} - {}^2F_{7/2}$		0.75569		
5s - 5p	${}^2S_{1/2} - {}^2P_{1/2}$		0.61204		
	${}^2S_{1/2} - {}^2P_{3/2}$		1.22678		
5s - 6p	${}^2S_{1/2} - {}^2P_{1/2}$		2.771(-3)		
	${}^2S_{1/2} - {}^2P_{3/2}$		5.789(-3)		
5p - 6s	${}^2P_{1/2} - {}^2S_{1/2}$		0.37715		
	${}^2P_{3/2} - {}^2S_{1/2}$		0.37964		
5p - 5d	${}^2P_{1/2} - {}^2D_{3/2}$		1.88856		
	${}^2P_{3/2} - {}^2D_{3/2}$		0.19083		
	${}^2P_{3/2} - {}^2D_{5/2}$		1.71708		
5d - 6p	${}^2D_{3/2} - {}^2P_{1/2}$				
	${}^2D_{3/2} - {}^2P_{3/2}$				
	${}^2D_{5/2} - {}^2P_{3/2}$				
5d - 5f	${}^2D_{3/2} - {}^2F_{5/2}$		0.11006		
	${}^2D_{5/2} - {}^2F_{5/2}$		5.416(-3)		
	${}^2D_{5/2} - {}^2F_{7/2}$		0.10834		
6s - 6p	${}^2S_{1/2} - {}^2P_{1/2}$		0.76690		
	${}^2S_{1/2} - {}^2P_{3/2}$		1.53734		

3.5 Conclusion

The MCDF-EOL method is applied to compute the excitation energies and the M2 transition probabilities of Be-like ions in the first section of this chapter. Apart from doubly ionized carbon, it is the first time this method has been applied to the calculation of the M2 transition probabilities for Be-like ions. The accuracy of the computed excitation energies is in excellent agreement with the NIST database. This work highlights a number of unique and desirable features of the MCDF-EOL method for highly ionized atoms. For instance, the MCDF-EOL calculations yield results with reasonable accuracy using fewer number of valence orbitals than with some other schemes. Also the importance of the Breit interaction is highlighted. For systems like Mg^+ and Ca^+ , any kind of large basis which is complete should give results close to the experimental values. But, the generation of a complete basis set is hard even for these small system. So one has to rely on FBSE. In all the FBSE method applied to atomic and molecular systems for solving DF equation, the optimization of orbitals' wavefunctions is done with respect to the numerical orbitals by suitably changing the parameters defined in any form of the analytical basis. Therefore, it is better to use numerical wavefunctions for those orbitals of interest, instead of wavefunctions obtained from the analytical basis. In addition, it is possible to get a few low lying bound valence orbitals with the new approach, which may not be bound if conventional analytical basis set expansion approaches are used. The accuracy of these orbitals is very important when calculations of interest are bound to bound transitions. In conclusion to the second section of this chapter, if one likes to use FBSE, the new method of generating basis will be one of the best approach to achieve better accuracy for any property of the systems.

In the previous section of this chapter focuses on the oscillator strengths for $3s - 4p$ transition as well as all allowed bound-bound transitions among the doublet states. Though the value of our calculated oscillator strength for $3s - 4p$ is larger than earlier calculated values using other methods, it is still a factor of ~ 2.5 smaller than the value expected by Morton and Hu [58] to fit the empirical curve of growth with the particular parameters $b=7.0$ and $\log N = 15.37$. However, it is in excellent agreement with the another recent empirical result obtained by Fitzpatrick [62]. Therefore, an

accurate experimental measurement is urgently needed. Our calculated excitation energies of various states have high accuracy. There is excellent agreement of our calculated oscillator strengths using the CCSD(T) method and the MCDF method (tested for a few transitions) with those obtained using the relativistic SD method wherever available. Among the features of our CCSD(T) calculations is the approximate inclusion of triple excitations from all the core orbitals into a large virtual space, leading to more accurate and reliable results.

References

- [1] I. P. Grant and H. M. Quiney, *Adv. At. Mol. Phys.*, **23**, 37 (1988)
- [2] P. Indelicato, *Phys. Rev. A*, **51**, 1132 (1995)
- [3] M. J. Seaton, in *Atoms and Molecules in Astrophysics*, ed. Carson and Roberts, Academic Press, London, (1972)
- [4] M Mizushima, *Phys. Rev.*, **134**, A883 (1964)
- [5] R. W. Munro, A. K. Dupree and G. L. Witbroe, *Sol. Phys.*, **19**, 347 (1971)
- [6] C. Jordan, in *Highlights of Astronomy*, C. de Jager (Ed.), pp.519, Reidel Publ. Dordrecht, The Netherlands (1971)
- [7] P. L. Dufton, K. A. Berrington, P. G. Burke and A. E. Kingston, *Astron. Astrophys.*, **62**, 111 (1978)
- [8] M. Malinovsky, *Astron. Astrophys.*, **43**, 101 (1975)
- [9] C. Jordan, *Astron. Astrophys.*, **34**, 69 (1974)
- [10] A. K. Dupree, P. V. Foukal and C. Jordan. *Astrophys. J.*, **209**, 621 (1976)
- [11] M. Louergue and H. Nussbaumer, *Astron. Astrophys.*, **51**, 163 (1976)
- [12] H. P. Mühlethaler and H. Nussbaumer, *Astron. Astrophys.*, **48**, 109 (1976)
- [13] R. C. Bohlin, P. A. Marioni and T. P. Stecher, *Astrophys. J.*, **202**, 415 (1975)
- [14] A. F. Kholtygin, *Astron. & Astrophys.*, **329**, 691 (1998)

-
- [15] P. A. Strittmater and R. E. Williams, *Annu. Rev. Astron. Astrophys.*, **14**, 307 (1976)
- [16] M. Hack, J. B. Hutchings, Y. Kondo, G. E. McCluskey and M. K. Tulloch, *Astrophys. J.*, **206**, 777 (1976)
- [17] D. C. Morton, *Astrophys. J.*, **203**, 386 (1976)
- [18] T. P. Snow and D. C. Morton, *Astrophys. J. Suppl.*, **32**, 429 (1976)
- [19] A. K. Dupree, *Astrophys. J. Lett.*, **200**, L27 (1975)
- [20] C. Rola and G. Stasinska, *Astron. & Astrophys.*, **282**, 199 (1994)
- [21] P. Jönsson and C. Froese Fischer, *Phys. Rev. A*, **57**, 4967 (1998)
- [22] R. H. Garstang, *Astrophys. J.*, **148**, 579 (1967)
- [23] R. Glass, *Astrophysics & Space Sc.*, **87**, 41 (1982)
- [24] H.P. Mühlethaler and H. Nussbaumer, *Astron. & Astrophys.*, **48**, 109 (1976)
- [25] H. Nussbaumer and P.J. Storey, *Astron. & Astrophys.*, **64**, 139 (1978)
- [26] C. D. Lin, C. Laughlin and G. A. Victor, *Astrophys. J.*, **220**, 734 (1978)
- [27] C. Laughlin, *J. Phys. B: Atom. Molec. Phys.*, **8**, 842 (1975)
- [28] R. Marrus & P. J. Mohr, *Adv. in Atomic & Molecular Phys.*, **14**, 181 (1978)
- [29] K. G. Dyall et al., *Comput. Phys. Commun.* **55**, 425 (1989)
- [30] G. Breit, *Phys. Rev.*, **34**, 553 (1929)
- [31] G. Breit, *Phys. Rev.*, **36**, 383 (1930)
- [32] G. Breit, *Phys. Rev.*, **39**, 616 (1932)
- [33] I. P. Grant and B. J. McKenzie, *J. Phys. B*, **13**, 2671 (1980)
- [34] I. P. Grant, *J. Phys. B*, **7**, 1458 (1974)

- [35] I P Grant, B J McKenzie, P H Norrington, D F Mayers and N C Pyper, *Comp. Phys. Comm.*, **21**, 207 (1980)
- [36] G Tachiev and C Froese Fischer, *J. Phys. B*, **32**, 5805 (1999)
- [37] A. Mohanty and F. Clementi, *Modern Techniques in Computational Chemistry: MOTECC-90*, pp. 141.
- [38] I.P. Grant and H.M. Quiney, *Adv. in Atom. and Mol. Phys.*, **23**, 37 (1988) and the references therein,
- [39] Y. Ishikawa, R.C. Binning and K.M. Sando, *Chem. Phys. Letters*, **101**, 111 (1983)
- [40] T. Helgaker and P.T. Taylor, *Modern Electronic Structure Theory*, ed. D.R. Yarkony, pp. 725 (1995)
- [41] P. Čársky and M. Urban, *Ab initio calculations: methods and applications in chemistry. Lecture Notes in Chemistry 16*. Springer-Verlag, Berlin.
- [42] R. C. Raffenetti, *J. Chem. Phys.*, **59**, 5936 (1972)
- [43] O. Matsuoka and S. Huzinaga, *Chem. Phys. Lett.*, **140**, 567 (1987); S. Okada and O. Matsuoka, *J. Chem. Phys.*, **91**, 4193 (1989); O. Matsuoka and S. Okada, *Chem. Phys. Letts.*, **155** 547 (1989).
- [44] E. Clementi and G. Corongio, *Chem. Phys. Lett.*, **90**, 359 (1982)
- [45] I P Grant and B J McKenzie, *J. Phys. B*, **13**, 2671 (1980)
- [46] R.K. Chaudhuri, P.K. Panda and B.P. Das, *Phys. Rev. A*, **59**, 1187 (1999)
- [47] Y.K.Kim, *Phys.Rev.*, **154**, 17(1967)
- [48] These works are compiled in a book by P.Pyykko, *Relativistic theory of atoms and molecules*(Springer,Berlin,1986)
- [49] F.A. Parpia, C.F.Fischer, and I.P. Grant(unpublished)

- [50] V.A.Dzuba,et.al.,Phys.Lett/A,141,147(1989),S.A.Blundell,et.al.,
Phys.Rev.A.,43,3407(1991),V.A.Dzuba,et.al.,Phys.Rev.A.,51,3454 (1995)
- [51] H.Merlitz,Geetha G.,R.K. Chaudhuri,B.P.Das, Uttam Sinha Mahapatra and
Debashis Mukherjee, Phys.Rev A(in press),
- [52] Geetha G., H.Merlitz, S. Majumder, R.K. Chaudhuri, B.P.Das, Uttam Sinha
Mahapatra and Debashis Mukherjee(to be submitted)
- [53] E.Eliav, U. Kaldor and Ishikawa, Phys. Rev.A.,53,3050,(1998).
- [54] U. Fano and J. W. Cooper, *Rev. Mod. Phys.*, 40, 441 (1968)
- [55] B. Bates, P.P.D. Carson, P.L. Dufton, C. D. McKeith, *Astron. Astrophys.*, 49,
81 (1976)
- [56] J.L. Linsky and B.E. Wood, *Astrophys. J.*, 463, 254 (1996)
- [57] M.Pettini, A.Boksenberg, B. Bates, R. F. McCaughan and C.D. McKeith, *Astron. Astrphys.*, 61, 839 (1977)
- [58] D. C. Morton and E. M. Hu, *Astrophys. J.*, 202, 638 (1975)
- [59] J.H. Black, J.C. Weisheit and E. Laviana, *Astrophys. J.*, 177, 567 (1972)
- [60] A. Hibbert, P.L.Dufton, M.J. Murray and D.G. York, *Mon. Not. R. astr. Soc.*,
205, 535 (1983)
- [61] U.J. Sofia, J.A. Cardelli and B.D. Savage, *Astrophys. J.*,430, 650 (1994)
- [62] E. L. Fitzpatrick, *Astrophys. J.*, 482, L199 (1997)
- [63] J. Fleming, A. Hibbert, K.L. Bell and Vaeck, *Mon. not. R. Astron. Soc.*, 300,
767 (1998)
- [64] M.S. Safronova, A. Derevianko and W.R. Johnson, *Phys. Rev. A*, 58, 1016
(1998)
- [65] R.J. Bartlett in *Modern Electronic Structure Theory*, edited by D.R. Yarkony,
World Scientific, Vol. II, pp 1047 (1995)

-
- [66] A.P. Jucys (Yutsis), I.B. Levinson and V.V. Vanagas, *Mathematical Apparatus of the Theory Angular Momentum*, Israel Program for Scientific Translation. Jerusalem, (1962)
- [67] E. Baz and E.B. Castel, *Graphical Methods of Spin Algebras in Atomic, Nuclear and Particle Physics*, Dekker, NY (1972)
- [68] P.G.H. Sandars, in *Atomic Physics and Astrophysics*, edited by M. Chretien and E. Lipworth, Gordon and Breach, London, (1971).
- [69] I. Lindgren and J. Morrison, in *Atomic Many-body Theory*, edited by G. Ecker. Lambropoulos, and H. Walther, Vol. 3, Springer-Verlag, Berlin (1985)
- [70] Z.W. Liu and H.P. Kelly, *Phys. Rev. A*, **43**, 3305 (1991)
- [71] H. Merlitz, Rajat K. Chaudhuri, Prafulla K. Panda, Uttam Sinha Mahapatra and Debashis Mukherjee, *Application of the Relativistic Coupled Cluster Method to Transition Probabilities : Boron Isoelectronic Sequence*, submitted to *Phys. Rev. A*.

Chapter 4

Applications of Molecular Studies to Astrophysics

4.1 Introduction

The study of atomic states and spectra proceeds along well-established directions, relying heavily on the concept of an average central symmetric field dominated by the nuclear field. The fact that the nucleus is a particle in motion can be ignored (or taken into account by the “reduced mass” of the electron) and the resulting description (Hartree-Fock) provides a very good basis for analysis of spectra and for further refinements (electron correlation effects, fine structures, hyperfine structures) [1].

In the case of molecules the situation is very different, for several reasons. The electrons in molecules move in an average potential field which is not even approximately central. For diatomic and linear polyatomic molecules, the field is axially symmetric; and the only ‘good’ quantum number related to this symmetry is the component of angular momentum along the symmetry axis. For a general polyatomic molecule even this point groups-symmetry is lacking, and only certain reflection and inversion symmetries remain [2]. Also, the nuclear motion is important for molecules. The Born-Oppenheimer approximation enables the electrons of the system to be described independently of the nuclear motion. This approximation is justified by

the fact that the heavy particle motions are slow and the quantum states adjust adiabatically to the rotations and vibrations of the nuclei. Because of this, the rotation and vibration of the molecules can be discussed separately from electronic motions. The approximation that have been there by made, however, give rise to certain typical “relative motion” effects of the electrons with respect to the nuclei and these do not have analogue in the atomic spectra. These rotations and vibrations of the nuclei are even important in the radio frequency spectra.

Observational data for several transitions of a molecular species, from levels covering a wide energy range, are very useful for the studies of excitation conditions. Besides more accurate measures of molecular abundances, this information may provide useful estimates of cloud temperatures. If we assume (i) emission regions covering the antenna beam, (ii) optically thin lines (of frequencies ν), and (iii) excitation temperatures $|T_x| \gg T_{BG}$ and $h\nu/k$, where T_{BG} is the background brightness, the following relation is valid between the observed integrated main beam brightness temperature ($\int T_{MB} dv$) and the population (column density) N_l of the relevant lower state molecular energy level E_l , for each observed transition,

$$\frac{N_l}{g_l} = \frac{3k}{8\pi^3 \mu^2} \frac{\int T_{MB} dv}{\nu S_{ul}}$$

Here g_l is the level degeneracy and S_{ul} the line strength. μ , h and k denote the dipole moment, and the Plank and Boltzmann constants, respectively. Therefore, accurate dipole moments and line strengths calculations are very important to estimate molecular abundance of the clouds.

The study of interstellar molecules began with the discovery of narrow absorption features in the ultra-violet spectra of a few distant stars, in the early thirties. Interstellar absorption lines of CN, CH and CH⁺ [3, 4, 5] were identified. Observation of these radicals revealed for the first time interesting chemical processes in the diffuse interstellar clouds. Both these and later radio studies of interstellar molecules have provided important clues for more profound physical properties of the Galaxy and beyond.

A few years ago, gas-phase interstellar chemical models of quiescent molecular clouds were able to reproduce the observed abundances of many small and complex species at so called early times of 10^5 - 10^6 years [6]. But recent models, however, have

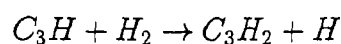
difficulty in reproducing the abundances of complex species [7, 8]. The cause of this failure is the introduction of many rapid, but highly uncertain neutral-neutral reactions. It had been assumed in the earlier models that most of the neutral-neutral reactions do not proceed at significant rates at quiescent cloud temperature (10K). Reaction between stable neutral species are undoubtedly slow at low temperatures, since such reactions have short-range potential barrier which prohibit their occurrence at low temperatures. There was, however, little evidence for the slowness of neutral reactions in which both the reactants are radicals, a term usually signifying an “open shell” atom or molecule with a non-singlet electronic state. Indeed, many oxygen atom-neutral radical reactions are now known to proceed rapidly at room temperature [9]. Also, rapid room temperature reactions involving neutral carbon atoms and stable hydrocarbons have been investigated by various groups [10, 11, 12]. Neutral reactions that are rapid at room temperature may well be rapid at low temperature. The inclusion of neutral-neutral reactions into gas-phase chemical models of dense interstellar clouds has occurred gradually.

The dark molecular cloud (DMC) within the Taurus molecular cloud 1 (TMC-1) is a cold cloud in the solar vicinity (~ 140 pc) [13]. IRC+10216 is an isolated and highly evolved star with a huge circumstellar shell, composed of expelled and at least partly processed matter. Despite its faint visual appearance ($m_v \sim 18$), it has been classified as a carbon star of spectral type C9. The circumstellar envelope (CSE) of the IRC+10216 contains over 40 molecular species [14]. Both the objects have extensively been studied by a number of radio astronomical observations and have been utilized for critical tests of gas-phase chemical models which have ever been postulated. There have been a number of attempts to clarify the detailed chemical processes which produce these molecules. The most prominent chemical feature common to these objects are the hydrocarbons.

After Bettens and Brown [7] remarkable work on carbon atom-hydrocarbon reactions, many studies [12, 15] were done to show that the dispersion interaction between the two neutral reactants dominates at long-range and is the cause of a large reaction rate coefficient at room temperature and below. Despite the assumed synthetic nature of the carbon atom-neutral hydrocarbon reactions included by Herbst

et al. [8], they obtained abundances of complex species far below the observed values for well-studied dark clouds such as TMC-1 and L134N.

The analyses of Bettens and Brown [7], and Herbst et al. [8] may underestimate the abundances of complex molecules for several reasons. First, Herbst has suggested that some of the destructive nature of the neutral-neutral reactions could be mitigated by inclusion of so-called hydrogen atoms abstraction reactions (HAARs) between hydrocarbon radicals and molecular hydrogen. One of the important example is this destruction mechanism of C_3H radical. C_3H which is produced via the carbon-insertion reaction between carbon atoms and acetylene could be converted into C_3H_2 via HAAR

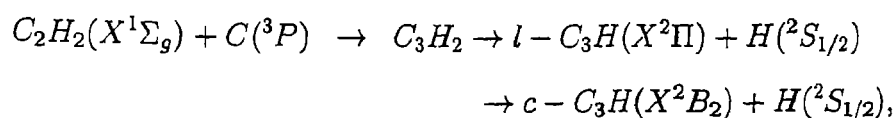


which would compete with the destructive reaction between C_3H and atomic oxygen. Subsequent reactions in which carbon insertion and hydrogenation alternate could produce large quantities of hydrocarbon efficiently. Reactions between the hydrocarbon radicals and molecular hydrogen need not occur rapidly for such an effect to become important [8] because there is so much H_2 in the interstellar gas. Secondly, their models suffer from sparse laboratory and theoretical data of electronic structure and reaction products. These models cannot elucidate the contribution to distinct structural isomers such as linear or cyclic C_3H . There are few calculations on these isomers and most of them have large uncertainty. Because of these, these models may not be able to explain why the interstellar abundance ratio of the above two isomers is unity in TMC-1 compared to 0.2 ± 0.1 around IRC+10216. Hence the structure and formation of interstellar C_3H isomers remains to be resolved. This has motivated us to take up the following project where we use a rigorous and accurate non-relativistic *ab initio* method (H^v) to calculate the ionization potential, excitation energies, oscillator strengths and dipole moments of C_3H isomers.

4.2 Determination of Properties of Propynlidyne Isomers using the H^v Method

The understanding of hydrocarbon syntheses in interstellar clouds provides one stimulus for increased recent interest in studying the hydrocarbon radical C_3H and its isomers. The linear C_3H radical (propynlidyne) was first detected in TMC-1 and the carbon star IRC+10216 by Thaddeus *et al.* [16] using microwave spectroscopy and by Gottlieb *et al.* [17] in the laboratory. Two years later Yamamoto *et al.* [18] discovered the cyclic isomer (cyclopropynlidyne) $c-C_3H$ in TMC-1. Standard reaction models, based on radiative association, dissociative recombination, and exothermic ion-molecule processes [19, 20], fail to reproduce the observed number densities and isomer ratios for the linear and cyclic C_3H isomers.

The computation of this isomer energy difference has been a major theoretical challenge. The earliest UHF/6-31G** *ab initio* calculations for C_3H by Yamamoto *et al.* [18] provided the belief that cyclic- C_3H is less stable than the linear C_3H isomer. However, this initial belief has been reversed by subsequent state-of-the-art theoretical calculations and experiments. Kaiser *et al.* [21, 22] use coupled cluster calculations with single, double and partial triple excitations [CCSD(T)] to supplement their experimental investigation of the mechanism for atom-neutral reaction,



in a study of the dynamical processes involved in the formation of various C_3H isomers. This system represents the prototype reaction of ubiquitous interstellar carbon atoms with the simplest unsaturated hydrocarbon molecule, acetylene, to synthesize hydrocarbon radicals via a single atom-neutral collision in interstellar environments. The circumstellar shell of IRC+10216, for example, contains C_2H_2 as well as $C(^3P)$ reservoirs at distances of 10^{14} to 10^{15} m from the central star [23]. Multireference configuration interaction (MRCI) calculations by Takahashi *et al.* [24] support the conclusions by Kaiser *et al.* [22] that the $c-C_3H$ (cyclic C_3H) radical is energetically more stable than the $l-C_3H$ (linear C_3H) isomer. While the computed ground state

4.2: Determination of Properties of Propynylidyne Isomers using the H^v Method 102

energy difference between these two isomers from the MRCI and CCSD(T) methods are quite close to experiment, the same quantity generated from other theoretical approaches departs widely [18, 25] from experiment. These large discrepancies emerge primarily from methodological differences among the various approaches and, perhaps, from basis set deficiencies. In addition, although considerable progress has been made in understanding the dynamics of the bond rupture reaction of the C_3H_2 radical and the geometries and the relative energies of the C_3H isomers, only a few studies [24, 26] have so far attempted to describe the properties of the lowest excited state of the C_3H isomers and their ionization potentials and electron affinities. Fig. 4.1 shows the proposed reaction pathway to the C_3H isomers.

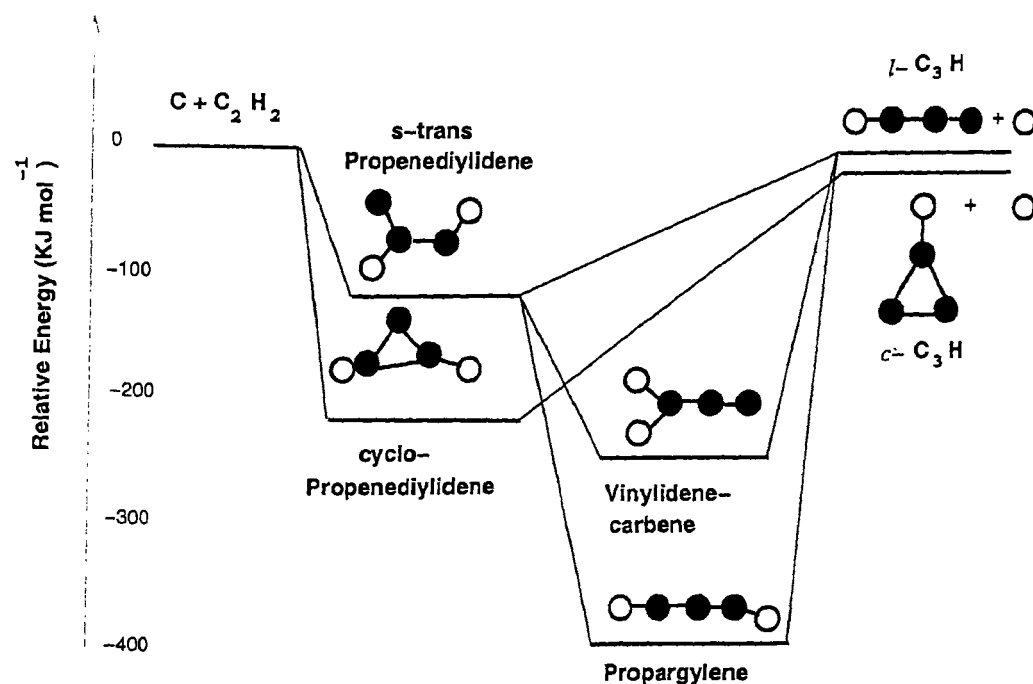


Figure 4.1: Calculated *ab initio* structures and relative energies of triplet C_3H_2 and doublet C_3H isomers. Filled circles are carbon atoms and void circles are hydrogen atoms. Figure taken from Kaiser's article [13]

The present work describes theoretical calculations for the ground and excited state properties of both C_3H isomers. Almost all previous theoretical works concur that a bent geometry (C_s point group) is energetically higher than the linear isomer [see refs. 23 and 43 for details] and that the cyclic isomer is more stable than the linear C_3H isomer. Since the earlier MP2/6-31G(d,p) optimization [24] pro-

duces a rather poor geometry, presumably partially because of the presence of two relevant resonance structures, we consider the geometry optimization using the H^v method with a two configuration reference space that contains these relevant resonance structures. The ground and excited state properties of the *l*- and *c*- C_3H radicals are computed through third order with the H^v method for both H^v optimized geometries, as well as for the experimental and MP2/6-31G(d,p) optimized geometries for comparison. Several harmonic vibrational frequencies are obtained as a by-product of the optimization procedure. Extensive theoretical studies [27, 28, 29, 30, 31, 32, 33, 34, 35, 36, 37, 38, 39] document the H^v formalism, its conceptual advantages, the computational algorithms for evaluating atomic and molecular properties, and the higher order convergence behavior of the method [40].

The computation of the conformational energy difference is complicated within a number of methods by symmetry breaking in the treatment of the linear isomer. The ground state of the *l*- C_3H isomer is of $^2\Pi$ symmetry, with one electron occupying the outer most degenerate π orbital. Maintaining this degeneracy during the optimization procedure often imposes significant technical problems. We impose the degeneracy of the *l*- C_3H isomer by using orbitals taken from a series of self-consistent field (SCF) calculations for the positive ion and the neutral species. More specifically, all doubly occupied orbitals for the ground state are determined from a closed shell SCF calculation for the ground state of the positive ion. The singly occupied π orbital and the other valence shell orbitals are generated as improved virtual orbitals (IVO's) for the neutral species [27]. Although symmetry breaking problems do not arise for the cyclic isomer, a similar procedure has also been applied for this case in order to treat both the isomers on an equal footing. Moreover, computations using this mixed orbital scheme for the cyclic isomer are in excellent agreement with those produced with our standard approach based on using neutral molecule ground SCF orbitals for all the occupied orbitals, an agreement similar to that demonstrated in many previous examples as emerging from the relative insensitivity of third order effective valence shell Hamiltonian calculations to a wide range of different orbital choices [41].

The theory of the H^v method is discussed in chapter 2 in details. The computed

results are presented and discussed in Secs. 4.2.1 and 4.2.2, respectively. We provide the first high level *ab initio* computations for excited electronic states above the lowest, the oscillator strengths for the transitions among these states, and the ionization potentials and electron affinities. An explanation is given for persistent theoretical difficulties in computing reasonable frequencies for the b_1 bending vibrations of the cyclic isomer.

4.2.1 Computational Details

All energies and molecular properties are evaluated for the *c*- and *l*- C_3H radicals at the experimental [42, 43] and theoretically optimized MP2 [24] and H^v geometries. [See Table 4.1 for details and the discussion below]. The ground states of the cyclic and linear C_3H isomers belong to the C_{2v} and $C_{\infty v}$ point groups, respectively. The restricted open-shell Hartree-Fock approximation (ROHF) to the ground state of the cyclic isomer is a single determinant with six doubly occupied a_1 orbitals, one doubly occupied b_2 orbital, and two doubly and one singly occupied b_1 orbitals. Thus, the ground state of cyclic C_3H radical is of 2B_1 symmetry. The ground state of linear C_3H , on the other hand, has ${}^2\Pi$ symmetry, with seven doubly occupied σ orbitals and two doubly and one singly occupied π orbitals.

The carbon atom basis set is constructed from a (10s7p2d)/[5s3p2d] contracted Gaussian basis of Sadlej [44] augmented by two *s* diffuse functions with exponents 0.021 and 0.0055, two *p* diffuse functions with exponents 0.021 and 0.0049, and one *d* diffuse function with exponent 0.015 for each of the carbon atoms. The hydrogen atom basis is a (5s2p)/[3s2p] basis [45]. This provides a basis of 120 contracted Gaussian type orbitals (CGTO). The number of CGTO used in this basis is quite close to that (a TZPP basis) employed by Ochsenfeld *et al.* [46]. The geometries of both isomers have been optimized by computing the third order H^v energy using a two-orbital reference space. The MP2 optimized geometries (see Table 4.1) are quite similar to the experimental geometry for the *c*- C_3H radical with the maximum deviation in bond lengths of 0.01 Å. In contrast, calculations for the linear isomer yield a much larger discrepancy between the MP2, on the one hand, and the H^v and experimental geometries on the other hand. The poor quality of

the MP2 geometry for the linear isomer arises because a one-configuration reference function is inadequate to describe the competition between the two dominant C-C≡C-H and C=C=C-H resonance structures. The MP2 geometry weighs the latter structure too heavily, while the H^v geometry optimization uses a minimal double reference treatment (see below) that adequately describes the mixing between these two resonance structures. All computations (optimization) produce a longer C-H bond length than experimentally observed [42] which actually only determines the projection of the C-H bond on the molecular axis. We, however, find no evidence for a bent C-H bond, although all atomic displacements have not been considered.

A four orbital H^v valence space (a complete active space) is used for computing the state energies and properties of both isomers at the experimental and optimized geometries. The choice of valence space orbitals is primarily based on energy considerations and the contributions of various orbitals to the states of interest [33] as illustrated below. The valence space generally spans a number of the highest occupied molecular orbitals in the ground state SCF approximations and a number of the lowest unoccupied orbitals in this state. For the cyclic geometry, the four orbital valence orbital space comprises two a_1 orbitals (one occupied and one unoccupied), one b_1 orbital (the singly occupied orbital in the ground state), and one b_2 (unoccupied) orbital. The complete active space for the linear geometry is composed of two σ (one occupied and one unoccupied) and two π (one singly occupied and one unoccupied) orbitals.

It is important to note the significant difference in the choice of both orbitals and orbital energies between the H^v and traditional multireference perturbation methods [47, 48]. The traditional approach generates all orbitals and their energies from a single Fock operator (the ground state Fock operator). Thus, all reference space orbitals and orbital energies, including those that are either occupied or unoccupied in the ground state SCF approximation, are evaluated using the same potential. The unoccupied reference space orbitals generated through this procedure describe an electron in the field of N others and are consequently more appropriate for describing negative ion states than the low lying excited states of interest. The H^v method, on the other hand, determines the unoccupied reference space orbitals and

their energies as improved virtual orbitals (IVOs) from a set V^{N-1} potential Fock operators in order to optimize the first order description (from PHP in Eq. (2.15) discussed in chapter 2 for atomic orbitals) and thereby to minimize the higher order perturbative corrections [32, 33, 39].

The H^v method thus yields unoccupied reference space orbital energies that are much lower than those from the ground state Fock operator due to the absence of an extra Coulomb operator in the H^v treatment for the IVOs. After the H^v valence space and orbital energies are computed in this fashion, the reference space orbital energies are replaced by their democratic average to eliminate (or greatly reduce) convergence difficulties from so-called intruder states [40].

The explicit procedure for obtaining the molecular orbitals and their energies involves a sequence of self-consistent field (SCF) calculations. [Some steps may actually be obtained using a single unitary transformation [35]]. For example, the four orbital reference space for the $c\text{-C}_3\text{H}$ radical is generated by the sequence of SCF calculations

- (1) $(\text{core})^{16}6a_1^2 3b_1^1$, 2B_1 ,
- (2) $[(\text{core})^{16}6a_1^2 3b_1^0]2b_2^1$, 2B_2 ,
- (3) $[(\text{core})^{16}6a_1^2 3b_1^0 2b_2^0]7a_1^1$, 2A_1 .

Here, the first step is a X^2B_1 state SCF calculation, and steps 2 and 3 are independent single orbital optimizations for the indicated states, where the orbitals inside the square brackets are frozen as the orbitals determined in the previous steps. The excited orbitals are then obtained by diagonalizing the X^2B_1 state Fock operator in the orbital space complementary to the union of the core and valence spaces. The H^v method incorporates correlation contributions arising from single and double excitations out of all the core orbitals and therefore requires fewer core orbitals in the valence space than CASSCF methods that omit the core excitations. As noted in the introduction, the retention of strict degeneracy for the linear isomer is accomplished by using a mixture of positive and neutral orbitals. When this type of scheme is applied to the cyclic isomer, step (1) of the above sequence is replaced by the two steps,

- (1) $(\text{core})^{16}6a_1^2$, 1A_1 ,

$$(1') [(core)^{16}6a_1^2]3b_1^1, \quad {}^2B_1,$$

while steps (2) and (3) remain unchanged. A comparison of computations for the cyclic isomer with both orbital choices provides a test of its accuracy.

Because of the large number of computed points required for optimizing the calculations for the H^v geometry optimization, the H^v geometries are performed with the more limited two-orbital reference space. The core and valence orbitals are determined from the SCF sequence,

$$(1) (core)^{16}7\sigma^2, \quad {}^1\Sigma,$$

$$(2) [(core)^{16}7\sigma^2]2\pi^1, \quad {}^2\Pi,$$

$$(3) [(core)^{16}7\sigma^2 2\pi^0]2\pi'^1, \quad {}^2\Pi,$$

for the linear isomer. This H^v geometry optimization is of interest as a nontrivial test for the H^v analytical derivative method [49] for which computer code are currently under development.

4.2.2 Results and Discussion

4.2.2.1 Cyclic C₃H

The first excited state electronic transition of *c*-C₃H has been assigned by Yamamoto *et al.* [18] to be of $X({}^2B_1) \rightarrow {}^2A_1$ symmetry, and is the only experimentally reported transition so far. Using a simple model, they deduce a vertical excitation energy of 10,800 cm⁻¹ (1.339 eV). This particular excited state involves a $6a_1 \rightarrow 3b_1$ transition rather than a $3b_1 \rightarrow 7a_1$ excitation. Hence, the doubly occupied $6a_1$ orbital must be retained in the valence space. This feature also explains why the EOMCC-IP computations have been performed using the negative ion $|\Phi_{C_3H^-}\rangle$ CSF as the closed shell zeroth order wavefunction. More specifically, the excited state of interest for the *c*-C₃H isomer has the CSF $|(core)^{16}6a_1 3b_1^2\rangle$. This particular CSF may be generated conveniently from a closed shell CSF $|(core)^{16}6a_1^2 3b_1^2\rangle$ by removing an electron from the occupied $6a_1^1$ orbital, thereby explaining why Stanton [26] employs the EOMCC-IP method to compute the excitation energies for the *c*-C₃H isomer.

Table 4.2 displays the vertical excitation energies and oscillator strengths of the *c*-C₃H isomers as computed through third order with the H^v method. The computed lowest excitation energy for the cyclic isomer is compared with experiment

[43] and with other high level calculations, the CASSCF calculations of Takahashi [24] and the equation of motion-coupled cluster singles and doubles for ionized states (EOMIP-CC) calculations of Stanton [26]. The errors in the estimation of vertical excitation energy for $X(^2B_1) \rightarrow ^2A_1$ from the CASSCF, EOMIP-CC and H^v methods (computed at the experimental geometry) are $\approx 14\%$, 4.2% , and 0.6% , respectively. However, the accuracy of the computed H^v excitation energy for the lowest $X(^2B_1) \rightarrow ^2A_1$ transition degrades when the MP2 (off by 2.8%) and H^v (off by 5.9%) optimized geometries are used in the calculations. Table 4.1 indicates that the deviation from experiment of the calculated C–H bond length $R_{C-H}^{(Opt.)} - R_{C-H}^{(Expt.)}$ is large (0.3%) compared to the deviation $R_{C-C}^{(Opt.)} - R_{C-C}^{(Expt.)}$ (0.2%) for the C–C bond length. Therefore, the slightly greater inaccuracy in the estimation of the transition energy at the optimized geometry presumably arises due to the overestimation of the C–H bond distance by the optimization procedure. Nevertheless, the estimated quantity is in accord with the experiment and state-of-art EOMIP-CC calculations. Interestingly, while both the CASSCF and EOMIP-CC calculations underestimate the $X(^2B_1) \rightarrow ^2A_1$ transition energy, the H^v method overestimates this quantity, with the H^v and EOMIP-CC energies of comparable accuracy.

Table 4.3 summarizes the computed third order H^v vertical ionization potentials and electron affinities for the cyclic form of the C₃H radical. To our knowledge, this table represents the first report for the ion state energies of this radical. Unlike the vertical excitation energy, the ionization energies and the electron affinities computed at the experimental, MP2 and H^v optimized geometry are quite close to each other, indicating that the ion state energies are quite insensitive to these small shifts in the geometrical parameters. The two negative electron affinities imply that the 1^1B_1 and 1^3B_1 anion excited states are metastable Feshbach resonances lying in the electron detachment continuum [50]. A separate computation for the negative ions should probably be used to provide a more accurate description for the interesting excited anion states.

Table 4.4 uses the two optimized and the experimental geometries to illustrate the slight variation of the computed dipole moment with the geometrical parameters. The table also compares the computed dipole moment from the third order H^v

calculations with experiment and with other correlated calculations. While the ground state dipole moments computed with the H^v method at the experimental and optimized geometries (MP2 and H^v) are reasonably close to experiment and to other correlated calculations, the dipole moment of the first excited state of A_1 symmetry is quite a bit larger than the other theoretical value, presumably because our calculations apply for the ground state geometry, while Ref. 26 uses the excited state geometry.

The vibrational frequencies obtained from the H^v method are compared with experiment [51] and with other theoretical calculations [24] in table 4.5. The H^v method estimate for the lowest vibrational frequency of a_1 symmetry is comparable to that from the CASSCF and MP2 calculations, but the H^v overestimates the other two vibrational frequencies of the same symmetry. Both the H^v and CASSCF treatments yield unphysical results for the b_1 vibration for which CASSCF computations yield an imaginary frequency. In addition, the lowest experimental [18] vibrational frequency of cyclic C₃H is 508 cm⁻¹ (a b_1 in-plane mode), and all the theoretical calculations, including the present, one fail to provide a comparable low frequency vibration. An explanation for these behaviors emerges from an analysis of the G-matrix [52] for the cyclic isomer in the five dimensional space considered (which contains two b_1 vibrations). Both computed b_1 vibrational frequencies are highly sensitive to an off-diagonal G-matrix element: changing the CCC equilibrium bond angle over a range of 2-3 degrees shifts the computed frequencies from 11000 to 6000 cm⁻¹ for the higher frequency b_1 vibration, and a change in the CCC bond angle of 1 degree converts the lower frequency mode from ≈ 1000 cm⁻¹ to an imaginary frequency. (Note that the root-mean-square zero point bending amplitude is ≈ 4 degrees.) Presumably, the theoretical force constants (F-matrix) are reasonable, but the vibrational frequencies should be evaluated with G-matrix elements that are explicit functions of the angle.

The third order H^v method compensates perturbatively for a wide range of different choices for the orbitals and orbital energies. For example, the third order H^v vertical transition energies and other related properties for the *c*-C₃H isomer have been computed separately by using the occupied orbitals generated from an

SCF sequence with the first step involving the $(core)^{16}6a_2^2$ (cation) configuration and those with the first step involving the $(core)^{16}6a_1^23b_1^1$ (neutral) ground state Fock-operators, respectively. The occupied orbitals from the $(core)^{16}6a_1^2$ positive ion Fock operator clearly experience a greater attractive potential and, therefore, are more tightly bound than those generated from the neutral $(core)^{16}6a_1^23b_1^1$ Fock operator. Because the two sets of orbitals and orbital energies differ considerably between these two extreme situations, one way to test practical convergence is the degree to which the computed properties differ with the two orbital choices since infinite order calculations should yield identical results in both cases. The use of cation and neutral occupied orbitals produces the third order H^v transition energy for $X(^2B_1) \rightarrow 1^2A_1$ transition as 1.347 eV and 1.288 eV, respectively, which is a rather minor difference. The two choices of orbitals and orbital energies yield virtually identical values for the dipole moment. Thus, both choices of orbitals are quite adequate for the cyclic isomer. However, the use of cation orbitals is more convenient and attractive computationally for the linear isomer, where this choice reduces the computational complexity during the orbital optimization.

4.2.2.2 Linear C₃H radical

Tables 4.6-4.9, respectively present the third order H^v vertical excitation energies, ionization potentials, electron affinities, and dipole moments as computed at three different geometries (experimental, MP2, and H^v optimized) and the vibrational frequencies obtained from the H^v optimization process. To our knowledge, no experimental or theoretical data (except the vibrational frequencies and ground state dipole moment) are available for comparison. However, based on our success for the cyclic isomer and several other systems [28, 29, 35, 36, 37, 38], we expect that our computed properties for the l -C₃H isomer should be quite accurate, and, therefore, of interest in spectroscopic studies.

It is evident from table 4.1 that all the optimization procedures appear to fail in reproducing the exceptionally short C-H bond length of 1.017 Å determined experimentally [42]. The short computed C-H distance was later interpreted by Oschenfeld *al.* [46] as occurring because of the Renner-Teller effect [53] which arises due to the

very low lying vibronic state involving the CCH bending mode and because the experiments only determine the projection of the C-H bond on the molecular axis. They have shown that the vibrational average for the projection of the C-H bond length on the molecular axis reduces the C-H bond length from 1.065 Å to 1.008 Å in much better accord with the experimentally quoted quantity. Using the same procedure, i.e., by evaluating the projection on the molecular axis of the C-H bond length as averaged over the CCH bending zero point motion, we obtain 1.019 Å for the projected C-H bond length which is very close to experiment.

Tables 4.6 and 4.7 demonstrate that the excitation energies and dipole moments of the *l*-C₃H isomer vary significantly between the different optimized geometries primarily because the single reference MP2 geometry optimization for this isomer encounters inaccuracies due to the importance of two dominant resonance structures. The MP2 geometry optimization produces a shorter C₁-C₂ bond length than experiment. The MP2 optimization yields the C₁-C₂ and C₂-C₃ bond lengths to be, respectively, of the order of the CC triple bond length in C₂H₂ (1.2033 Å) and the CC double bond length in C₂H₄ (1.3384 Å). Both the MP2 and H^v methods agree on the C-H bond length as discussed above, but the H^v geometry compares more favorably to experiment for the CC bond lengths. Since all of the theoretical methods yield the actual C-H bond length as opposed to experiment which only obtains its projection on the molecular axis, we compute the excitation energies using a "mixed experimental" geometry in which the C-C bond lengths are taken from experiment while the C-H bond length is taken from theory (the H^v optimized value). In contrast to the excitation energies evaluated for the poor MP2 geometry, the relative ordering of the excited states (except the rather nearby 1²Σ⁻ and 2²Δ excited states) computed at the experimental and "mixed" geometries agrees with that calculated at the H^v geometry. The small differences arise from a slight variation in the C-C bond lengths. This analysis confirms that the significant variation in the computed excitation energies and dipole moments between the MP2 and H^v methods as well as between the MP2 and experimental geometries arises mostly due to the poor MP2 estimate of the C-C bond lengths rather than errors in the C-H bond length.

Table 4.8 presents the ionization potentials and electron affinities of the linear isomer from third order H^v calculations at the experimental and theoretically optimized geometries. The table clearly indicates that the singlet and triplet Π states of l - C_3H^- are bound, with the $^1\Pi$ state lower energetically than the $^3\Pi$ electronic state as expected. It is also interesting to note that the positive and negative ion states of the l - C_3H display a dependence on geometry. While the H^v vertical ionization potentials for the H^v optimized geometry are quite close to those for the experimental geometry, the electron affinities differ substantially. A separate optimization for the positive and negative ions of the l - C_3H radical may be useful to provide a more accurate description for these interesting excited ionic species.

The harmonic vibrational frequencies obtained from the H^v geometry optimization are compared with those obtained from the CASSCF and MP2 calculation of Takahashi *et al.* [24] and the MCSCF calculation of Kanada *et al.* in table 4.9. The experimentally [54] estimated lowest vibration frequency this isomer is as low as 28 cm^{-1} which corresponds to the C–H bending mode. The present and all earlier theoretical calculations, including CASSCF, MP2 and MCSCF calculations fail to account for such a low frequency vibrational mode. The estimated vibrational frequency for this C–H bending mode with the H^v , MP2, and CASSCF methods is 262, 245 and 325 cm^{-1} , respectively, departing considerably from experiment.

4.2.2.3 Conformational energy difference

Table 4.10 compares the ground state energy difference between the cyclic and linear C_3H radicals as computed through third order with the H^v method and as obtained from experiment and from other theoretical calculations [13, 24]. Table 4.10 indicates that the third order H^v conformational energy difference at the experimental geometry is fairly close to that obtained from the CCSD(T) method but does not fall within the experimental range. However, as noted above the experimental C–H bond length corresponds only to the projection on the molecular axis, not the actual bond length. The third order H^v estimate for the ground state energy difference between these two isomeric forms at the respective H^v optimized geometries not only lies within the experimental range but is also quite close to the MRCI value. The

computations in table 4.10 should be modified for differences in zero point energies between the isomers. Reference 24 estimates that the zero point differences reduce the computed energy difference by 1.1 Kcal/mole, bringing the H^v calculations well within the experimental range. Further reduction in the small discrepancies between the optimized and experimental geometries may help in pinning down a more precise theoretical prediction.

4.3 Conclusion

We describe highly correlated *ab initio* computations for the ground state energy difference between the cyclic and linear isomers of propynlidyne (C_3H), as well as their harmonic vibrational frequencies, ionization potentials, electron affinities, excited state energies, dipole moments and oscillator strengths, some of which have not been reported before. The difficulties in computing these isomers energy difference are illustrated by contrasting our computations using the theoretically optimized geometries and the experimental geometries. The third order H^v conformational energy difference between the two C_3H isomers at the experimentally quoted geometry is in good agreement with that obtained from the CCSD(T) method but departs considerably ($\approx 6-10$ KJ/mole) from experiment, mainly because experiment for the linear geometry only provides the projection of the C-H bond on the molecular axis. On the other hand, the third order H^v isomer energy difference computed for the H^v and MP2 optimized geometries lie at the opposite extremes of the experimental range, although inclusion of approximate zero point energy corrections place the H^v value squarely within the experimental range and the MP2 value slightly below this range. The main source of uncertainty in the energy difference probably stems from residual discrepancies between the theoretical and experimental geometries.

The H^v calculations for the ground state isomer energy difference, the cyclic C_3H lowest excitation energy, and the dipole moments in both isomers are in good agreement with experiment and with other state-of-art correlated computations. These agreements once again demonstrate the high accuracy obtainable with the H^v method for complex atomic and molecular systems. We provide the first high level calculations for excitation energies and oscillator strengths to higher excited

Table 4.1: Structural data for the C_3H isomers.

Parameter	Linear				Cyclic			
	MP2 [1]	Expt.[2]	H^v	CCS-	MP2 [1]	Expt.[4]	H^v	CCS-
	geom.		geom.	D(T)[3]	geom.		geom.	D(T)[3]
R(C1-H)	1.0631Å	1.0171Å	1.07Å	1.065Å	1.0790Å	1.0760Å	1.079Å	1.078Å
R(C1-C2)	1.2005Å	1.2539Å	1.255Å	1.243Å	1.3747Å	1.3739Å	1.03709Å	1.377Å
R(C2-C3)	1.3640Å	1.3263Å	1.340 Å	1.347	1.3878Å	1.3771Å	1.3763Å	1.378Å

[1]Ref. [24], [2]Ref. [42] [3]Ref. [22] [4]Ref. [43]

states of both isomers, as well as several lowest vertical ionization potentials and electron affinities. This new information emerges as a bonus of the H^v method which generates all states of the neutral and ions from a single computation. The computations suggest that linear anion has bound excited state. A strong sensitivity of the computed b_1 vibrational frequencies for the cyclic isomer on a G-matrix elements explains the persistent difficulties in computing accurate values.

Table 4.2: Vertical excitation energies (in eV) and oscillator strengths (in parentheses) of the $c-$ C_3H radical.

State	Third Order H^v			CASSCF[1]	EOMCC-IP[2]	Expt. [3]
	MP2 geom.	Expt. geom.	H^v geom.			
1^2A_1	1.377 (0.037)	1.347 (0.037)	1.418 (0.039)	1.149	1.283	1.339
1^4A_2	3.735	3.754	3.754			
1^2B_2	3.891	3.908	3.858			
1^2A_2	4.573 (0.014)	4.578 (0.014)	4.590 (0.014)			
2^2A_1	7.825	7.775	7.778			
2^4B_1	8.439	8.313	8.427			
2^2B_1	8.572	8.445	8.559			
2^2A_2	8.814	8.733	8.767			

[1]Ref. [24],[2]Ref. [26],[3]Ref. [43].

Table 4.3: Vertical ionization potentials and electron affinities (in eV) of the $c\text{-C}_3\text{H}$ radical.

State	Third Order H^ν		
	MP2 geometry	Experimental geometry	H^ν geometry
Ionization potential			
1^1B_1	10.708	10.665	10.666
1^1A_1	10.711	10.674	10.706
Electron affinity			
1^1A_1	1.804	1.732	1.741
1^1B_1	-0.509	-0.494	-0.512
1^3B_1	-0.522	-0.505	-0.524

Table 4.4: Dipole moments (in Debye) of the $c\text{-C}_3\text{H}$ radicals

State	Third Order H^ν			EOMCC-IP	MP2[2]	CASSCF[2]	Expt.
	MP2	Expt.	H^ν				
	geom.	geom.	geom.				
X^2B_1	2.43	2.42	2.44	2.35	2.34	2.37	2.30 ³
1^2A_1	4.31	4.25	4.28	3.03			
1^4A_2	1.80	1.72	1.75				
1^2B_2	1.56	1.49	1.53				

1- C_3H

[1]Ref. [26]. [2]Ref. [46]. [3]Ref. [55].

Table 4.5: Vibrational frequencies (in cm^{-1}) of the $c\text{-C}_3\text{H}$ radical.

Symmetry	H^ν	CASSCF[1]	MP2 [1]	Expt.
a_1	1050	1191	1206	1160 [2]
a_1	1554	1670	1657	1832 [2]
a_1	3712	3450	3325	3238 [2]
b_1	1117	1047	969	508 [3]
b_1	8303	890i	12526	

[1]Ref. [24] [2]Ref. [51] [3]Ref. [43]

Table 4.6: Vertical excitation energies (in eV) and oscillator strengths (in parentheses) of the $l-C_3H$ radical.

State	Third Order H ^v			
	MP2 geom.	Experimental geom.	H ^v geom.	Mixed geom.
1 ⁴ Δ	1.970	4.329	4.064	4.370
1 ² Σ ⁺	3.320 (0.003)	5.461 (0.009)	5.219 (0.008)	5.506
1 ² Δ	3.429 (0.016)	5.155 (0.021)	4.969 (0.020)	5.207
1 ² Σ ⁻	3.978	5.957	5.697	6.000
2 ² Δ	5.226	5.912	5.806	5.917

Table 4.7: Dipole moments (in Debye) of the $l-C_3H$ radical.

State	Third Order H ^v			MP2[1]	CASSCF[1]	Expt.
	MP2	Expt.	H ^v			
	geom.	geom.	geom.			
X ² Π	1.83	2.46	2.41	3.31	3.42	3.1 ²
1 ⁴ Δ	0.59	1.66	1.62			
1 ² Σ ⁺	1.38	2.35	2.35			
1 ² Δ	2.16	3.31	3.31			

[1] Ref. [24] [2] Ref. [56]

Table 4.8: Vertical ionization potentials and electron affinities (in eV) of the $l-C_3H$ radicals.

State	Third Order H ^v		
	MP2 geometry	Experimental geometry	H ^v geometry
Ionization potential			
1 ¹ Σ	8.701	9.327	9.208
1 ¹ Π	12.831	15.223	14.969
Electron affinity			
1 ¹ Π	0.298	0.221	0.305
1 ³ Π	0.204	0.131	0.215

Table 4.9: Vibrational frequencies (in cm^{-1}) of the $l\text{-C}_3\text{H}$ radical.

Isomer	Symmetry	H^v	CASSCF[1]	MP2 [1]	MCSCF[2]
	π	262	325	245	247
	σ	1020	1095	1117	1139
	σ	1829	1925	2467	1906
	σ	3291	3613	3601	3607

[1]Ref. [24] [2]Ref. [42]

Table 4.10: Energy difference (in KJ mole^{-1}) between the $c\text{-C}_3\text{H}$ and $l\text{-C}_3\text{H}$ radicals.

Experimental geometry	Third order H^v		CCSD(T)[1]	MRCI[2]	Approx. Expt.[3]
	MP2 geometry	H^v geometry			
14.12	4.58	8.39	13.00	9.01 (8.62)	4.18-8.32

[1]Ref. [46]. [2]Ref. [24]. [3] Ref. [22].

References

- [1] D.R. Yarkony, *Molecular Structure*, Atom. Mol. & Opt. Phys. Handbook, Ed. G.W.F. Drake, AIP press (1996)
- [2] G.W. King, *Spectroscopy and Molecular Structure*, Holt.Rinehart and Winston, Inc., NY, pp252 (1964)
- [3] P. Swings and I. Rosenfeld, *Astroph. J.*, **86**, 483 (1937)
- [4] A. McKellar, *Publ. Dominion Ap. Obs.*, Victoria, B.C., No. 15, **7**, 251 (1941)
- [5] A.E. Douglas and G. Herzberg, *Astroph. J.*, **94**, 381 (1941)
- [6] E. Herbst & C. M. Leung, *Astroph. J. Suppl.*, **69**, 271 (1989)
- [7] R. P. A. Bettens and R.D. Brown, *MNRAS*, **258**, 347 (1992)
- [8] E. Herbst, H.-H. Lee, D.A. Howe & T.J. Millar, *MNRAS*, **268**, 335 (1994)
- [9] D. L. Baulch, et al., *J. Phys. Chem. Ref. Data*, **21**, 411 (1992)
- [10] D. Husain, *J. Chem. Soc. Faraday Trans.*, **89**, 2164 (1993)
- [11] N. Haider & D. Husain, *J. Photochem. Photobiol.* **A70**, 119 (1993)
- [12] D. C. Clary, N. Haider, D. Husain & M. Kabir, *Astroph. J.*, **422**, 416 (1994)
- [13] Y. Hirahara, et. al, *Astroph. J.*, **394**, 539 (1992)
- [14] T.J.Millar and Eric Herbst, *Astron. Astrophys.*, **288**, 561 (1994).
- [15] D. C. Clary, T.S. Stoecklin & A.G. Eichham, *J. Chem.Soc. Faraday Trans.*, **89**, 2185 (1993)
- [16] P. Thaddeus, C. A. Gottlieb, A. Hjalmarson, L. E. B. Johansson, W. M. Irvine. P. Friberg and R. A. Linke, *Astrophys. J. Lett.*, **294**, L49 (1985).
- [17] C. A. Gottlieb, J. M Vrlitek, E. W. Gottlieb, P. Thaddeus and A. Hjalmarson. *Astrophys J. Lett.*, **294**, L55 (1985).

- [18] S. Yamamoto, S. Saito, M. Ohishi, H. Suzuki, S. Ishikawa, N. Kaifu and A. Murakami, *Astrophys. J. Lett.* **322**, L55 (1987).
- [19] T. J. Miller, C. M. Leung, and E. Herbst, *Astron. Astrophys.* **183**, 109 (1987).
- [20] D. Smith, *Chem. Rev.* **92**, 1580 (1992).
- [21] R. I. Kaiser, Y. T. Lee, and A. G. Suits, *J. Chem. Phys.* **103**, 10395 (1995).
- [22] R. I. Kaiser, C. Ochsenfeld, M. Head-Gordon, Y. T. Lee and A. G. Suits; *Science* **274**, 1508 (1996) and references therein.
- [23] J. Keene, K. Young, T.G. Phillips, T.H. Büttgenbach, *Astrophys. J.*, **415**, L131 (1993)
- [24] J. Takahshi and K. Yamashita, *J. Chem. Phys.* **104**, 6613 (1996).
- [25] K. Akoi, K. Hashimoto, S. Ikuta and A. Murakami, *Astrophys. J* (in press).
- [26] J. F. Stanton, *Chem. Phys. Lett.* **237**, 20 (1995).
- [27] K. F. Freed, *Lecture Notes in Chemistry, Vol 52* (Springer, Berlin, 1989), p. 1.
- [28] H. Sun, K. F. Freed, M. Herman and D. L. Yeager, *J. Chem. Phys.*, **72**, 4158 (1980).
- [29] R. K. Chaudhuri, A. Mudholkar, K. F. Freed, C. H. Martin and H. Sun, *J. Chem. Phys.* **106**, 9252 (1997) and references therein.
- [30] R. K. Chaudhuri and K. F. Freed, *J. Chem. Phys.* (to be published).
- [31] S. Majumder, B. P. Das and R. K. Chaudhuri, *Phys. Rev. A* **59**, 3432 (1999).
- [32] J. E. Stevens, K. F. Freed, F. Arendt and R. L. Graham, *J. Chem. Phys.* **101**, 4832 (1994).
- [33] C. M. Taylor, R. K Chaudhuri and K. F. Freed, (to be submitted).
- [34] R. K. Chaudhuri, B. P. Das, and K. F. Freed, *J. Chem. Phys.* **108**, 2556 (1998).
- [35] J. P. Finley and K. F. Freed, *J. Chem. Phys.* **102**, 1306 (1995).

- [36] R. L. Graham and K. F. Freed, *J. Chem. Phys.* **96**, 1304 (1992).
- [37] A. W. Kanzler, H. Sun, and K. F. Freed, *Int. J. Quantum Chem.* **39**, 269 (1991).
- [38] C. M. Martin and K. F. Freed, *J. Chem. Phys.* **100**, 7454 (1994).
- [39] J. E. Stevens, R. K. Chaudhuri, and K. F. Freed, *J. Chem. Phys.* **105**, 8754 (1996).
- [40] (a). J. P. Finley, R. K. Chaudhuri and K. F. Freed, *J. Chem. Phys.* **103**, 4990 (1995); (b). J. P. Finley, R. K. Chaudhuri and K. F. Freed, *Phys. Rev. A* **54**, 343 (1996); (c) R. K. Chaudhuri, J. P. Finley and K. F. Freed, *J. Chem. Phys.* **106**, 4067 (1997).
- [41] (a). M. G. Sheppard and K. F. Freed, *J. Chem. Phys.* **75**, 4525 (1981). (b). M. G. Sheppard and K. F. Freed *Int. J. Quantum Chem.* **15**, 21 (1981).
- [42] S. Kanada, S. Yamamoto, S. Saito and Y. Osamura, *J. Chem. Phys.* **104**, 2192 (1996).
- [43] S. Yamamoto and S. Saito, *J. Chem. Phys.* **101**, 5484 (1994).
- [44] A. J. Sadlej, *J. Chem. Phys.* **75**, 320 (1981).
- [45] T. H. Dunning, *J. Chem. Phys.* **90**, 1007 (1989).
- [46] C. Ochsenfeld, R. I. Kaiser, Y. T. Lee, A. G. Suits and M. Head-Gordon, *J. Chem. Phys.* **106**, 4141 (1997) and references therein.
- [47] B. H. Brandow, *Rev. Mod. Phys.* **39**, 771 (1967).
- [48] I. Lindgren and J. Morrison, *Atomic Many-Body Theory. 2nd ed. Springer Series on Atoms and Plasmas* (Springer, New York, 1986).
- [49] R. K. Chaudhuri, J. E. Stevens, and K. F. Freed. *J. Chem. Phys.* **108**, 9685 (1998).
- [50] H. Sun and K. F. Freed, *J. Chem. Phys.* **76**, 5051 (1982).

- [51] M. E. Jacox, in *Vibrational and Electronic Energy Levels of Polyatomic Transient Molecules*, edited by J. W. Gallagher (American Chemical Society and American Institute of Physics for NIST., Gaithersburg, Maryland (USA), 1993), p. 156.
- [52] E. Bright Wilson, Jr. J. C. Decius and Paul C. Cross, *Molecular Vibrations (The Theory of Infrared and Raman Vibrational Spectra)*, Dover Publications, New York,(1980).
- [53] G. Herberg, *Molecular Spectra and Molecular Structure* (Krieger, Malabar, 1991), Vol. III.
- [54] S. Yamamoto, S . Saito, H. Suzuki, S. Deguchi, N. Kaifu, S. Ishikawa and M. Ohishi, *Astrophys. J.* **348**, 363 (1990).
- [55] J. M. Vrtilek, C. A. Gottlieb, T. C. Killian and P. Thaddeus, *Astrophys. J. Lett.* **364**, L53 (1989).
- [56] F. J. Lovas, R. D. Suenram, T. Ogata and S. Yamamoto, *Astrophys. J.* **399**, 325 (1992).

Chapter 5

Conclusion and Future Directions

5.1 Conclusion

In this thesis work we have calculated various electronic properties of atomic and molecular systems of astrophysical interest using many-body theory. We have attempted to improve the accuracies of the existing calculations and predict strengths of unobserved lines using highly correlated and accurate theoretical methods.

We have started with neutral carbon, a small but complicated open shell system. A multireference non-relativistic many-body perturbation theory, the third order effective valence shell Hamiltonian method was employed to calculate excitation energies (EE) of various states of the system and oscillator strengths (*f*-values) of allowed transitions among them. There are no experimental measurements for many of these transitions among the excited states, only a few theoretical computations have been carried out. Using the H^v method we could achieve better accuracy for the EE values for all the states than those obtained with other accurate methods such as the closed coupling [1], the SUPERSTRUCTURE [2] approaches and the coupled cluster theory based on the similarity transformed equation of motion [3]. This was possible because of the multireference structure of our method, which enabled us to be captured the non-dynamical correlation (correlation internal to the valence orbitals) necessary to describe open-shells accurately. In these calculations we obtained the oscillator strengths by using wavefunctions computed through third

order in perturbation and the effective dipole operators evaluated through second order. The accuracies achieved for the f -values by our calculations are comparable with other theoretical calculations, but they are not in good agreement with the experimental values. The present H^v computations strongly suggest the use of multiple reference spaces for the excited state computations because of the different nature of correlation in various classes of excited states.

We have chosen neutral calcium for our next calculation. This is a very important system for the spectroscopic studies in astrophysics. The electronic properties of the excited states of this atom were not calculated accurately or measured experimentally with high precision. Our successful calculations on neutral carbon motivated us to calculate the binding energies (energies relative to first ionization threshold), excitation energies, oscillator strengths and transition probabilities of Ca I using the third order H^v method. The difficulties in accurately estimating these properties of Ca I arise mainly due to i) the lack of a balanced description of the ground and excited states, ii) the use of an inadequate basis which leads to difficulties in describing the excited states and an unbalanced treatment of dynamical correlation (correlations describing coulomb holes) and polarization effects. We have shown that by using the improved virtual orbitals (IVO) basis and the appropriate selection of the valence space the third order H^v method produces accurate results of the electronic properties by overcoming the above difficulties. We obtained better agreement for all the properties with the experiments, wherever available, than the corresponding results obtained from other correlated methods. This work highlights a number of important features of the H^v method. It also demonstrates that the success of the H^v method largely depends on two competing factors- the trade off between the large valence space to produce more accurate results and better perturbative convergence to avoid intruder states. This calculations provide a uniform accuracy for more excited states than those obtained with some other schemes such as MCHF [4] and CI [5].

With the advent of high resolution spectrographs with large signal to noise ratio, the observations of forbidden lines become common for precise determination of the column densities of the ISM. But very few accurate calculations have been performed

on them and experimental measurements are difficult. The magnetic quadrupole transition from $2s2p$ (3P_2) to $2s^2$ (1S_0) is one of those frequently observed transitions, whose weak transition rates were not calculated precisely for Be-like ions with low Z -values and for higher Z -values no attempt being made. At present, observations [6, 7] near these ultraviolet and visible lines of highly ionized systems are of immense interest. We employed the relativistic counterpart of the MCHF method, the MCDF method based on the EOL approximation to calculate accurate excitation energies and transition probabilities of these transitions. In these calculations, the relativistic correction of the Coulomb interaction; the Breit interaction was included via first-order perturbation theory. We have shown that the effect of the inclusion of the Breit interaction to the excitation energies is important as one increases the atomic number. The computed excitation energies are in excellent agreement with the NIST database. Apart from doubly ionized carbon, to our knowledge, this method was applied for the first time to the M2 transition probabilities for Be-like ions. As expected for low- Z ions, our results are not different from all other results obtained using relativistic corrections. But for heavier ions the relativistic motions of the electrons become effective, so the discrepancies are larger. This work highlights a number of unique and desirable features of the MCDF-EOL method for highly ionized atoms.

Solutions of the Dirac-Fock equation for many-electron atoms using the method of finite basis set expansion (FBSE) have found a number of applications. The accuracy of the many-body theoretical computations depends on the basis to a large extent. The quality of a particular basis set is determined by physical considerations and numerical tests. The most widely used FBSE method in the framework of Gaussian-type orbitals, which yields good results, but, it depends largely on the exponent parameter and size of the basis set. We have developed an approach which uses numerical wavefunctions for occupied and a few low lying unoccupied orbitals. This has important implications, especially, for the correlated many-body methods. We have used this formalism to obtain a new orbital basis. In our work we have applied this approach to two systems; Mg^+ and Ca^+ and verified the improvements of the calculated results.

Intrinsically much weaker lines of Mg^+ are the best candidates to determine the Mg II column densities in the neutral region of ISM. But all the calculated f -values of these lines are ambiguous (see Sect. 3.4) and there are large discrepancies among the *ab initio* calculations and empirical calculations. Therefore, an improved and accurate *ab initio* calculation was necessary. We have employed one of the most successful *ab initio*, highly correlated all order many-body method namely, the coupled cluster method to calculate those quantities. The excitation energies obtained using this method are in excellent agreement with the experimentally measured values. We have calculated improved oscillator strengths for $3s - 4p$ transitions which agree well with the empirical estimations [8]. Our calculated oscillator strengths of other strong lines are in excellent agreements with the all order relativistic SD method [9], wherever available. We have carried out calculations for many of the above mentioned transitions which to our knowledge, has not been performed earlier.

We have chosen one of the most important molecules in astrophysics for our theoretical studies, which has received relatively little attention. Hydrocarbon radicals are of recent interest in astronomical observations because they provide accurate estimations of cloud temperature, chemical processes inside molecular clouds. One of them is propynlidyne, C_3H radical first detected in TMC-1 and the carbon star IRC+10216 [10]. We have employed the third order H^v method to calculate the vertical excitation energies, ionization potentials, electron affinities, dipole moments, oscillator strengths and some harmonic vibrational frequencies of the two isomers of the C_3H radicals within MP2 geometry [11] and experimental geometry [12]; some of these calculations have not been reported before. The computations of these isomers' ground states energy difference has been a major theoretical challenge. We confirmed the experimental investigations and the CCSD(T) calculations by Kaiser et al. [13] that linear C_3H isomer is less stable than the cyclic one. Our calculated energy differences using two different geometries lie within the experimental range if we consider approximate zero point energy corrections. Other calculated properties are in good agreement with experiment and other state-of-art correlated computations. We have carried out calculations for the first time in literature of the excitation energies and oscillator strengths of high-lying excited states of isomers,

as well as several lowest vertical ionization potentials and electron affinities. This work shows many advantageous features of the H^v method as well as its limitations. In brief, we calculated various electronic properties of single and multi-reference atomic and molecular systems of immense astronomical interest with high accuracy using many-body processes. To do that we modified the existing approaches and codes; at some places, we had to develop new theories and codes depends on the requirements of the problems.

5.2 Future Directions

We have seen in this thesis that better accuracies are required in lots of cases, which serves as a motivation for extending this work in the following contexts. The H^v method; one of the most successful MR-MBPT methods, improves the agreement between theory and experiment for excitation energies and oscillator strengths of atomic systems like calcium and molecular systems like propylidyne isomers, but for other systems like carbon improvements are not uniform through out the spectrum. One can try to improve the accuracies by improving the quality of the basis and increasing the reference space in the H^v framework. But, in the latter case, as it has been argued over the past few years, the numerical stability of the calculations are affected by the ever present intruder states. However, this has been mitigated by extensive studies of the convergence of the perturbation series [14]. As explained in chapter 2, the selection of the model space plays a crucial role as it influences the convergence and accuracy of the results. Without the clear separation of the model and complementary space with large energy gap between them, the so-called intruder states appear and spoil the convergence. Such separation cannot be achieved in many cases if a complete model space (consisting of all possible distributions of the valence electrons in the valence orbitals) is used. Convergence may often be achieved by resorting to the incomplete-model-space scheme [15], where only low-energy determinants deemed important for the state under consideration are calculated accurately. It is desirable to develop MR-MBPT method may satisfy all these requirements.

The results obtained from the MCDF-EOL method could improve if one considers

more excitations from the core and valence spaces to larger virtual space, which again leads to the convergence problem to optimize those virtual orbitals. A large CI calculation may yield better results than ours. But conventional large CI calculations is time consuming and need huge disk space. Therefore, the non-conventional CI approach, like the Epstein-Nesbet approach may be useful in such cases.

It is possible to improve on several aspects of coupled cluster calculations. One way to apply the all order single reference coupled cluster approach (SRCC) of Kállay and Surján [16] to all the atomic properties. The multi-reference systems, like neutral carbon, may be calculated with better accuracy than presented in this thesis, if we use a multi-reference version of the state-specific coupled cluster theory, suggested by Mukherjee et al. [17].

The selection of basis functions is one of the most important ingredient of the atomic and molecular calculations, as we have experienced in this thesis work. We have developed a approach to generate basis functions which yields better results for atomic and molecular properties than by using the conventional basis functions. The inclusion of the inter-electron separation in the basis functions, the geminal basis, may be important in various accurate many-body calculations to describe many-body states and improve those results.

In many-body methods, in general, accuracies improve with extensions of the reference space or virtual space. And in the case of perturbative method, it is the increase in the order of perturbation. To do such calculations, bigger parallel computers with more memory and more CPUs are necessary.

References

- [1] H. Nussbaumer and P.J. Storey, *Astron. Astrophys.*, **140**, 383 (1984)
- [2] A. Hibbert and E. Biémont, *Astron. Astrophys. Suppl.*, **99**, 179 (1993)
- [3] Nooijen and R.J. Bartlett, *J. Chem. Phys.*, **107**, 6812 (1997)
- [4] N. Vaeck, M. Godefroid and J.E. Hansen, *J. Phys. B*, **24**, 361 (1991)
- [5] J. Mitroy, *J. Phys. B*, **26**, 3703 (1993)

- [6] J.D. Gillaspay, *Physica Scripta*, **T65**, 168 (1996)
- [7] S.J. Adelman and A.F. Gulliver, *Physica Scripta*, **T83**, 97 (1999)
- [8] E. L. Fitzpatrick, *Astrophys. J.*, **482**, L199 (1997)
- [9] M.S. Safronova, A. Derevianko and W.R. Johnson, *Phys. Rev. A*, **58**, 1016 (1998)
- [10] P. Thaddeus, C.A. Gottlieb, H. Hjalmarson, L.E.B. Johansson, W.M. Irvine, P. Friberg and R.A. Linke, *Astrophys. J. Lett.*, **294**, L49 (1985)
- [11] J. Takahshi and K. Yamashita, *J. Chem. Phys.*, **104**, 6613 (1996)
- [12] S. Kanada, S. Yamamoto, S. Saito and Y. Osamura, *J. Chem. Phys.*, **104**, 2192 (1996)
- [13] R.I. Kaiser, C. Ochsenfeld, M. Head-Gordon, Y.T. Lee and A.G. Suits, *Science*, **274**, 1508 (1996) and references therein.
- [14] R.K. Chaudhuri, J.P. Finley and K.F. Freed, *J. Chem. Phys.*, **106**, 4067 (1997)
- [15] L. Meissner and R.J. Bartlett, *J. Chem. Phys.*, **92**, 562 (1990) and references therein.
- [16] M.Kállay and P.R.Surján, *J.Chem.Phys*, **113**, 1359 (2000)
- [17] S. Chattopadhyay, U.S. Mahapatra and D. Mukherjee, *J. Chem. Phys.*, **111**, 3820 (1999)
- [18] U. Kaldor, *Theor. Chim. Acta*, **80**, 427 (1991) and references therein.

Appendix:A

DF and MCDF method

A.1 Rayleigh-Ritz Variational Principle

Theorem 1: Let H be the Hamiltonian of a system, then the functional,

$$E(\Psi) = \frac{\langle \Psi | H | \Psi \rangle}{\langle \Psi | \Psi \rangle}$$

is minimized when $|\Psi\rangle$ is the ground state wavefunction.

Proof : Let $\{|n\rangle\}$ be a set of eigenvectors of H .

$$H|n\rangle = E_n|n\rangle$$

$$|\Psi\rangle = \sum_n a_n|n\rangle$$

$$\begin{aligned} E(\Psi) &= \frac{\langle \Psi | H | \Psi \rangle}{\langle \Psi | \Psi \rangle} \\ &= \sum_n |a_n|^2 E_n \end{aligned}$$

$$\Rightarrow E(\Psi) \geq \sum_n |a_n|^2 E_0 = E_0$$

$$\Rightarrow E(\Psi) \geq E_0$$

when the equal sign holds if all $a_n=0$ for $n \neq 0$. In that case, however, $|\Psi\rangle = |0\rangle$ is the eigenfunction corresponding to E_0 as required.

A.2 Dirac-Fock equation for Atoms

For a relativistic N -particle system we get the relativistic HF equation which is also known as the Dirac-Fock equation. In this case the Dirac Hamiltonian with Coulomb potential and central potential $V_N(r_i)$ is

$$H = \sum_i c\alpha_i \cdot \mathbf{P}_i + (\beta_i - 1)mc^2 + V_N(r_i) + \sum_{i<j} \frac{e^2}{r_{ij}} \quad (\text{A.1})$$

We represent the ground state wavefunction Φ as a $N \times N$ determinant

$$\Psi = \frac{1}{\sqrt{N!}} \begin{bmatrix} \phi_1(x_1) & \phi_1(x_2) & \cdots & \phi_1(x_N) \\ \phi_2(x_1) & \phi_2(x_2) & \cdots & \phi_2(x_N) \\ \vdots & \vdots & \ddots & \vdots \\ \phi_N(x_1) & \phi_N(x_2) & \cdots & \phi_N(x_N) \end{bmatrix} \quad (\text{A.2})$$

Where Φ s are the eigenvectors of \mathbf{J}^2 and J_z . Where the single particle wavefunctions ϕ_i s are the eigenvectors of \mathbf{J}^2 and J_z and can be expressed in terms of Dirac form as,

$$\phi_a = \begin{pmatrix} g(r)\chi_{\kappa_a, m_a} \\ if(r)\chi_{-\kappa_a, m_a} \end{pmatrix} \quad (\text{A.3})$$

where $g(r)$ and $f(r)$ are space parts and χ_{κ_a, m_a} part is spin angular function. And the quantum number $\kappa = \pm(j + \frac{1}{2})$ for $l = j \pm \frac{1}{2}$.

Using the variational principle:

$$\delta E[\Psi] = 0$$

$$\Rightarrow \delta[\langle \Psi | H | \Psi \rangle - \sum_{ab} \lambda_{ab} \langle \phi_a | \phi_b \rangle] = 0$$

The radial part of the single particle Hamiltonian in atomic unit ($e = m = \hbar = 1$ and $c = \frac{1}{\alpha}$) is

$$h_a = \frac{1}{\alpha} \begin{pmatrix} \sum_i V_N(r_i) & \sum_i c\sigma_i \cdot \mathbf{P}_i \\ \sum_i c\sigma_i \cdot \mathbf{P}_i & -[\sum_i V_N(r_i) + 2mc^2] \end{pmatrix} \begin{pmatrix} \psi_A \\ \psi_B \end{pmatrix}$$

And let V represent the Coulomb part of the electron-electron interactions.

$$\begin{aligned} E[\phi] &= \sum_a \langle a | h_a | a \rangle + \sum_{ab} \{ \langle ab | V | ab \rangle - \langle ab | V | ba \rangle \} \\ &= \sum_a q_a I(a) + \sum_{ab} \sum_k [f^k(ab) F^k(ab) + g^k(ab) G^k(ab)] \end{aligned} \quad (\text{A.4})$$

where q_a is the occupation number of orbital a .

$$\text{Let } u_a = \frac{1}{r} \begin{pmatrix} f_a(r) \\ ig_a(r) \end{pmatrix} \text{ and } u_b = \frac{1}{r} \begin{pmatrix} f_b(r) \\ ig_b(r) \end{pmatrix}$$

Then, the one particle integral can be written as :

$$I(a) = \langle u_a | h_a | u_a \rangle$$

and direct and exchange part of the two particle radial integrals are given by :

$$F^k(ab) = \langle a | \frac{1}{r} Y_{bb}^k | a \rangle = \int u_a^\dagger(r) u_a(r) Y_{bb}^k \frac{dr}{r}$$

$$G^k(ab) = \langle a | \frac{1}{r} Y_{ba}^k | b \rangle = \int u_a^\dagger(r) u_b(r) Y_{ba}^k \frac{dr}{r}$$

where

$$Y_{ab}^k(r) = r \int_0^\infty \frac{r'^k}{r'^{k+1}} u_a^\dagger(r') u_b(r') dr'$$

$$= \frac{1}{r^k} \int_0^r r'^k u_a^\dagger(r') u_b(r') dr' + r^{k+1} \int_r^\infty \frac{1}{r'^{k+1}} u_a^\dagger(r') u_b(r') dr'$$

$f^k(ab)$ and $g^k(ab)$ are angular coefficients.

Using the Variational Principle, we get

$$\delta \{ E[\phi] - \sum_{ab} \lambda_{ab} \langle a | b \rangle \} = 0 \quad (\text{A.5})$$

$$\sum_a q_a \delta I(a) + \sum_{ab} \sum_k [f^k(ab) \delta F^k(ab) + g^k(ab) \delta G^k(ab)] - \sum_{ab} \lambda_{ab} \delta \langle a | b \rangle = 0$$

$$\delta I(a) = 2 \langle \delta u_a | h_a | u_a \rangle$$

$$\delta_a F^k(ab) = \delta_a \int u_a^\dagger(r) u_a(r) Y_{bb}^k \frac{dr}{r}$$

$$= 2(1 + \delta_{ab}) \langle \delta u_a | \frac{1}{r} Y_{bb}^k | u_a \rangle$$

and

$$\Rightarrow \delta_a \sum_{bk} f^k(ab) F^k(ab) = 2q_a \langle \delta u_a | V_a(r) | u_a \rangle \quad (\text{A.6})$$

where $V_a(r) = \frac{1}{q_a r} \sum_{bk} (1 + \delta_{ab}) f^k(ab) Y_{bb}^k$: Direct DF potential.

$$\Rightarrow \delta_a \sum_{bk} g^k(ab) G^k(ab) = -2q_a \langle \delta u_a | \chi_a(r) \rangle \quad (\text{A.7})$$

Where $\chi_a(r) = -\frac{1}{q_a r} \sum_{bk} (1 + \delta_{ab}) g^k(ab) Y_{ba}^k u_a(r)$: Exchange DF potential.

By define $\epsilon_a = \frac{1}{q_a} \lambda_{aa}$, we get from Eq. 3.26,

$$2q_a \langle \delta u_a | [h_a + V_a(r) - \chi_a(r)] | u_a \rangle - 2q_a \epsilon_a \langle \delta u_a | u_a \rangle - 2 \sum_{b \neq a} \lambda_{ab} \langle \delta u_a | u_b \rangle = 0$$

Note, $\lambda_{ab} = \lambda_{ba}$

$$(h_a + V_a(r) - \epsilon_a) u_a(r) = \chi_a(r) + \frac{1}{q_a} \sum_{b \neq a} \lambda_{ab} u_b(r) \quad (\text{A.8})$$

This is the Dirac-Fock equation for relativistic particle.

A.3 Multiconfiguration Dirac-Fock Equations for Atoms :

In the multiconfiguration approach, each atomic state function (ASF) is expressed in terms of configuration state functions (CSFs) by

$$\Psi(\Pi J M) = \sum_r c_r \Phi_r(\gamma_r \Pi J M)$$

where Π is the parity, J and M are quantum numbers representing angular momentum, γ_r represents other informations needed to specify Ψ .

Then the energy expression in terms of ASF can be written in terms of CSFs by the following way,

$$E = \langle \Psi | H | \Psi \rangle = \sum_{rs} c_r^* H_{rs} c_s \quad (\text{A.9})$$

where,

$$H_{rs} = \langle \Phi_r(\gamma_r \Pi J M) | H | \Phi_s(\gamma_s \Pi J M) \rangle$$

$$H_{rr} = \sum_a q_a(r) I(aa) + \sum_{ab} \sum_k [f^k(ab) F^k(ab) + g^k(ab) G^k(ab)]$$

where q_a is the occupation of orbital a in configuration r .

$$H_{rs} = \sum_{ab} T_{rs}(ab) I(ab) + \sum_{abcd} \sum_k V_{rs}^k(abcd) R^k(abcd), \quad \text{for } r \neq s$$

where,

$$I(ab) = \langle a | h_\kappa | b \rangle \quad (\kappa = \kappa_a = \kappa_b)$$

$T_{rs}(ab) = 0$ for $\kappa_a \neq \kappa_b$

$$\begin{aligned} R^k(abcd) &= \langle a | \frac{1}{r} Y_{bd}^k | c \rangle = R^k(cbac) = R^k(adcb) \\ &= R^k(badc) = \langle b | \frac{1}{r} Y_{ac}^k | d \rangle \end{aligned}$$

$$F^k(ab) = R^k(abab) \quad G^k(ab) = R^k(abba)$$

The normalization condition is $\langle \Psi | \Psi \rangle = 1, \Rightarrow \sum_r |c_r|^2 = 1$.

Applying the variational principle on Eq. (3.30) with respect to mixing coefficients, we get

$$\begin{aligned} \frac{\partial}{\partial c_n^*} [\langle \Psi | H | \Psi \rangle - \lambda \langle \Psi | \Psi \rangle] &= 0 \\ \frac{\partial}{\partial c_n^*} [\sum_{rs} c_r^* H_{rs} c_s - \lambda \sum_r |c_r|^2] &= 0 \\ \frac{\partial}{\partial c_n^*} [\sum_{rs} c_r^* H_{rs} c_s - \lambda \sum_{rs} c_r^* c_s \delta_{rs}] &= 0 \\ \Rightarrow \sum_s (H_{ns} - \lambda \delta_{ns}) c_s &= 0 \end{aligned}$$

Thus the matrix eigenvalue equation can be written as

$$\tilde{H} \tilde{c} = \lambda \tilde{c} \quad (\text{A.10})$$

where, $\lambda = \sum_{rs} c_r^* H_{rs} c_s = E$. Therefore,

$$\delta E = \sum_{rs} c_r^* \delta H_{rs} c_s$$

Evaluating of δH_{rr} and δH_{rs} ,

$$\begin{aligned} \delta_a H_{rr} &= 2 \left[\langle \delta u_a | q_a(r) h_k | u_a \rangle + \frac{1}{r} \sum_{bk} (1 + \delta_{ab}) f_r^k(ab) \langle \delta u_a | Y_{bb}^k | u_a \rangle \right. \\ &\quad \left. + \frac{1}{2} (1 + \delta_{ab}) g_r^k(ab) \langle \delta u_a | Y_{ab}^k | u_b \rangle \right] \end{aligned}$$

Let, $\bar{q}_a = \sum_r |c_r|^2 q_a(r)$, $\bar{f}^k = \sum_r |c_r|^2 f_r^k$, $\bar{g}^k = \sum_r |c_r|^2 g_r^k$,

$$\begin{aligned} V_a(r) &= \frac{1}{\bar{q}_a r} \sum_{bk} (1 + \delta_{ab}) \bar{f}^k(ab) Y_{bb}^k(r) \\ \chi_a(r) &= -\frac{1}{\bar{q}_a r} \sum_{bk} (1 + \delta_{ab}) \bar{g}^k(ab) Y_{ab}^k(r) u_b(r) \end{aligned}$$

Then,

$$\delta_a \sum_r |c_r|^2 H_{rr} = 2\bar{q}_a \left[\langle \delta u_a | h_k + V_a(r) | u_a \rangle - \langle \delta u_a | \chi_a(r) \rangle \right]$$

Similarly, we can write,

$$\delta_a H_{rs} = 2 \left[\langle \delta u_a | \left\{ \sum_b T_{rs}(ab) h_k | u_b \right\} + \sum_{bcd} bcd V_{rs}^k(abcd) \frac{1}{r} Y_{bd}^k | u_c \right\rangle \right]$$

where, $T(ab) \equiv \sum_{rs} c_r^* c_s T_{rs}(ab)$, $V^k(abcd) \equiv \sum_{rs} c_r^* c_s V_{rs}^k(abcd)$

$$\Rightarrow \delta_a \sum_{rs} c_r^* H_{rs} c_s = 2 \left[\sum_b T(ab) \langle \delta u_a | h_k | u_b \rangle + \sum_{k,bcd} V^k(abcd) \langle \delta u_a | \frac{1}{r} Y_{bd}^k | u_b \rangle \right]$$

Now

$$\begin{aligned} \delta_a E &= \delta_a \sum_r |c_r|^2 H_{rr} + \delta_a \sum_{rs} c_r^* c_s H_{rs} \\ &= 2\bar{q}_a \left[\langle \delta u_a | h_k + V_a(r) | u_a \rangle - \langle \delta u_a | \chi_a(r) \rangle \right] \\ &\quad + \frac{1}{\bar{q}_a} \langle \delta u_a | \left[\sum_b T(ab) h_k | u_b \right] + \sum_{k,bcd} V^k(abcd) \frac{1}{r} Y_{bd}^k | u_c \rangle \end{aligned}$$

Let

$$\begin{aligned} |\bar{\chi}_a\rangle &= |\chi_a\rangle - \frac{1}{\bar{q}_a} \sum_{k,bcd} V^k(abcd) \frac{1}{r} Y_{bd}^k | u_c \rangle \\ &= -\frac{1}{\bar{q}_a r} \left[\sum_{bk} \bar{g}^k(ab) Y_{ba}^k | u_b \right] + \sum_{k,bcd} V^k(abcd) Y_{bd}^k | u_c \rangle \end{aligned}$$

The variation of the orthogonality condition shows,

$$\begin{aligned} \delta_a \left[\sum_b \lambda_{ab} \langle u_a | u_b \rangle \right] &= \lambda_{aa} 2 \langle \delta u_a | u_a \rangle + \sum_{b \neq a} \lambda_{ab} \langle \delta u_a | u_b \rangle \\ &= \bar{q}_a \varepsilon_a 2 \langle \delta u_a | u_a \rangle + \sum_{b \neq a} \lambda_{ab} \langle \delta u_a | u_b \rangle \end{aligned}$$

where $\lambda_{aa} = \bar{q}_a \varepsilon_a$. From the variational principle equation,

$$\begin{aligned} \delta_a \left[E - \sum_b \lambda_{ab} \langle u_a | u_b \rangle \right] &= 0 \\ \Rightarrow 2\bar{q}_a \langle \delta u_a | h_k + V_a - \varepsilon_a | u_a \rangle - 2\bar{q}_a \langle \delta u_a | \bar{\chi}_a \rangle - \frac{1}{\bar{q}_a} \sum_{b \neq a} \langle \delta u_a | [\lambda_{ab} - T(ab) h_k] | u_b \rangle &= 0 \\ \Rightarrow (h_k + V_a(r) - \varepsilon_a) u_a(r) = \chi_a(r) + \frac{1}{\bar{q}_a} \sum_{b \neq a} [\lambda_{ab} - T(ab) h_k] u_b(r) &\quad (\text{A.11}) \end{aligned}$$

where $\kappa = \kappa_a = \kappa_b$. The coupled equations (3.31) and (3.32) are called the **Multi-configuration Dirac-Fock equations**.